UNIVERSIDADE FEDERAL DE VIÇOSA

ELIARA ACIPRESTE HUDSON

FORMAÇÃO DE COMPLEXOS SUPRAMOLECULARES ENTRE ESTRUTURAS CARREADORAS E MOLÉCULAS BIOATIVAS

VIÇOSA - MINAS GERAIS
2021

ELIARA ACIPRESTE HUDSON

FORMAÇÃO DE COMPLEXOS SUPRAMOLECULARES ENTRE ESTRUTURAS CARREADORAS E MOLÉCULAS BIOATIVAS

Tese apresentada à Universidade Federal de Viçosa, como parte das exigências do Programa de Pós-Graduação em Ciência e Tecnologia de Alimentos, para obtenção do título de *Doctor Scientiae*.

Orientadora: Ana Clarissa dos Santos Pires

Coorientadores: Luis Henrique Mendes da Silva
Márcia Cristina Teixeira R. Vidigal

VIÇOSA - MINAS GERAIS
2021

Ficha catalográfica elaborada pela Biblioteca Central da Universidade Federal de Viçosa - Campus Viçosa

T
H885f
2021

Hudson, Eliara Acipreste, 1989-
Formação de complexos supramoleculares entre estruturas carreadoras e moléculas bioativas / Eliara Acipreste Hudson. – Viçosa, MG, 2021.
102 f. : il. (algumas color.) ; 29 cm.

Orientador: Ana Clarissa dos Santos Pires.
Tese (doutorado) - Universidade Federal de Viçosa.
Inclui bibliografia.

1. Compostos bioativos. 2. Ciclodextrinas. 3. Caseínas. 4. Curcumina. 5. Resveratrol. 6. Quercetina. I. Universidade Federal de Viçosa. Departamento de Tecnologia de Alimentos. Programa de Pós-Graduação em Ciência e Tecnologia de Alimentos. II. Título.

CDD 22. ed. 613.282

ELIARA ACIPRESTE HUDSON

FORMAÇÃO DE COMPLEXOS SUPRAMOLECULARES ENTRE ESTRUTURAS CARREADORAS E MOLÉCULAS BIOATIVAS

Tese apresentada à Universidade Federal de Viçosa, como parte das exigências do Programa de Pós-Graduação em Ciência e Tecnologia de Alimentos, para obtenção do título de *Doctor Scientiae*.

APROVADA: 02 de junho de 2021.

Assentimento:

Eliara Acipreste Hudson
Autora

Ana Clarissa dos Santos Pires
Orientadora

AGRADECIMENTOS

A Deus por todas as graças concedidas, pelo cuidado e preparo do caminho até aqui.

À Universidade Federal de Viçosa (UFV), ao Departamento de Tecnologia de Alimentos (DTA) e ao Programa de Pós-Graduação em Ciência e Tecnologia de Alimentos (PPGCTA) pela oportunidade de realização do doutorado e disponibilização de recursos.

Ao Conselho Nacional de Desenvolvimento Científico e Tecnológico (CNPq) pela concessão da bolsa de estudos. À Fundação de Amparo à Pesquisa do Estado de Minas Gerais (FAPEMIG) pela concessão de recursos financeiros ao projeto. O presente trabalho foi realizado com apoio da Coordenação de Aperfeiçoamento de Pessoal de Nível Superior – Brasil (CAPES) – Código de Financiamento 001.

À professora Ana Clarissa pelos ensinamentos, atenção, exemplo e cuidado como orientadora durante graduação e pós-graduação. Agradeço também pela amizade, confiança e carinho sempre presentes ao longo desses anos de convívio e parceria.

Ao professor Luis Henrique por toda a disponibilidade durante a coorientação e, em especial, pelos valiosos ensinamentos, paciência e apoio na escrita científica.

À Professora Márcia pela colaboração e disponibilidade como coorientadora neste trabalho.

À Jaqueline e à Yara por terem aceitado participar da banca de defesa.

Ao grupo "Termodinâmica Molecular Aplicada" (THERMA), do qual tenho imenso orgulho de fazer parte, pela trajetória e aprendizados nele construídos. Aos colegas de grupo pela colaboração e convívio. De forma especial, meu agradecimento à Jaqueline e à Natália, pela parceria na caminhada.

Ao grupo "Química Verde Coloidal e Macromolecular" (QUIVECOM), pela parceria, colaboração nas atividades e disponibilização de equipamentos.

Aos meus amados pais, Maria do Carmo e Reginaldo, por todo amor, apoio e incentivo em cada um dos momentos da minha caminhada, especialmente nos mais difíceis. Ao meu amado irmão Pedro, pela amizade e carinho que sempre me deram forças. Aos meus queridos avós pelo apoio e orações, em especial ao meu vô Ari, pela imensa confiança em mim e por seu exemplo de fé e otimismo. Essa conquista é, orgulhosamente, dedicada a vocês.

Houve um atraso de 03 meses na defesa da tese devido às limitações impostas pela pandemia da COVID-19. Este atraso foi regulamentado pelo Ministério da Educação por meio da Portaria n° 544, de 16 de junho de 2020.

RESUMO

HUDSON, Eliara Acipreste, D.Sc., Universidade Federal de Viçosa, junho de 2021. **Formação de complexos supramoleculares entre estruturas carreadoras e moléculas bioativas.** Orientadora: Ana Clarissa dos Santos Pires. Coorientadores: Luis Henrique Mendes da Silva e Márcia Cristina Teixeira Ribeiro Vidigal.

Os compostos bioativos apresentam a propriedade de modular diversos processos metabólicos, mas sua bioatividade é dependente de suas estabilidade e biodisponibilidade. Dessa forma, a formação de complexos supramoleculares entre moléculas bioativas e macromoléculas naturais, como proteínas e ciclodextrinas, é uma estratégia interessante para a incorporação dos bioativos em diferentes matrizes de forma a manter sua bioatividade. Para isso, é fundamental que se caracterize as interações que promovem e sustentam a formação desses complexos, assim como se conheça sua cinética de formação e dissociação. Este trabalho foi dividido em três artigos científicos e objetivou caracterizar as interações intermoleculares dos seguintes sistemas: micela de caseína-curcumina (MC-CUR), β-caseína-quercetina (β-cas-Qct), β-ciclodextrina-resveratrol/análogo estrutural (β-CD-RES e β-CD-RESAn1). No primeiro artigo, estudou-se a formação do complexo MC-CUR, a capacidade carreadora da MC e sua proteção térmica para CUR em um pH de 6,6. Mostrou-se que uma MC pode transportar cerca de 18.000 moléculas de CUR. Os parâmetros termodinâmicos indicaram um processo de formação de complexo entalpicamente dirigido ($\Delta H° = –64,63$ kJ/mol e $T\Delta S°$ variando de –42,45 a –44,46 kJ/mol) e o aumento da temperatura reduziu a taxa de formação do complexo MC-CUR e aumentou sua taxa de dissociação. A energia de ativação para a formação dos complexos ativados MC-CUR foi negativa para a etapa de associação de moléculas livres de MC e CUR (–62,8 kJ/mol) e positiva para a dissociação dos complexos termodinamicamente estáveis (1,80 kJ/mol). A MC protegeu a CUR contra sua degradação térmica. No segundo artigo, foi demonstrado que β-cas e Qct formam complexos supramoleculares termodinamicamente estáveis em um processo dirigido por um aumento na entropia do sistema ($\Delta H° = 25,86$ e $T\Delta S° = 53,49$ kJ/mol a 25 °C), via formação de um complexo ativado dirigido por uma redução entrópica ($T\Delta S^{‡}_{(a)} = -15,31$ kJ/mol e $T\Delta S^{‡}_{(d)} = -68,80$ kJ/mol a 25 °C) e um ganho entálpico ($\Delta H^{‡}_{(a)} = 30,87$ e $\Delta H^{‡}_{(d)} = 5,0$ kJ/mol a 25 °C). A adição de ambos os sais, KCl ou KSCN, aumentou a estabilidade do complexo por diminuição dos valores das entalpias cinética e termodinâmica. No terceiro artigo, a cinética de interação entre β-CD modificada (β-CD-NH_2) e RES, bem como seu análogo estrutural (RESAn1) foi determinada. A inclusão de RESAn1, bem como sua dissociação da β-CD-NH_2, foram mais rápidos que os mesmos processos que

ocorreram tendo RES como molécula hóspede ($k_a^{\beta-CD\ \ \ _2/RES}$ =3,10x10^4 $M^{-1}s^{-1}$, $k_a^{\beta-CD-NH_2/RES}$=1,87 x10^3 $M^{-1}s^{-1}$; $k_d^{\beta-CD\ \ \ _2/RES}$ =0,39 s^{-1}, $k_d^{\beta-CD\ \ \ _2/RES}$=0,30 s^{-1}, a 25 °C). As diferenças estruturais entre os polifenóis (RES e RESAn1) afetaram mais os parâmetros energéticos de formação do complexo ativado entre estes e a β-CD-NH_2 via associação das moléculas livres que via dissociação dos complexos termodinamicamente estáveis ($E_{act,a}^{\beta-CD-\ \ _2/RES}$ =14,81 kJ/mol, $E_{act,a}^{\beta-CD\ \ \ _2/RESAn}$ =-15,01 a 82,35 kJ/mol, $E_{act,d}^{\beta-CD-\ \ _2/RES}$ =5,19 kJ/mol e $E_{act,d}^{\beta-CD-\ \ _2/RES}$ =6,29 kJ/mol). Essas diferenças são devidas, principalmente, ao processo de dessolvatação das moléculas que interagiram. Conclui-se que os parâmetros termodinâmicos e cinéticos obtidos para cada um dos sistemas estudados, bem como os resultados das análises complementares, são importantes fundamentos para otimização da aplicação desses complexos moleculares bioativos em diferentes sistemas alimentícios ou farmacêuticos.

Palavras-chave: Compostos bioativos. Complexos supramoleculares. Caseínas. β-ciclodextrina. Curcumina. Quercetina. Resveratrol. Termodinâmica. Cinética.

ABSTRACT

HUDSON, Eliara Acipreste, D.Sc., Universidade Federal de Viçosa, June, 2021. **Supramolecular complex formation between carrier structures and bioactive molecules.** Adviser: Ana Clarissa dos Santos Pires. Co-advisers: Luis Henrique Mendes da Silva and Márcia Cristina Teixeira Ribeiro Vidigal.

Bioactive compounds have the property of modulating several metabolic processes, but their bioactivity is dependent on their stability and bioavailability. Thus, the formation of supramolecular complexes between bioactive molecules and natural macromolecules, such as proteins and cyclodextrins, is an interesting strategy for the incorporation of bioactive substances in different matrices to maintain their bioactivity. For this, it is essential to characterize the interactions that promote and sustain the formation of these complexes, as well as to know their formation and dissociation kinetics. This work was divided into three scientific articles and aimed to characterize the intermolecular interactions of the following systems: micelle of casein-curcumin (MC-CUR), β-casein-quercetin (β-cas-Qct), β-cyclodextrin-resveratrol/structural analog (β-CD-RES and β-CD-RESAn1). In the first article, the formation of the MC-CUR complex, the carrying capacity of MC and its thermal protection for CUR at a pH of 6.6 was studied. It has been shown that an MC can carry around 18,000 molecules of CUR. The thermodynamic parameters indicated an enthalpically driven complex formation process ($\Delta H° = -64.63$ kJ·mol^{-1} and $T\Delta S°$ ranging from –42.45 to –44.46 kJ·mol^{-1}). The increase in temperature reduced the rate of formation of the MC-CUR complex and increased its rate of dissociation. The activation energy for the formation of activated MC-CUR complexes was negative for the association of free MC and CUR molecules (–62.8 kJ·mol^{-1}) and positive for the dissociation of thermodynamically stable complexes (1.80 kJ·mol^{-1}). MC protected CUR against its thermal degradation. In the second article, it was demonstrated that β-cas and Qct form thermodynamically stable supramolecular complexes in a process driven by an increase in the entropy of the system ($\Delta H°= 25.86$ and $T\Delta S°= 53.49$ kJ·mol^{-1} at 25 °C), via formation of an activated complex driven by an entropic reduction ($T\Delta S^{‡}_{(a)}= -15.31$ kJ·mol^{-1} and $T\Delta S^{‡}_{(d)}= -68.80$ kJ·mol^{-1} at 25 °C) and an enthalpic increase ($\Delta H^{‡}_{(a)} = 30.87$ and $\Delta H^{‡}_{(d)} = 5.0$ kJ·mol^{-1} at 25 °C). The addition of both salts, KCl or KSCN, increased the stability of the complex by decreasing the values of the kinetic and thermodynamic enthalpies. In the third article, the interaction kinetics between modified β-CD (β-CD-NH_2) and RES, as well as its structural analog (RESAn1) was determined. The inclusion of RESAn1, as well as its dissociation from β-CD-NH_2, were faster than the same processes that occurred with RES as a guest molecule

($k_a^{\beta-CD-NH_2/RESAn1}$=3.10x10^4 M^{-1}s^{-1}, $k_a^{\beta-CD-NH_2/RES}$=1.87x10^3 M^{-1}s^{-1}; $k_d^{\beta\beta-CD-NH_2/RESAn1}$=0.39 s^{-1}, $k_d^{\beta-CD-NH_2/RES}$=0.30 s^{-1}, at 25 °C). The structural differences between the polyphenols (RES and RESAn1) affected the energetic parameters of formation of the activated complex more via the association of free molecules than via dissociation from the thermodynamically stable complexes ($E_{act,a}^{\beta-CD-NH_2/RES}$ =14.81 kJ·mol^{-1}, $E_{act,a}^{\beta-CD-\ _2/RESAn1}$ =-15.01 to 82.35 kJ·mol^{-1}), ($E_{act,d}^{\beta-CD-NH_2/RES}$ =5.19 kJ·mol^{-1} and $E_{act,d}^{\beta-CD-NH_2/RESA}$ =6.29 kJ·mol^{-1}). These differences are mainly due to the desolvation process of the interacting molecules. It is concluded that the thermodynamic and kinetic parameters obtained for each of the studied systems, as well as the results of the complementary analyzes, are important foundations for optimizing the application of these bioactive molecular complexes in different food or pharmaceutical systems.

Keywords: Bioactive compounds. Supramolecular complexes. Caseins. β-cyclodextrin. Curcumin. Quercetin. Resveratrol. Thermodynamics. Kinetics.

SUMÁRIO

INTRODUÇÃO GERAL

Há muito tempo, plantas são utilizadas com fins medicinais para tratamento de diversas doenças. Os metabólitos secundários das plantas, também conhecidos como compostos bioativos, apresentam a propriedade de modular diversos processos metabólicos, o que interfere na indução ou inibição de enzimas, na atividade de receptores celulares, na expressão de genes, além de influenciar na redução de estados pró-inflamatórios, estresse oxidativo e diversos distúrbios metabólicos (SANTOS et al., 2019). Essas propriedades conferem a compostos bioativos efeitos terapêuticos sobre diversas doenças, como cânceres (WU et al., 2018), diabetes (ZHENG et al, 2021), doenças infecciosas e inflamatórias (PENG; ZHAO; BIWAS, 2017), Alzheimer e outras doenças degenerativas (GIACOMELI et al., 2019). Além disso, estudos recentes têm apresentado vários compostos bioativos, como curcumina, quercetina, ácido gálico, resveratrol e naringina, como potenciais inibidores de enzimas diretamente relacionadas à infecção por SARS-CoV-2, vírus causador da Covid-19, declarada como doença pandêmica global pela OMS em 11 de março de 2020 (KELFIE; BIESALSKI, 2021; KHAERUNNISA et al., 2020; RANGSINTH et al., 2021).

A bioatividade de compostos bioativos é, no entanto, dependente da estabilidade destes ao processo de digestão e consequente biodisponibilidade (CARBONELL-CAPELLA et al., 2014). Além das transformações químicas pelas quais passam estes compostos em condições fisiológicas, a limitada solubilidade em meios aquosos e instabilidade química frente a luz e determinados valores de pH e temperatura apresentados pelos compostos bioativos também são fatores que diminuem sua biodisponibilidade e eficácia terapêutica (WANG et al., 2016). Portanto, é de grande interesse nas áreas de farmácia e de alimentos o desenvolvimento de estratégias que viabilizem a incorporação de compostos bioativos em diferentes matrizes de forma a reduzir sua instabilidade química, entregando-os aos seus locais de ação no organismo sem que percam sua bioatividade. Nesse campo, a formação de complexos supramoleculares entre moléculas bioativas e macromoléculas naturais, como proteínas e ciclodextrinas, é uma estratégia que vem sendo cada vez mais explorada.

As proteínas do leite são veículos naturais de micronutrientes, como cálcio e fosfato. Devido a suas estruturas predominantemente hidrofóbicas, as proteínas do leite são também veículos promissores para compostos bioativos hidrofóbicos, sendo capazes de liberar esses compostos nos locais adequados no corpo humano, preservando sua bioatividade (DE KRUIF et al., 2012). Essas proteínas são subdivididas em caseínas, que representam cerca de 80% do

total de proteínas do leite, e em proteínas do soro, presentes em cerca de 20% do total proteico do leite (BELLOMARIA et al., 2016).

Micelas de caseína são partículas coloidais formadas por complexos de proteínas e fosfato de cálcio coloidal. Atualmente, o modelo estrutural mais aceito para descrever a organização das micelas de caseína é o modelo do "nanocluster", que descreve a micela de caseína como uma matriz homogênea de caseínas, formada pelas interações entre os centros de fosforilação dessas proteínas e "nanoclusters", ou nanoagregados, de fosfato de cálcio coloidal, além de interações fracas entre as próprias moléculas de caseínas. A fração proteica das micelas (aproximadamente 93% de sua massa seca) é constituída por quatro componentes individuais de produtos gênicos: α_{s1}-, α_{s2}-, β- e κ-caseínas (DE KRUIF et al., 2012). A estrutura aberta das micelas de caseína, com seus canais e cavidades preenchidos com material da fase contínua do leite (soro), a torna uma molécula de grande potencial para a ligação de pequenas moléculas, como as moléculas bioativas hidrofóbicas vitamina D (HAHAM et al., 2012), ômega-3 (ZIMET; ROSENBERG; LIVNEY, 2011) e β-caroteno (GONZÁLEZ-FERRERO et al., 2013). Não apenas na forma de agregados as caseínas apresentam potencial carreador para moléculas bioativas. Por possuírem ambas regiões hidrofílicas e hidrofóbicas em suas estruturas, as moléculas individuais das caseínas também podem se ligar a diferentes compostos e atuar como veículos para essas moléculas (MA et al., 2021).

A β-caseína representa cerca de 36% das caseínas do leite bovino e é a mais hidrofóbica dentre elas. A conformação da molécula dessa caseína é flexível e aberta, com pouca estrutura terciária (PORTNAYA et al., 2006). Além disso, suas regiões hidrofílicas e hidrofóbicas são muito bem definidas: em valores de pH próximos à neutralidade, a região C-terminal da β-caseína é altamente hidrofóbica, praticamente não apresentando cargas elétricas líquidas, enquanto seu N-terminal é altamente polar e negativamente carregado (O'CONNELL; GRINBERG; DE KRUIF, 2003). Essas características conferem a essa proteína a propriedade de se auto organizar na forma de micelas formadas, principalmente, por interações hidrofóbicas entre 15 a 60 moléculas de β-caseína, quando em concentrações acima de sua concentração micelar crítica (0,5 a 2,0 mg/mL, em pH próximo a 7,0 e a 25 ºC) (PORTNAYA et al., 2006). Micelas de β-caseína mostram uma alta eficiência de encapsulação e efeito protetor contra a degradação de várias moléculas (LI et al., 2019). Moléculas individuais de β-caseína também formam complexos com moléculas de baixo peso molecular, como curcumina (BAHRI et al., 2019), resveratrol (CHENG et al., 2020) e ácido fólico (ZHANG et al., 2014), via interações

hidrofóbicas, forças de van der Waals e ligações de hidrogênio (SHAPIRA; ASSARAF; LIVNEY, 2010).

Além das proteínas do leite, as ciclodextrinas também são potenciais carreadores para diversas moléculas, incluindo compostos bioativos, devido à sua capacidade de encapsulação via formação de um complexo de inclusão "hóspede-hospedeiro" (PINHO et al., 2014). Os complexos de inclusão modulam características da molécula bioativa hóspede, aumentando sua solubilidade, estabilidade e biodisponibilidade, protegendo-a das condições do meio (pH, temperatura e luz). Dessa forma, o tempo de meia-vida da molécula pode ser aumentado, e a concentração necessária para alcançar o efeito bioativo da mesma pode ser reduzida (FANG; BHANDARI, 2010; ROY et al., 2018). Entre as ciclodextrinas naturais, a β-ciclodextrina é a mais utilizada como veículo para compostos bioativos devido à sua cavidade de tamanho mais adequado à ligação dessas moléculas, à sua maior disponibilidade e a seu menor custo (DAS; SUBUDDHI, 2015).

Apesar de já serem bem estabelecidas as capacidades carreadoras das caseínas e das ciclodextrinas, é fundamental que se caracterize as interações que promovem e sustentam a formação dos complexos bioativo-proteína ou bioativo-ciclodextrina, assim como se conheça a cinética de formação e dissociação desses complexos para sua melhor aplicação como sistemas bioativos, bioacessíveis e biodisponíveis. A ressonância plasmônica de superfície se apresenta como uma técnica poderosa para a caracterização da termodinâmica e da cinética de formação desses complexos em tempo real (SCHNEIDER et al., 2015).

Neste trabalho, utilizou-se a ressonância plasmônica de superfície para caracterizar energeticamente e/ou cineticamente a formação de complexo entre três importantes estruturas carreadoras e três importantes moléculas bioativas nos seguintes sistemas: micelas de caseína e curcumina; β-caseína e quercetina; β-ciclodextrina e resveratrol. Além disso, avaliou-se a capacidade carreadora e o efeito protetor das micelas de caseína sobre a degradação térmica da curcumina, o efeito de sais da série de Hofmeister sobre a interação β-caseína-quercetina e o efeito da estrutura química da molécula hóspede sobre a formação de complexos de inclusão, por meio da comparação de resultados da interação entre β-ciclodextrina e resveratrol e β-ciclodextrina e um análogo estrutural do resveratrol.

ARTICLE 1

Curcumin-Micellar Casein Multisite Interactions elucidated by Surface Plasmon Resonance

Article published in the *International Journal of Biological Macromolecules*. doi: 10.1016/j.ijbiomac.2019.04.166.

Abstract

Determine the thermodynamic and kinetic parameters of interaction between micellar casein (MC) and curcumin (CUR) is useful for the application of MC-CUR systems in food products. We used surface plasmon resonance (SPR) and ultraviolet-visible spectrophotometry (UV-vis) to study the MC-CUR complex formation, MC carrying capacity, and thermal protection for CUR at a pH of 6.6. An MC could carry about 18,000 molecules of CUR. SPR suggested an enthalpy-driven process ($\Delta H° = –64.63$ kJ·mol$^{–1}$ and $T\Delta S°$ ranging from –42.45 to –44.46 kJ·mol$^{–1}$). Temperature increased reduced the rate of MC-CUR complex formation and increased its dissociation rate. The activation energy for the formation of MC-CUR activated complexes was negative for association of free MC and CUR molecules (–62.8 kJ mol$^{–1}$) and positive for dissociation of the thermodynamically stable complexes (1.80 kJ mol$^{–1}$). MC protected the CUR against its thermal degradation. This study shows the importance of characterizing MC-small molecules interactions for better application of MC as a nanocarrier.

Highlights

- 180 nm - Micellar casein (MC) can carry about 18,000 molecules of curcumin (CUR).
- SPR measurements showed that the MC-CUR complex formation was exothermic.
- Temperature increasing reduced MC-CUR association but increased its dissociation rate.
- MC exhibited thermal protection for CUR.

1. Introduction

Milk proteins are natural, easily available, and nutritious molecules, which can carry several bioactive hydrophobic compounds due to their structural and functional characteristics.

Bovine micellar casein (MC) has often been used as a nanocarrier for various bioactive molecules (KIMPEL; SCHMITT, 2015a; LIVNEY, 2010; ZHUANG et al., 2018).

The properties of hydrophobic bioactive molecules (e.g., curcumin (CUR)), such as stability, solubility, and bioavailability, can be improved using MC as a nanocarrier system. CUR is a natural dye that has limitations in its application in food and pharmaceutical systems because of its high hydrophobicity, chemical instability, including its thermal degradation behavior (RAGHAV; SEBASTIAN; RATHINASAMY, 2018). For a better application of protein nanocarrier systems, it is necessary to understand the interaction mechanism and determine the thermodynamic and kinetic parameters involved in the formation of complexes between these biopolymers and the carried compounds.

Surface plasmon resonance (SPR) is a powerful tool that offers valuable information about molecular interactions, such as the kinetic and thermodynamic parameters in real time (LIU et al., 2017). In addition, this technique allows label-free qualitative and quantitative detection, uses a small amount of reagents, and reuses the sensor chips (FATHI et al., 2018).

The MC-CUR complex formation and its application as a vehicle for CUR to cancer cells *in vitro* using HeLa cells at a pH of 7.4 was studied (SAHU; KASOJU; BORA, 2008). The binding constant of the MC-CUR complex was 10^4 L·mol^{-1}, and these complexes exhibited cytotoxic effects similar to those of an equal dose of free CUR. The influence of using heated milk on the interactions between MC and CUR was evaluated and was observed a higher CUR-binding capacity upon heating (YAZDI; CORREDIG, 2012); this result can be attributed to the denaturation of whey proteins bound to the MC surface. Unfortunately, the thermodynamic and kinetic parameters of binding in MC-CUR complexes were not determined in these studies.

Khanji et al. and Nadi et al. determined, using fluorescence spectroscopy, the thermodynamic parameters of interaction between CUR and MC in the pH range of 5.0 to 7.4 and at a pH of 7.0, respectively (KHANJI et al., 2015; NADI et al., 2015). In both studies, the MC-CUR complex-formation process was entropically driven. However, fluorescence measurements only access the interactions occurring at sites close to the fluorophores in the proteins. To the best of our knowledge, the thermodynamics of CUR interacting at any site of the casein molecules in an MC were not analyzed thus far. In addition, the kinetics of MC-CUR complex formation has not yet been reported. As SPR accesses the interaction between CUR and any site in the MC, we attempted to determine the kinetic and thermodynamic parameters of MC-CUR complex formation. In addition, we determined the amount of CUR that can be carried by an MC and analyzed its protective effect against the thermal degradation of CUR.

2. Material and methods

2.1. Materials

Curcumin (≥80 wt.%), chloroform, and dimethyl sulfoxide (DMSO) (analytical grade) were obtained from Sigma Aldrich (USA). Sodium phosphate and sodium azide (analytical grade) were acquired from Vetec (Brazil), while sensor chips CM5, 3-(N,N-dimethylamino)propyl-N-ethylcarbodiimide (EDC) (>99 wt.%), N-hydroxysuccinimide (NHS) (>99 wt.%), ethanolamine-HCl (1 M, pH 8.5), and sodium acetate (>99 wt.%) were purchased from General Electric Healthcare Company (Sweden). Micellar casein was obtained by the centrifugation of skimmed milk according to the procedure described by Sahu et al. (SAHU; KASOJU; BORA, 2008).

2.2. Partitioning experiments

Partitioning experiments were performed in triplicate according to a protocol described by Cárdenas, Jiménez, & Martínez with a few changes (CÁRDENAS; JIMÉNEZ; MARTÍNEZ, 2015). CUR was solubilized in chloroform at 5×10^{-4} mol·L^{-1} and stored in glass bottles in the dark. MC dispersions (0 to 3×10^{-10} mol·L^{-1} at a pH of 6.6) were added to the bottles containing the CUR solutions. These bottles were then stored in water baths maintained at different temperatures (25, 30, and 35 °C) for 24 h to reach thermodynamic equilibrium. Later, aliquots from the aqueous phases were collected and CUR concentrations were measured by measuring the absorbance at 425 nm using a Lambda 35 ultraviolet-visible (UV-vis) spectrophotometer (Perkin Elmer Inc., Waltham, USA).

2.3. Surface plasmon resonance experiments

Thermodynamic and kinetic analyses by SPR were carried out on a two channel Biacore X100 instrument (General Electric Healthcare Company, USA). To determine the thermodynamic and kinetic parameters, MC was immobilized on a CM5 sensor chip by covalent amine coupling according to the manufacturer's recommended protocol. The carboxylic groups in the sensor chip were initially activated for 7 min with a 1:1 EDC/NHS solution at a flow rate of 20 μL·min^{-1} at 25 °C. Subsequently, a solution of MC (2 mg·mL^{-1}) prepared in sodium acetate buffer at a pH of 4.0 (10 mmol·L^{-1}) was injected for 7 min through the sample channel of the chip, leading to a low density of MC immobilization (around 670

resonance units (RU)). In the reference channel, only the buffer was injected. Posteriorly, the injection of ethanolamine-HCl blocked non-specific interactions (HUDSON et al., 2018b).

For MC-CUR interaction experiments, CUR solutions (10 to 120 μM) were prepared in sodium phosphate buffer at a pH 6.6 with 1% of DMSO. For each experiment, CUR solutions of a known concentration were injected and flowed over the both chip channels. MC-CUR complex formation was evaluated at six temperatures (12 to 28 °C). The experiments were performed in triplicate and a new sensor chip was used in each of these experiments.

2.4. Thermal-degradation kinetics of CUR

Solutions of CUR (1×10^{-5} mol·L^{-1}) at a pH of 6.6 were stored in glass flasks in the absence and presence of MC suspensions of increasing concentration; oxygen was removed from these glass flasks by nitrogen ablation and they were then conditioned in water baths of different temperatures (30, 40, 50, and 60 °C). Aliquots were withdrawn at different time intervals (0 to 5.5 h) and their absorbance was determined at 425 nm using quartz cells in a Lambda 35 UV-vis spectrophotometer (Perkin Elmer Inc., Waltham) (DA SILVA, 2017). The degradation experiments were performed in triplicate.

3. Results and discussion

3.1. Partitioning experiments

Considering that MC is a rather porous structure, CUR molecules may have access to different binding sites of this protein aggregate (HOLT et al., 2013). One way to study these interaction sites is to determine the ability of MC to extract CUR molecules solubilized in an organic phase (chloroform) to an aqueous phase (sodium phosphate buffer). We performed CUR partition experiments at 25, 30, and 35 °C. Figure 1 shows the amount of CUR extracted from the organic phase to the aqueous phase per mole of MC present in the buffer at 25 °C. The plots at 30 and 35 °C are included in the Supplementary Material (Figure S1).

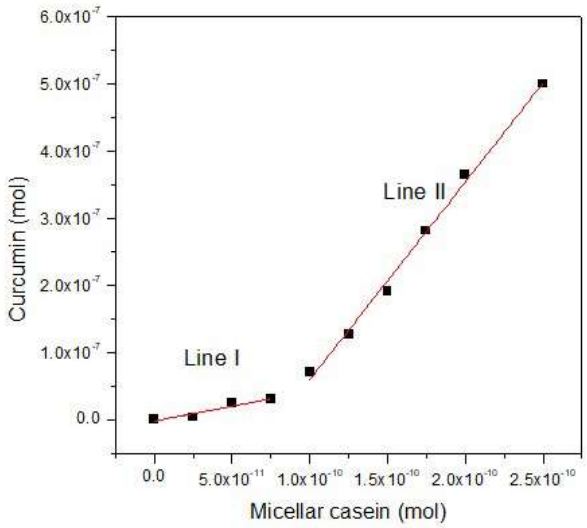

Figure 1. Number of moles of curcumin extracted from the organic phase to the buffer *versus* the number of moles of micellar casein present in the aqueous phase at 25°C.

At all temperatures, in the absence of MC in the aqueous phase, there was no extraction of CUR from the organic phase to the buffer. However, for all thermodynamic conditions, the number of moles of extracted CUR in the aqueous phase increased with an increase in the amount of MC. The plots of [CUR] vs. [MC] showed two straight lines and their slopes indicate the amount of CUR extracted per aggregate of casein. At 25 °C, the slope of the first line (I) indicated that about 2,273 molecules of CUR are bound to MC, suggesting that at lower [CUR]/[MC] ratios, CUR binds preferentially to sites with a higher interaction energy. The higher slope of the second line (II) suggests that about 15,838 are carried by a MC aggregate and here, CUR probably binds to sites with less interaction energy than those indicated by line I. To relate the amount of casein molecules present in an MC with the amount of CUR molecules it carries, we make an estimation considering the general composition of an MC.

It is well established that MC is composed of approximately 39% αs1-casein, 11% αs2-casein, 36% β-casein, and 14% κ-casein (FOX; BRODKORB, 2008). Considering that the average molecular weight of MC is 10^9 g·mol^{-1} (FOX; BRODKORB, 2008; SCHMIDT et al., 1974; SHUKLA; NARAYANAN; ZANCHI, 2009), there are about 1.7×10^4, 4.8×10^3, 1.6×10^4, and 6.0×10^3 molecules of αs1-, αs2-, β-, and κ-casein, respectively. Therefore, there are about 4.43×10^4 casein molecules in a nanoaggregate (MC), while only 2.3×10^3 molecules of CUR (5.19%) interacted with the highest-energy interaction sites and 1.58×10^4 molecules of CUR (35.66%) interacted with the lowest-energy sites. Therefore, considering an interaction model of 1:1, only 40.85% of caseins interacted with CUR.

To determine the kinetic and the thermodynamic parameters of complex formation between CUR and MC, we performed SPR experiments.

3.2. SPR measurements

By analyzing the dependence of the SPR signal (resonance units - RU) on time, it is possible to obtain valuable kinetic and thermodynamic information on the molecular interactions between MC and CUR (SHARIFI et al., 2017). In a typical SPR experiment, one partner (ligand) is anchored to a surface of a sensor chip, while the other (analyte) is free in solution and may bind to the ligand (SANDOVAL-ALTAMIRANO et al., 2017).

After the immobilization of MC on a sensor chip, solutions of CUR (10–120 μM) were injected into the sample and reference cells, generating a signal (RU), which changed with time. The RU versus time curve is called a sensorgram and it is depicted in Figure 2.

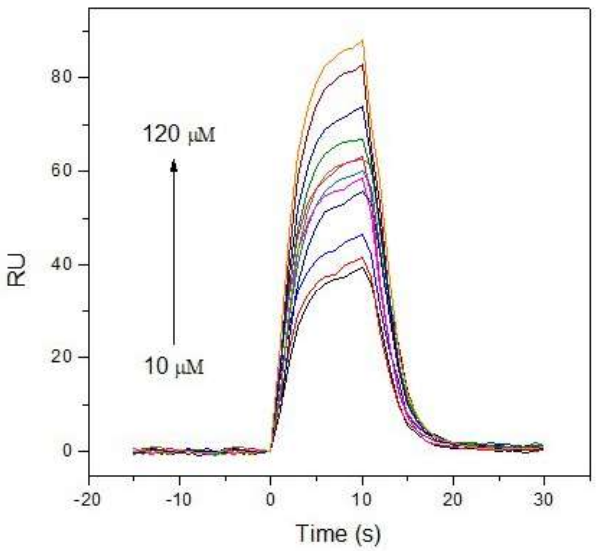

Figure 2. Resonance units *versus* time curves of immobilized micellar casein when it interacts with curcumin of various concentrations (10–120 μM) at pH 6.6 and 25 °C.

Initially, for 15 s, the RU signal was zero because only the buffer solution flowed in the reference and sample SPR cells, producing the same change in the refractive index. At 0 s, the CUR solution started to flow in both SPR cells, resulting in an abrupt increase in the RU value, which increased for 10 s after the CUR solution started to flow. Simultaneous association of free MC and CUR particles and dissociation of MC-CUR complexes caused this enhancement in RU. However, it is important to stress that in this step, the association rate is higher than the dissociation rate. In sequence, the CUR solution flow ended, and a buffer solution began to flow again in both SPR cells, causing only the dissociation of MC-CUR and decreasing the RU value to zero.

3.2.1 Kinetics of MC-CUR complex formation by SPR

Determining the kinetic parameters (association rate constant, k_a, and dissociation rate constant, k_d) of the MC-CUR interaction and their dependence on temperature allows us to determine how fast this process occurs and obtain the energetic parameters involved in the formation of an activated complex. This activated complex is formed by the association of free ligands or due to the dissociation of the thermodynamically stable MC-CUR complex. These energy parameters provide information on the conformational changes occurring at the binding sites of different proteins present in MC. These biopolymer-induced site conformational changes are caused by protein-CUR interactions, which can break the intramolecular interactions (amino-acid residue-amino-acid residue) present at each interacting site.

As previously discussed, MC is an aggregate formed by thousands of proteins; thus, when we talk about the fitting of MC-CUR interaction kinetic data to a simple bimolecular interaction model, we should assume that each CUR-MC site of interaction has its own kinetic constants. Thus, k_x (x = "*a*" (association) or "*d*" (dissociation)) is a weighted average of k_x of each site of interaction ($k_{x,i}$) (Equation 1).

$$k_x = \frac{\sum n_i k_{x,i}}{n_t} \quad (1)$$

Here, n_i is the number of MC sites with association ($k_{a,i}$) and dissociation ($k_{d,i}$) rate constants and n_t is the total number of sites present in a MC.

Based on the above discussion, our bimolecular model is better expressed as $MC_{site} + CUR \underset{kd}{\overset{ka}{\rightleftarrows}} MC_{site} - CUR$, where k_a is the number of CUR molecules that form complexes with each site in MC and k_d is the fraction of these complexes that dissociate per second. From Equations 2 and 3, global numerical fitting of *RU* versus *t* was performed and the k_d and k_{obs} values were obtained. Later, k_a values were determined from the following relationship, $k_{obs} = k_a[curcumin] + k_d$. Supplementary Table 1 (Table S1) shows the k_a and k_d values at different temperatures.

$$RU(t) = RU(t_m)\, e^{-k_d(t-t_m)} \quad (2)$$

$$RU(t) = RU_{max}[1 - e^{-k_{obs}(t)}] \quad (3)$$

Here, RU (t_m) denotes the resonance units at the start of the descendent part of the sensorgram, where only dissociation occurs, and RU_{max} denotes the resonance units obtained at infinity.

The value of k_a decreased (4.66×10^3 to 1.32×10^3 M^{-1} s^{-1}) and that of k_d increased (0.403 to 0.419 s^{-1}) as temperature increased, demonstrating that an increase in temperature reduced the MC-CUR complex-formation rate and increased its dissociation rate. This result shows that at low temperatures, CUR incorporation in MC becomes more efficient, while its release would be more effective at higher temperatures. The high efficiency of CUR incorporation at low temperatures could be explained as follows. At low temperatures, the interaction between caseins inside MC is weaker than at high temperatures (WALSTRA; WOUTERS; GEURTS, 2006). Thus, this might increase the rate of MC-CUR formation. On the other hand, high temperatures favor interactions between caseins inside the MC, consequently increasing the MC-CUR dissociation rate.

Based on the Arrhenius approach, the energetic parameters involved in activated-complex formation can be determined from the temperature dependence of k_a and k_d values (DE PAULA et al., 2017). The activation energy (E_{act}) for activated-complex formation from the association of free MC and CUR molecules ($E_{act(a)}$) or from the dissociation of thermodynamic stable MC-CUR complexes ($E_{act\ (d)}$) were obtained by the application of Equation 4 to data shown in the plot of *ln* k_x *versus 1/T (x = a or d)* (Arrhenius plot) (Figure 3). Other energetic parameters associated with MC-CUR activated complexes (Gibbs free energy change of activation ($\Delta G_x^{\ddagger}$), enthalpy change of activation ($\Delta H_x^{\ddagger}$), and entropy change of activation ($T\Delta S_x^{\ddagger}$)) were obtained from Equations 5, 6, and 7, respectively. The values of the energetic parameters are shown in Table 1.

$$E_{act(x)}\,(T) = -R\left(\frac{d\ln K_x}{d\ 1/T}\right) \tag{4}$$

$$\Delta G_x^{\ddagger}(T) = -RTln(k_x h/k_B(T)) \tag{5}$$

$$\Delta H_x^{\ddagger}(T) = E_{act(x)}(T) - RT \tag{6}$$

$$T\Delta S_x^{\ddagger}(T) = \Delta H_x^{\ddagger}(T) - \Delta G_x^{\ddagger}(T) \tag{7}$$

In these equations, the subscript "x" indicates "a" for association and "d" for dissociation, respectively, and R is the universal gas constant (8.3145 J·mol^{-1}·K^{-1}), h is the Planck's constant and k_B is the Boltzmann's constant.

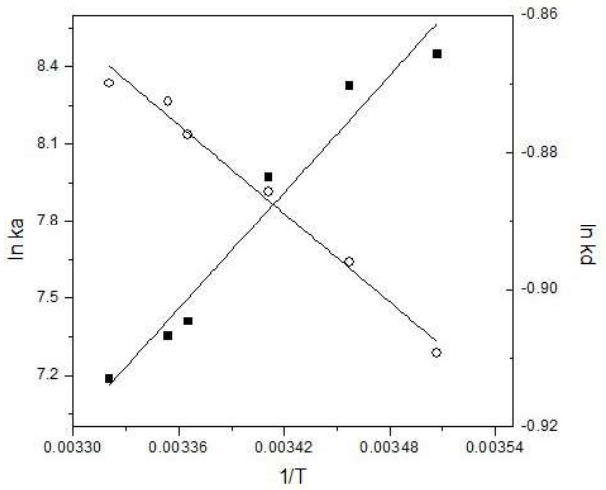

Figure 3. ln k_a and ln k_d *versus* 1/T for MC-CUR activated-complex formation in the temperature range of 12 to 28 °C. Association (■) and dissociation (○).

Table 1. Energetic parameters associated with MC-CUR activated-complex formation at 25 °C

Association phase (*a*)	Dissociation phase (*d*)
$E_{act(a)} = -62.8$ kJ mol^{-1}	$E_{act(d)} = 1.80$ kJ mol^{-1}
$\Delta H^{\ddagger} = -65.3$ kJ mol^{-1}	$\Delta H^{\ddagger} = -0.68$ kJ mol^{-1}
$T\Delta S^{\ddagger} = -120.1$ kJ mol^{-1}	$T\Delta S^{\ddagger} = -75.8$ kJ mol^{-1}
$\Delta G^{\ddagger} = 54.8$ kJ mol^{-1}	$\Delta G^{\ddagger} = 75.2$ kJ mol^{-1}

The E_{act} value was negative for association and positive for dissociation, indicating that the formation of the activated complex due to interactions between free CUR molecules and protein sites present in the MC was accompanied by energy release, while the dissociation of the thermodynamically stable MC-CUR complex to form the activated complex needs to absorb energy. E_{act} is a result of the contributions of molecular processes that occur in each of these phases.

In the association phase, E_{act} might be attributed to the following sub-processes – i) desolvation of ligands, ii) conformational changes in the biopolymer interaction sites, and iii) direct interaction between CUR and protein sites. The first two processes occur with energy absorption, while the CUR-protein site interaction releases energy. During the formation of MC

nanoaggregates, the secondary structure of caseins is lost because of protein-protein interactions and energy is not required to change the conformation of proteins sites caused by MC-CUR interactions. Furthermore, as the $E_{act(a)}$ value was negative, the energy cost for the desolvation of free ligands was lower than the energy released during CUR-protein site interaction. On the other hand, in the dissociation phase, the energy cost for breaking the interactions in the thermodynamically stable complex predominantly contributes to the positive $E_{act(d)}$. It is important to emphasize that this is a low-energy cost.

The entropy change related to the process of activated-complex formation from the free ligands was negative. This entropy decrease should be attributed to the reduction in the degree of translational freedom of both CUR and casein molecules due to their interaction, which overcomes the entropy gain resulted from the release of the water molecules from the solvation layer of these molecules. Activated-complex formation by the association of free ligands or the dissociation of the thermodynamically stable MC-CUR complexes was enthalpically driven and it occurred with a decrease in entropy. Thus, the formation of a thermodynamically stable MC-CUR complex from the activated complex was entropically driven and enthalpically unfavorable.

3.2.2 Thermodynamics of the MC-CUR complex-formation process by SPR

The determination of thermodynamic parameters, such as the binding constant (K_b), standard Gibbs free energy change (ΔG°), standard enthalpy change (ΔH°), and standard entropy change (ΔS°) can contribute to the understanding of the main interaction forces involved in complex-formation processes (SILVA et al., 2018).

To determine the K_b values related to MC-CUR complexes, we used the relationship $K_b = k_a/k_d$ for each of the studied temperatures. The ΔH° value was obtained from the van't Hoff equation (Equation 8) and the ΔG° and TΔS° values were determined from Equation 9 and 10, respectively. All the thermodynamic parameters of the MC-CUR complex-formation process are presented in Table 2.

$$ln\frac{Kb_2}{Kb_1} = -\frac{\Delta H^\circ}{R}\left(\frac{1}{T_2} - \frac{1}{T_1}\right) \quad (8)$$

$$\Delta G^\circ = -RTlnK_b \quad (9)$$

$$\Delta G^\circ = \Delta H^\circ - T\Delta S^\circ \quad (10)$$

Here, R is the universal gas constant (8.3145 $J \cdot mol^{-1} \cdot K^{-1}$) and T is the temperature (K).

Table 2. Binding constant (K_b), standard Gibbs free energy ($\Delta G°$), enthalpy ($\Delta H°$), and entropy ($T\Delta S°$) changes corresponding to the MC-CUR complex-formation process at different temperatures, as determined by SPR

T *	K_b ** ($\times 10^3$)	$\Delta H°$ ***	$\Delta G°$***	$T\Delta S°$***
12	11.6 ± 0.58	–64.6 ± 3.27	–22.18 ± 1.11	–42.45 ± 2.12
16	10.1 ± 0.60		–22.18 ± 1.10	–42.46 ± 2.12
20	7.0 ± 0.35		–21.59 ± 1.07	–43.04 ± 2.15
24	3.9 ± 0.27		–20.47 ± 1.23	–44.16 ± 2.64
25	3.7 ± 0.18		–20.38 ± 1.02	–44.25 ± 2.64
28	3.1 ± 0.15		–20.17 ± 1.00	–44.46 ± 2.66

*°C, **$L \cdot mol^{-1}$, ***$kJ \cdot mol^{-1}$

The K_b values were of the order of 10^3 $L.mol^{-1}$, and these values decrease with an increase in temperature, which demonstrates a reduction in complex formation with an increase in temperature. Nadi et al. studied the interactions between whole casein and CUR at pH 7.0 and obtained K_b values of the order of 10^6 $L \cdot mol^{-1}$ (NADI et al., 2015). Khanji et al. also studied the interactions between MC and CUR and obtained $K_b = 7.8 \times 10^4$ $L \cdot mol^{-1}$ at pH 6.5 and 25 °C (KHANJI et al., 2015). The discrepancy in K_b values found by different authors can be explained considering that the studies cited above used fluorescence spectroscopy to follow the casein-CUR binding, while our study used SPR, a broader technique able to detect interaction in all binding sites. Hence, the K_b values measured are averages of all the interacting sites for CUR in MC.

There are four main forces of molecular interaction – hydrophobic interactions, hydrogen bonds, van der Waals forces, and electrostatic interactions (JIA et al., 2017; ROSS; SUBRAMANIAN, 1981). To elucidate the nature of interaction between CUR and MC, the thermodynamic parameters of complex formation were determined.

The $\Delta G°$ values were negative, indicating that the MC-CUR complex formation was favored in relation to free ligands (MC and CUR). The negative $\Delta H°$ and $T\Delta S°$ values demonstrate that the process of complex formation was enthalpically driven (Table 2).

The $\Delta H°$ value comes from the sum of enthalpy change associated to different processes, such as: enthalpy change of desolvation of MC and CUR molecules (ΔH_{des}), enthalpy change of MC-CUR interaction ($\Delta H_{MC\text{-}CUR}$), and enthalpy change of water-water interaction ($\Delta H_{w\text{-}w}$).

Considering that ΔH° is negative (–64.63 kJ·mol^{-1}), we can consider that $|\Delta H_{MC-CUR} + \Delta H_{W-W}| >> |\Delta H_{des}|$, probably due to the amount of complexes formed inside the protein aggregate, and consequently, the interaction between water molecules formed outside the MC. There are only two reports in the available literature on the measurement of the thermodynamic parameters of MC-CUR interactions; a comparison between the values reported in these two studies and our values shows a dissonance. Khanji et al. (2015), using native-like casein micelles obtained by microfiltration and diafiltration of a milk ultrafiltrate followed by spray-drying stabilization, determined ΔH° to be 114.5 kJ·mol^{-1} at pH 6.5, while Nadi et al. (2015), using whole casein obtained from Sigma Chemical Co., found ΔH° to be 35 kJ·mol^{-1} at pH 7.0. These discrepancies illustrate the effect of the use of another technique to study the biding between proteins or protein aggregates and bioactive molecules. While the cited authors used fluorescence to determine the thermodynamic parameters, we used the SPR. Therefore, the thermodynamic parameters obtained in our work are related to all binding sites presented in MC, and they are not restricted to the tryptophan (Trp) residues. Our results demonstrate that there are more interaction sites in caseins apart from those close to the Trp residues; these sites release more energy when CUR-protein site interactions occur.

There was an entropic reduction in the system upon MC-CUR complex formation (Table 2), which is different from the positive TΔS° values obtained in the fluorescence studies of casein-CUR interaction (Khanji et al., 2015, Nadi et al., 2015). Similarly to it was discussed for the ΔH° values, this difference in our results can be attributed to the SPR is able to detect interactions at sites far from the Trp residues, and probably these interactions occur with less desolvation of CUR and proteins. Further, the decrease in the degree of translational freedom of these molecules due to interaction contributes more than the effect of water-molecule release from the solvation layer of caseins and CUR, resulting in a negative entropy change. However, we can not despise the contribution of the immobilization of MC on the chip surface to the entropy reduction because it can reduce the number of spatial positions that this nanoaggregate could occupy when the interactions occurred.

3.3. Protective effect of MC against CUR thermal degradation

Thermal processing is often applied to increase the shelf life of foods. However, heat treatment may decrease the levels of bioactive compounds present in the food matrix (DOMENEGHINI et al., 2013). It is known that CUR is thermally sensitive and can degrade, losing its health-related properties, but milk proteins are known for their ability to stabilize

bioactive compounds against various environmental conditions (PARAMERA; KONTELES; KARATHANOS, 2011; SAIZ-ABAJO et al., 2013). Kinetic analysis is frequently carried out to predict the degradation rates, half-life times, and thermal stability of several chemical compounds (CHEN et al., 2014; SARKIS et al., 2013). To verify the efficiency of MC to protect CUR from thermal degradation, we performed a kinetic analysis of CUR heat degradation in the presence of different concentrations of MC at four temperatures.

We determined the kinetic thermal degradation constant (K_{TD}) and half-life time ($t_{1/2}$) of CUR in the presence of different MC concentrations using Equations 11 and 12, respectively. The K_{TD} values were obtained from the slope of the plot of $-\ln A/A_0$ versus the heat-exposure time.

$$-ln\, A/A_0 = K_{TD}\, t \tag{11}$$

$$t_{1/2} = ln2/K_{TD} \tag{12}$$

Here, A is the absorbance at the end time, A_0 is the absorbance at time 0, and t is the storage time.

Figure S2 shows the K_{TD} and $t_{1/2}$ values of CUR as functions of MC concentration at 30, 40, 50 and 60 °C and a pH of 6.6.

An increase in the MC concentration led to a reduction in the K_{TD} value and an increase in half-life time of CUR. This reduction in K_{TD} occurs at all temperatures, at a ratio of approximately 3 times at 30 and 40 °C, and 1.5 times at 50 and 60 °C (reduction in relation to the K_{TD} of free curcumin). The half-life was increased by about 2.5 times at 30 and 40 °C and 1.45 times at 50 and 60 °C

As described earlier, in a mixture of MC and CUR, there is a chemical equilibrium, MC + CUR ⇋ MC-CUR, and as the MC concentration increases, the system favors complex formation between MC and CUR. The decrease in the free energy of the system (observed when CUR interacts with MC) confers greater stability to CUR molecules bonded to MC sites. Therefore, more energy is required to degrade CUR molecules, resulting in a decrease in the K_{TD} and an increase in the $t_{1/2}$ values. It should be stressed that these determined kinetic parameters are weighted averages resulting from parameters related to free CUR (CUR_{free}) and CUR bound to MC ($CUR_{complex}$), i.e., $K_{TD} = f\, K'_{TD} + (1-f)K''_{TD}$ and $t_{1/2} = f\, t'_{1/2} + (1-f)\, t''_{1/2}$, where f is the fraction of CUR bound to MC, K'_{TD} and $t'_{1/2}$ are the thermal

degradation constant and half-life time of bound CUR, respectively, and K''_{TD} and $t''_{1/2}$ are parameters corresponding to free CUR.

Haham et al. studied the effect of nanoencapsulation of vitamin D in MC on its stability and bioavailability and reported that there was no significant loss of vitamin D when the nanoencapsulated system was heated at 353 K for 1 min, unlike the 13% and 14% loss observed when the vitamin was emulsified with Tween-80 and when it was unencapsulated, respectively (HAHAM et al., 2012). Saiz-Abajo et al. found that MC protected β-carotene for up to 8 h at 80 °C and during industrial heat treatment, such as pasteurization and sterilization (SAIZ-ABAJO et al., 2013). These results show the thermal protective effect of MC for a bioactive molecule, which corroborates with the results of our study.

We also determined the activation enthalpic energy of degradation ($\Delta H^{\ddagger}_{d}$) of CUR in the presence of five different concentrations of MC using the slopes of ln K_{TD} versus 1/T plots (Arrhenius plot). The Arrhenius plot of CUR in the presence of 1×10^{-10} mol·L^{-1} of MC at four temperatures (30, 40, 50 and 60 °C) and pH 6.6 is presented in Figure 4. The plots for other MC concentrations are shown in Figure S3.

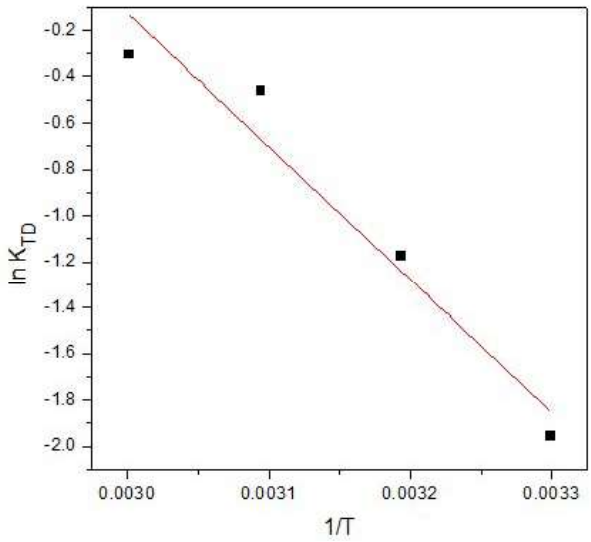

Figure 4. Arrhenius plot of curcumin degradation in the presence of 1×10^{-10} mol·L^{-1} of micellar casein at four different temperatures and pH 6.6.

The $\Delta H^{\ddagger}_{d}$ values were dependent on MC concentration; these values are also weighted averages of $\Delta H^{\ddagger}_{d}$ for free CUR and $\Delta H^{\ddagger}_{d}$ for CUR bound to MC. The dependence of $\Delta H^{\ddagger}_{d}$ as a function of MC concentration at a pH of 6.6 is shown in Figure S4.

As the concentration of MC increased, $\Delta H^{\ddagger}_{d}$ also increased, indicating that a greater amount of energy is needed to thermally degrade CUR when there is more MC in the system. In fact, as MC concentration increases, there is more complex formation between MC and CUR

occur, conferring greater stability to CUR molecules. By exponentially fitting the $\Delta H^{\ddagger}_{d}$ versus [MC] curve and by extrapolating the analytical function to an infinite MC concentration, we determined $\Delta H^{\ddagger}_{d}$ to be 59.76 $kJ \cdot mol^{-1}$; this is the mean energy required for the thermal decomposition of CUR bound to MC.

4. Conclusion

Thermodynamic and kinetic analyses performed in this study provided important insights into the interactions between MC and CUR. For the first time, the partitioning experiments showed that about 18,000 CUR molecules interact with caseins present in MC, demonstrating the potential carrier capability of this protein nanoaggregate. These interactions occurred at different protein sites, which could be divided into two groups, high- and low-energy interactions. The MC-CUR complex formation process was enthalpically driven. Kinetic analysis by SPR also indicated that at low temperatures, CUR incorporation into MC is more efficient and its release would be more effective at higher temperatures. The thermal degradation of CUR was reduced by up to three times after interaction with MC. Therefore, it is possible that MC offer a suitable carrying for CUR and possibly for other bioactive compounds that can be used as functional ingredients in different food systems.

Declarations of interest

There are no conflicts of interest to declare.

Acknowledgments

This work was supported by the Conselho Nacional de Desenvolvimento Científico e Tecnológico (Brazil), Coordenação de Aperfeiçoamento de Pessoal de Nível Superior (Brazil), and Fundação de Apoio à Pesquisa de Minas Gerais (Brazil).

References

CÁRDENAS, Z. J.; JIMÉNEZ, D. M.; MARTÍNEZ, F. Thermodynamic study of the partitioning of methyl and propyl parabens in some organic solvent/buffer systems. **The Journal of Chemical Thermodynamics**, [s. l.], v. 86, p. 180–187, 2015.

CHEN, Z.; XIA, Y.; LIAO, S.; HUANG, Y.; LI, Y.; HE, Y.; TONG, Z.; LI, B. Thermal degradation kinetics study of curcumin with nonlinear methods. **Food chemistry**, [s. l.], v. 155, p. 81–86, 2014.

DA SILVA, R. M. Caseína Micelar como Nanocarreador para Curcumina. 2017. Universidade Federal de Viçosa, [s. l.], 2017.

DE PAULA, H. M. C.; COELHO, Y. L.; AGUDELO, A. J. P.; REZENDE, J. de P.; FERREIRA, G. M. D.; FERREIRA, G. M. D.; PIRES, A. C. dos S.; DA SILVA, L. H. M. Kinetics and thermodynamics of bovine serum albumin interactions with Congo red dye. **Colloids and Surfaces B: Biointerfaces**, [s. l.], v. 159, p. 737–742, 2017.

DOMENEGHINI, G.; ⇑ M.; JAESCHKE, D. P.; TESSARO, I. C.; DAMASCENO, L.; MARCZAK, F. Degradation kinetics of anthocyanins in acerola pulp: Comparison between ohmic and conventional heat treatment. **Food Chemistry**, [s. l.], v. 136, p. 853–857, 2013.

FATHI, F.; MOHAMMADZADEH-AGHDASH, H.; SOHRABI, Y.; DEHGHAN, P.; EZZATI NAZHAD DOLATABADI, J. Kinetic and thermodynamic studies of bovine serum albumin interaction with ascorbyl palmitate and ascorbyl stearate food additives using surface plasmon resonance. **Food Chemistry**, [s. l.], v. 246, p. 228–232, 2018.

FOX, P. F.; BRODKORB, A. The casein micelle: Historical aspects, current concepts and significance. **International Dairy Journal**, [s. l.], v. 18, n. 7, p. 677–684, 2008.

HAHAM, M.; ISH-SHALOM, S.; NODELMAN, M.; DUEK, I.; SEGAL, E.; KUSTANOVICH, M.; LIVNEY, Y. D. Stability and bioavailability of vitamin D nanoencapsulated in casein micelles. **Food & Function**, [s. l.], v. 3, n. 7, p. 737, 2012.

HOLT, C.; CARVER, J. A.; ECROYD, H.; THORN, D. C. Invited review: Caseins and the casein micelle: Their biological functions, structures, and behavior in foods1. **Journal of Dairy Science**, [s. l.], v. 96, n. 10, p. 6127–6146, 2013.

HUDSON, E. A.; MAXIMILER, H.; DE PAULA, C.; MAX, G.; FERREIRA, D.; MAX, G.; DO, M.; HESPANHOL, C.; MENDES DA SILVA, L. H.; CLARISSA, A.; PIRES, S. Thermodynamic and kinetic analyses of curcumin and bovine serum albumin binding. **Food Chemistry**, [s. l.], v. 242, p. 505–512, 2018.

JIA, J.; GAO, X.; HAO, M.; TANG, L. Comparison of binding interaction between beta-lactoglobulin and three common polyphenols using multi-spectroscopy and modeling methods. **Food Chemistry**, [s. l.], v. 228, p. 143–151, 2017.

KHANJI, A. N.; MICHAUX, F.; JASNIEWSKI, J.; PETIT, J.; LAHIMER, E.; CHERIF, M.; SALAMEH, D.; RIZK, T.; BANON, S. Structure and gelation properties of casein micelles doped with curcumin under acidic conditions. **Food & function**, [s. l.], v. 6, n. 12, p. 3624–33, 2015.

KIMPEL, F.; SCHMITT, J. J. Review: Milk Proteins as Nanocarrier Systems for Hydrophobic Nutraceuticals. **Journal of Food Science**, [s. l.], v. 80, n. 11, p. 2361–2366, 2015.

LIU, X.; LUO, F.; LI, P.; SHE, Y.; GAO, W. Investigation of the interaction for three Citrus flavonoids and α-amylase by surface plasmon resonance. **Food Research International**, [s. l.], v. 97, p. 1–6, 2017.

LIVNEY, Y. D. Milk proteins as vehicles for bioactives. **Current Opinion in Colloid & Interface Science**, [s. l.], v. 15, n. 1, p. 73–83, 2010.

NADI, M. M.; REZA, M.; KOOSHK, A.; MANSOURI, K.; GHADAMI, S. A.; AMANI, M.; GHOBADI, S.; KHODARAHMI, R. Comparative Spectroscopic Studies on Curcumin Stabilization by Association to Bovine Serum Albumin and Casein: A Perspective on Drug-

Delivery Application. **International Journal of Food Properties**, [s. l.], v. 18, p. 638–659, 2015.

PARAMERA, E. I.; KONTELES, S. J.; KARATHANOS, V. T. Stability and release properties of curcumin encapsulated in Saccharomyces cerevisiae, β-cyclodextrin and modified starch. **Food Chemistry**, [s. l.], v. 125, n. 3, p. 913–922, 2011.

RAGHAV, D.; SEBASTIAN, J.; RATHINASAMY, K. Biochemical and Biophysical characterization of curcumin binding to human mitotic kinesin Eg5: Insights into the inhibitory mechanism of curcumin on Eg5. **International Journal of Biological Macromolecules**, [s. l.], v. 109, p. 1189–1208, 2018.

ROSS, P. D.; SUBRAMANIAN, S. Thermodynamics of protein association reactions: forces contributing to stability. **Biochemistry**, [s. l.], v. 20, n. 11, p. 3096–102, 1981.

SAHU, A.; KASOJU, N.; BORA, U. Fluorescence Study of the Curcumin−Casein Micelle Complexation and Its Application as a Drug Nanocarrier to Cancer Cells. **Biomacromolecules,** [s. l.], v. 9, n. 10, p. 2905–2912, 2008.

SAIZ-ABAJO, M. J.; GONZALEZ-FERRERO, C.; MORENO-RUIZ, A.; ROMO-HUALDE, A.; GONZALEZ-NAVARRO, C. J. Thermal protection of β-carotene in re-assembled casein micelles during different processing technologies applied in food industry. **Food Chemistry**, [s. l.], v. 138, n. 2–3, p. 1581–1587, 2013.

SANDOVAL-ALTAMIRANO, C.; SANCHEZ, S. A.; FERREYRA, N. F.; GUNTHER, G. Understanding the interaction of concanavalin a with mannosyl glycoliposomes: A surface plasmon resonance and fluorescence study. **Colloids and Surfaces B: Biointerfaces,** [s. l.], v. 158, p. 539–546, 2017.

SARKIS, J. R.; JAESCHKE, D. P.; TESSARO, I. C.; MARCZAK, L. D. F. Effects of ohmic and conventional heating on anthocyanin degradation during the processing of blueberry pulp. **LWT - Food Science and Technology**, [s. l.], v. 51, p. 79–85, 2013.

SCHMIDT, D. G.; BOTH, P.; VAN MARKWIJK, B. W.; BUCHHEIM, W. The determination of size and molecular weight of casein micelles by means of light-scattering and electron microscopy. **Biochimica et Biophysica Acta (BBA) - Protein Structure**, [s. l.], v. 365, n. 1, p. 72–79, 1974.

SHARIFI, M.; EZZATI, J.; DOLATABADI, N.; FATHI, F.; ZAKARIAZADEH, M.; BARZEGAR, A.; RASHIDI, M.; TAJALLI, H.; RASHIDI, M.-R. Surface plasmon resonance and molecular docking studies of bovine serum albumin interaction with neomycin: kinetic and thermodynamic analysis. **BioImpacts**, [s. l.], v. 7, n. 2, p. 91–97, 2017.

SHUKLA, A.; NARAYANAN, T.; ZANCHI, D. Structure of casein micelles and their complexation with tannins. **Soft Matter**, [s. l.], v. 5, n. 15, p. 2884, 2009.

SILVA, C. E. L.; HUDSON, E. A.; AGUDELO, Á. J. P.; DA SILVA, L. H. M.; PINTO, M. S.; DO CARMO HESPANHOL, M.; BARROS, F. A. R.; DOS SANTOS PIRES, A. C. β-Carotene and Milk Protein Complexation: a Thermodynamic Approach and a Photo Stabilization Study. **Food and Bioprocess Technology**, [s. l.], v. 11, n. 3, 2018.

WALSTRA, P.; WOUTERS, J. T. M.; GEURTS, T. J. **Dairy science and technology**. [s.l.] : CRC/Taylor & Francis, 2006.

YAZDI, S. R.; CORREDIG, M. Heating of milk alters the binding of curcumin to casein micelles. A fluorescence spectroscopy study. **Food Chemistry**, [s. l.], v. 132, p. 1143–1149, 2012.

ZHUANG, Y.; UEDA, I.; KULOZIK, U.; GEBHARDT, R. Influence of β-lactoglobulin and calcium chloride on the molecular structure and interactions of casein micelles. **International Journal of Biological Macromolecules**, [s. l.], v. 107, n. PartA, p. 560–566, 2018.

Supplementary Material

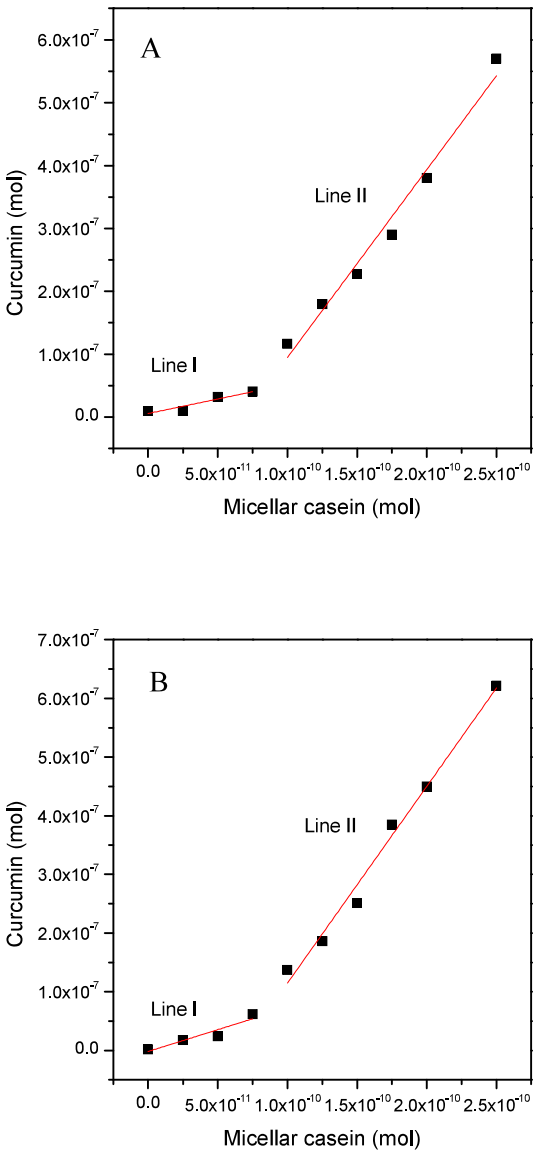

Figure S1. Number of moles of curcumin extracted from the organic phase *versus* the number of moles of micellar casein present in the aqueous phase at 30 °C (A) and 35 °C (B).

Table S1. Association (k_a) and dissociation (k_d) rate constants of MC-CUR complexes at different temperatures

Temperature (°C)	k_a (10^3 M^{-1} s^{-1})	k_d (s^{-1})
12	4.66	0.403
16	4.13	0.408
20	2.90	0.412
24	1.65	0.416
25	1.56	0.418
28	1.32	0.419

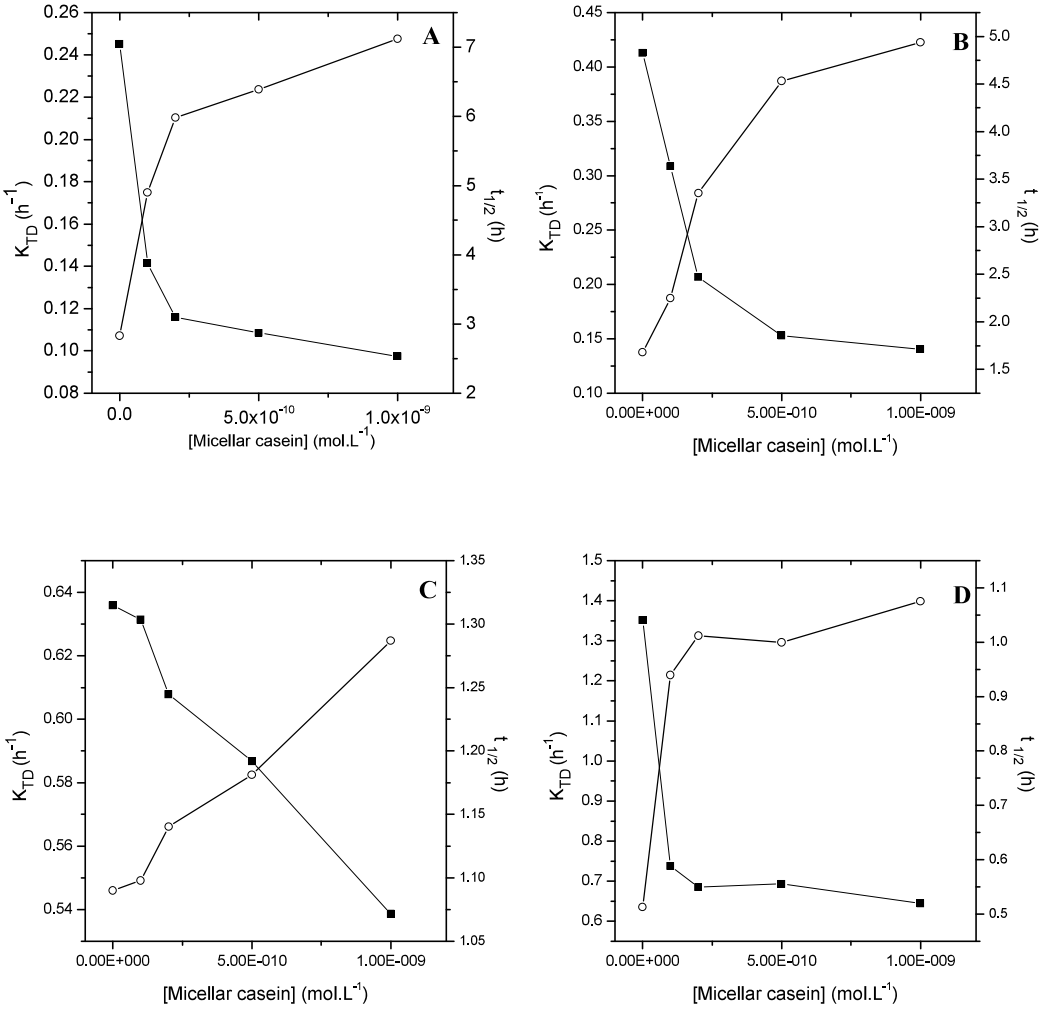

Figure S2. Kinetic thermal degradation constant (K_{TD}) (■) and half-life ($t_{1/2}$) (○) of CUR as a function of MC concentration at 30 (A), 40 (B), 50 (C), and 60 °C (D) and pH 6.6.

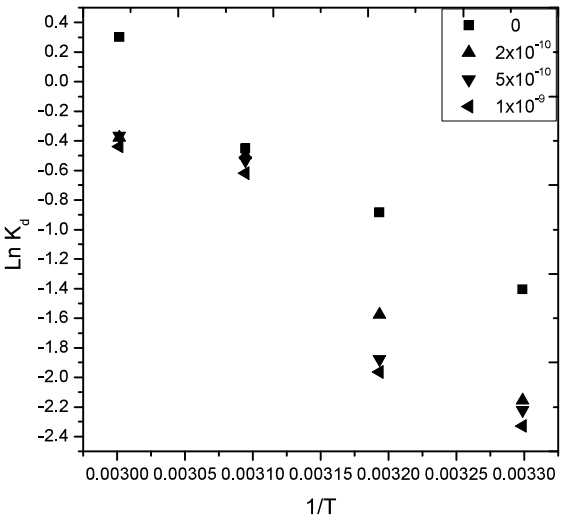

Figure S3. Arrhenius plot for curcumin degradation in the presence of different micellar casein concentrations at four temperatures and pH 6.6.

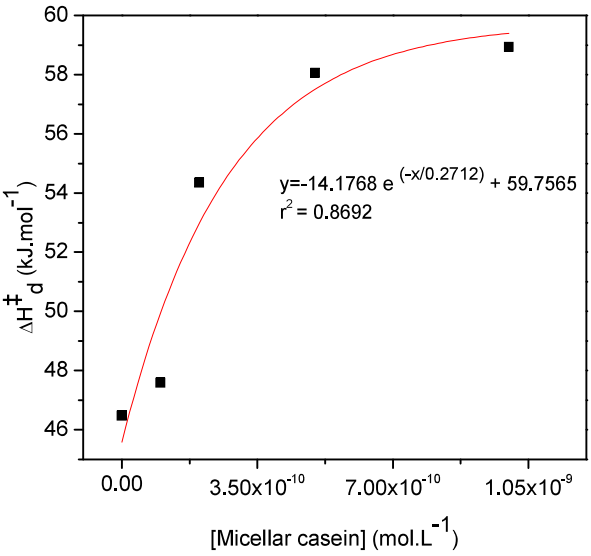

Figure S4. Dependence of activation enthalpic energy of curcumin degradation as a function of micellar casein concentration at pH 6.

ARTICLE 2

Energetic parameters of β-casein/quercetin activated and thermodynamically stable complex formation accessed by Surface Plasmon Resonance

Article published in the journal *Colloids and Surfaces B: Biointerfaces*. doi: 10.1016/j.colsurfb.2019.06.048

Abstract

Characterizing the energetics and molecular dynamics of binding between proteins and bioactive compounds is strategic. Using surface plasmon resonance, we demonstrated that β-casein (β-cas) and quercetin (Qct) form supramolecular complexes driven by an increase in entropy ($\Delta H° = 25.86$ and $T\Delta S° = 53.49$ kJ·mol^{-1} at 25 °C). It was possible to infer that the β-cas/Qct complex was formed via an activated complex synthesized by an entropic reduction ($T\Delta S^{‡}_{(a)} = -15.31$ kJ·mol^{-1} and $T\Delta S^{‡}_{(d)} = -68.80$ kJ·mol^{-1} at 25 °C) and an enthalpic increase ($\Delta H^{‡}_{(a)} = 30.87$ and $\Delta H^{‡}_{(d)} = 5.0$ kJ·mol^{-1} at 25 °C). Independent of the nature of the Hofmeister ions, the salts KCl or KSCN increased complex stability by decreasing both the kinetic and thermodynamic enthalpy values, through shielding of the electrostatic interactions at the electric double layer of the interacting molecules. An increase in temperature favored both the association of the free interacting molecules and the dissociation of the thermodynamically stable β-cas/Qct complexes. These results provide insights into the β-cas/Qct interaction process and contribute to the understanding of how Hofmeister ions can modulate intermolecular interactions between proteins and small molecules.

Keywords

protein-bioactive interaction, β-casein, quercetin, supramolecular complex, Hofmeister ions.

1. Introduction

The flavonol quercetin (Qct) (3,3´,4´,5,7-pentahydroxyflavone) has shown therapeutic potential with a high antioxidant capacity (CHEN et al., 2016), anti-inflammatory and anti-proliferative effects (KLEEMANN et al., 2011), antiviral and antibacterial activities (LU et al., 2016; VAQUERO; ALBERTO; DE NADRA, 2007), anti-cancer properties (WU et al., 2018), and potential as a cardiovascular agent (PATEL et al., 2018). However, the use of Qct as a

therapeutic agent is limited due to the chemical transformations it undergoes in physiological conditions, its poor water solubility, and its short half-life, which leads to low bioavailability (CAI et al., 2013). Furthermore, in food formulations enriched with Qct, the pH and temperature of processing and storage can affect the stability of this bioactive compound (WANG et al., 2016).

For these reasons, several studies have been carried out to improve the bioavailability of Qct and other hydrophobic bioactive agents (WANG et al., 2016). For this purpose, different carrier systems have been developed to incorporate Qct and modify its undesirable characteristics, including its encapsulation within lipid-based vehicles, such as solid lipid nanoparticles (LI et al., 2009), inclusion complexes with cyclodextrins (AZZI et al., 2018), nano-emulsions (CHEN et al., 2018; GAO et al., 2009), liposomes (GANG et al., 2012), nanomicelles (WANG et al., 2019), and polymer nanoparticles (PANDEY et al., 2015). Proteins are also promising carrier systems for Qct due to their availability, food-grade characteristics, and specific physicochemical properties (GHAYOUR et al., 2019).

Indeed, molecular complexes between Qct and milk proteins, such as serum albumins(POÓR et al., 2018), β-lactoglobulin (MIRPOOR; HOSSEINI; NEKOEI, 2017), and lactoferrin (HUANG et al., 2018), have shown that proteins can improve the solubility, stability, and bioavailability of Qct. β-casein (β-cas) is a good candidate for the delivery of several hydrophobic compounds (BAHRI et al., 2019; DEZHAMPANAH; ESMAILI; KHORSHIDI, 2017), including Qct (MEHRANFAR; BORDBAR; PARASTAR, 2013a; WEI et al., 2018). β-cas has well-defined hydrophilic and hydrophobic regions and can form micelle-like structures under defined conditions (HORNE, 2002; MOITZI et al., 2008; PORTNAYA et al., 2008). Using fluorescence spectroscopy and molecular docking, Mehranfar et al. (2013) performed thermodynamic and molecular analyses of the binding process between β-cas micelles and Qct at pH 7.0. This revealed that the interaction was enthalpically driven and that Qct probably binds to a site located in the hydrophobic core of the β-cas molecule (MEHRANFAR; BORDBAR; PARASTAR, 2013b). Wei et al. (2018) also studied the thermodynamics of β-cas/Qct binding using UV-vis spectroscopy and chemometrics, and found that at pH 6.0 the interaction process was entropically driven (WEI et al., 2018). However, the kinetics of complex formation between β-cas and Qct were not addressed in these previous studies. Determining kinetic parameters provides important information about the dynamics of the interaction and the stability of the protein/bioactive complex (FATHI et al., 2016).

Despite the potential of proteins as nanocarriers, it is well known that their structure, function, and dynamics are strongly dependent on the characteristics of their buffering medium (KIMPEL; SCHMITT, 2015b). Therefore, medium composition can affect bioactive-protein binding. For example, the presence of ions modulates water-protein and ion-protein interactions, which can change, promote, or disfavor protein-analyte binding (BASU; SURESH KUMAR, 2015; HIRT et al., 2014). Furthermore, the ion-specific effects of the Hofmeister series on water structure and the colloidal surface hydration of proteins can also modify intermolecular interactions (HIRT et al., 2014; METRICK; MACDONALD, 2015). Although recognized in 1888 (HOFMEISTER, 1888; KUNZ; HENLE; NINHAM, 2004), the effects of these ions are still extensively investigated as there are many unanswered questions (LEONTIDIS, 2017). For example, there are no studies on the effects of Hofmeister ions on the molecular dynamics or on the parameters involved in activated complex formation. In previous papers on the β-cas/Qct interaction, the effects of Hofmeister ions were not explored.

Therefore, using Surface Plasmon Resonance (SPR) we determined the kinetic and thermodynamic parameters involved in complex formation between β-cas and Qct in the absence and presence of two salts belonging to the Hofmeister series.

2. Material and methods

2.1. Materials

Carboxymethylated dextran sensor chips (CM5), N-Hydroxysuccinimide (NHS), N-(3-dimethylaminopropyl)-N-ethylcarbodiimide hydrochloride (EDC), ethanolamine-HCl (1 M, pH 8.5), HBS-P buffer (pH 7.4), and immobilization buffer (pH 4.0), were purchased from General Electric Healthcare Company (Pittsburgh, PA, USA). β-cas (≥98% wt.), Qct (≥95% wt.), potassium thiocyanate (KSCN), potassium chloride (KCl), and dimethyl sulfoxide (all of analytical grade) were obtained from Sigma-Aldrich (St. Louis, MO, USA).

2.2. SPR analysis

Real-time analysis of complex formation between β-cas and Qct were performed at pH 7.4 on a two-channel Biacore X100 system (GE Healthcare Life Sciences, PA, USA) at six temperatures (12, 16, 20, 24, 25 and 28 °C).

β-cas immobilization on the CM5 sensor chip

β-cas was immobilized on the dextran surface of a standard optical CM5 sensor chip by a standard covalent amine coupling procedure. Covalent couplings are stable, do not require ligand modifications, and are commonly used to immobilize proteins on biosensors (FATHI et al., 2018). The CM5 sensor chip was inserted into the SPR machine and rinsed with acetate buffer. The carboxylic groups on the chip surface were activated using an amine coupling reagent containing EDC and NHS (1:1) for 7 minutes. The β-cas solution was prepared in acetate buffer (pH 4.0) at a concentration of 30 $\mu g \cdot ml^{-1}$ (1.25×10^{-6} $mol \cdot L^{-1}$) and injected into channel 1 (sample channel) of the sensor chip for 10 min, resulting in protein immobilization with a density of 4463 RU (resonance units). This pH favored the interaction between the negatively charged carboxymethyl dextran layer of the sensor chip and the positively charged chain of β-cas, which has an isoelectric point of approximately 4.8 (ATAMER et al., 2017). Acetate buffer without β-cas was injected into channel 2 (reference channel) as a control. Non-specific interactions on the chip surface were blocked through the addition of an ethanolamine-HCl solution to the chip channels (HUDSON et al., 2018a).

Analysis of the β-cas/Qct complex formation process

Increasing concentrations of Qct (5 to 13 μM) prepared in HBS-P buffer at pH 7.4 with 1% DMSO were injected for 3 minutes into both sensor chip channels at a flow rate of 30 $\mu l \cdot min^{-1}$. This flow rate was chosen to avoid mass transport which would affect accurate determination of the interaction kinetics. Mass transport is a common phenomenon in SPR experiments and may result in erroneous binding models and kinetic data (TERAN; NUGENT, 2019). We tested the flow of the Qct solution over the chip surface with immobilized β-cas at different flow rates, and at 30 $\mu L \cdot min^{-1}$ mass transport was not observed. The specific response of the β-cas/Qct surface was acquired by subtracting the response of the reference channel from that of the sample channel. The generated signal, given as RU, at different temperatures (12 to 28 °C) was monitored over time, producing multiple sensorgrams.

Effect of the type and concentration of ions on β-cas/Qct complex formation

The effects of two ions of the Hofmeister series on the β-cas/Qct interaction were investigated using KCl and KSCN at different concentrations (25, 40, 60, 80, and 100 mM). Qct solutions (5, 7, 9, 11, and 13 μM) containing KCl (25-100 mM) or KSCN (25-100 mM) were injected over both channels, and thermodynamic and kinetic analysis were performed as

described in 2.2.2. All SPR experiments were performed in triplicate to ensure accuracy and the results were expressed as the mean ± standard deviation.

2.3. Zeta potential analysis

To evaluate the effect of KCl and KSCN on the zeta potential of β-cas and β-cas/Qct complexes, samples of β-cas alone at 10 μM and of β-cas (10 μM) added to Qct (13 μM) prepared in buffer (pH 7.0) containing 0, 15, 25, 30, or 40 mM of KCl or KSCN, were measured on a Zetasizer Nano ZS system (Malvern Instruments, Worcestershire, UK). For this, water at 25 °C (with a refraction index of 1.330, viscosity of 0.8872 cP, and a dielectric constant of 78.5) was used as a dispersant for the equipment.

3. Results and discussion

3.1. Kinetics of β-cas/Qct complex formation

The refractive index of the solution flowing over the CM5 chip surface is dependent on the local concentration (around 100 nm above the chip surface) (LEE et al., 2018). As β-cas/Qct binding occurs there is a real-time change in the local concentration, and consequently an alteration in the refractive index of the solution near the chip surface occurs, producing an SPR resonance signal over time (sensorgram) (LEE et al., 2018). Figure 1 shows representative SPR sensorgrams of the interaction between β-cas and Qct (5, 7, 9, 11, and 13 μM) at 25 °C.

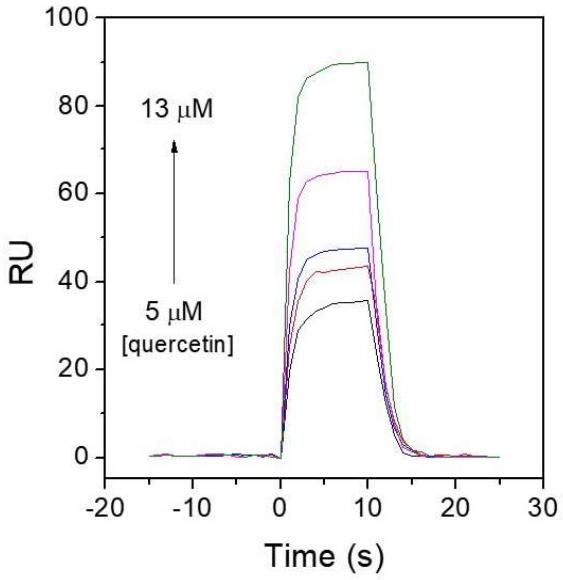

Figure 1. Sensorgrams (resonance units (RU) *versus* time) of immobilized β-casein interacting with different concentrations of quercetin (5, 7, 9, 11, and 13 μM) at 25 °C, at pH 7.4.

At the beginning of the SPR experiment, buffer flow over the sample and reference channels of the microfluidic system generated the background signal and produced an RU signal of approximately 0 (from -15 to 0 s). However, when a solution containing Qct was flown across the chip channel with immobilized β-cas, the fast association rate of binding and lower dissociation rate (ascending part of the sensorgrams) caused an increase in the RU signal. The difference between the rates of association and dissociation decreased over time until reaching a plateau, where the difference is equal to 0 (close to 10 s). Then, further flow of buffer across the chip surfaces led to dissociation of β-cas/Qct complexes (descending part of the sensorgrams), resulting in a decrease of the RU signal (10 to 25 s).

Global kinetic analysis of the ascending and descending parts of the sensorgrams was performed to determine the dissociation (k_d), observed (k_{obs}), and association (k_a) rate constants of β-cas/Qct complex formation based on a 1:1 molecular binding model (Equations 1, 2, and 3, respectively) (DE PAULA et al., 2017).

$$RU(t) = RU(t_m)\, e^{-k_d(t-t_m)} \quad (1)$$

$$RU(t) = RU_{max}[1 - e^{-k_{obs}(t)}] \quad (2)$$

$$k_{obs} = k_a[quercetin] + k_d \quad (3)$$

In these equations, RU (t) is the SPR response at time t, RU (t_m) denotes the SPR signal where the descendent exponential curve of the sensorgram starts, and RU_{max} indicates the resonance units obtained at an infinite time.

The k_d and k_{obs} values were obtained by global fitting of the data at phases from 0 to 10 s and from 10 to 25 s to Eq. (1) and (2), respectively. The behavior of k_{obs} values with Qct concentrations were linear and are shown in Supplemental Materials (Figure S1). The slope of these plots represents the k_a values.

Determining the k_a and k_d values allow us to evaluate the dynamics of an intermolecular interaction, expressing the number of β-cas/Qct complexes formed per second and the fraction of these complexes that decay per second, respectively (FATHI et al., 2016). The k_a and k_d values increased linearly with increasing temperature (Figure S2), indicating that the rate of association of free Qct and β-cas molecules and the rate of dissociation of β-cas/Qct complexes increased at higher temperatures.

Based on transition state theory, we can consider that during the process of β-cas/Qct nanoaggregate formation, a transition (or activated) complex is formed by the association of free β-cas and Qct molecules or by dissociation of the thermodynamically stable β-cas/Qct complexes (FERNÁNDEZ-RAMOS et al., 2006a). As activated complex formation requires spatial atomic reorganization of the interacting species, we should consider the existence of a potential energy barrier (activation energy) associated with the change in distance between Qct and β-cas molecules (PHILLIPS; HEBEN, 2015). The activation energies involved in the association of free molecules ($E_{act(a)}$) and dissociation of stable complexes ($E_{act(d)}$) were determined using the Arrhenius equation (Eq. 4).

$$E_{act(x)}(T) = -R\left(\frac{d\ln k_x}{d\ 1/T}\right) \quad (4)$$

In this equation, the subscript "*x*" represents the association ("*a*") or dissociation ("*d* ") phases, and R is the universal gas constant (8.3145 $J{\cdot}mol^{-1}{\cdot}K^{-1}$).

The temperature dependence of the k_a and k_d values allowed the change in Gibbs free energy ($\Delta G_x^{\ddagger}$), enthalpy ($\Delta H_x^{\ddagger}$), and entropy ($T\Delta S_x^{\ddagger}$), related to activated complex formation, to be calculated (Eq. 5, 6 and 7). These values are presented in the Table 1.

$$\Delta G_x^{\ddagger}(T) = -RTln(k_x h/k_B(T)) \quad (5)$$

$$\Delta H_x^{\ddagger}(T) = E_{act(x)}(T) - RT \quad (6)$$

$$T\Delta S_x^{\ddagger}(T) = \Delta H_x^{\ddagger}(T) - \Delta G_x^{\ddagger}(T) \quad (7)$$

In the Eq. 5, h is the Planck's constant and k_B is the Boltzmann's constant.

Table 1. Energetic parameters related to β-casein/Quercetin activated complex formation

[a]T	Association step (*a*)				Dissociation step (*d*)			
	[b]E_{act}	[b]$\Delta H^{\ddagger}$	[b]$\Delta G^{\ddagger}$	[b]$T\Delta S^{\ddagger}$	[b]E_{act}	[b]$\Delta H^{\ddagger}$	[b]$\Delta G^{\ddagger}$	[b]$T\Delta S^{\ddagger}$
12	33.35 ±0.5	30.98 ±0.6	45.49 ±0.8	-14.52 ±0.2	7.48 ±0.2	5.11 ±0.1	70.82 ±0.9	-65.70 ±0.7
16		30.94 ±0.5	45.81 ±0.8	-14.87 ±0.2		5.08 ±0.1	71.78 ±0.9	-66.70 ±0.6
20		30.91 ±0.6	46.05 ±0.9	-15.14 ±0.2		5.05 ±0.2	72.67 ±0.9	-67.63 ±0.6
24		30.88 ±0.6	46.22 ±0.9	-15.34 ±0.3		5.01± 0.2	73.60 ±0.9	-68.59 ±0.7
25		30.87 ±0.7	46.18 ±0.7	-15.31 ±0.3		5.00± 0.1	73.81 ±0.8	-68.80 ±0.6
28		30.84 ±0.5	46.34 ±0.8	-15.49 ±0.2		4.98± 0.1	74.51 ±0.8	-69.54 ±0.7

The formation of the activated complex from the β-cas and Qct free molecules required a higher activation energy (33.35 kJ·mol^{-1}) than the formation of the transition complex from the dissociation of the thermodynamically stable β-cas/Qct complexes (7.48 kJ·mol^{-1}). This result ($E_{act(a)} > E_{act(d)}$) showed that desolvation of the ligands, conformational changes at the interaction sites of the protein, and the direct interaction of Qct with each site in β-cas, absorb more energy during association than dissociation. This suggests that the ligand-analyte interactions and conformations in the thermodynamically stable complex are similar to those of the activated complex, thus requiring less energy for the formation of this transition nanoaggregate. On the contrary, a higher energy barrier needs to be overcome when this process occurs from the association of free β-cas and Qct molecules.

Despite the higher E_{act} value determined in the association phase, the net energetic cost ($\Delta G^{\ddagger}$) showed that activated complex formation from the association of free β-cas and Qct molecules occurs faster than the same process occurring from dissociation of the thermodynamically stable β-cas/Qct complexes (REZENDE et al., 2019). This higher β-cas/Qct binding velocity is due to entropic contributions. By analyzing $\Delta G^{\ddagger}$ and $T\Delta S^{\ddagger}$, we can conclude that synthesis of the activated complex occurred with a decrease in configurational, conformational, and solvation entropy for both association and dissociation steps; however, the $T\Delta S^{\ddagger}$ decrease was remarkably higher for the dissociation step. The higher $T\Delta S^{\ddagger}$ value in the association step can be explained if one considers that sites in the activated complex become more structured when Qct binds to β-cas. Thus, the entropic cost to form the β-cas/Qct activated complex from the dissociation of stable complexes is a determinant factor that influences the speed of this process. The kinetics of activated complex formation between another milk protein, bovine serum albumin (BSA), and a protein aggregation inhibiting dye, congo red (CR), was studied by de Paula et al. (2017). Although BSA is a globular protein and the CR molecule is larger than Qct, a similar activation energy was required for BSA-CR association when compared with our results for β-cas/Qct association, at 25 °C ($E_{act(a)\ BSA\text{-}CR}$ = 35.88 kJ·mol^{-1}). Activated complex formation from the association of free BSA and CR molecules also occurs faster than the dissociation of thermodynamically stable BSA/CR complexes ($\Delta G^{\ddagger}_{(a)}$ = 33.35 kJ·mol^{-1} and $\Delta G^{\ddagger}_{(d)}$ = 66.25 kJ·mol^{-1}). However, the globular structure and conformational changes in BSA seem to contribute strongly to the entropy of BSA-CR activated complex formation ($T\Delta S^{\ddagger}_{(a)}$ = 0.05 and $T\Delta S^{\ddagger}_{(d)}$= - 48.55 kJ·mol^{-1}).

3.2. Thermodynamics of β-cas/Qct complex formation

From the k_a and k_d values determined for each temperature, the binding constant (K_b) was determined (Eq. 8). Thus, the standard Gibbs free energy change (ΔG°) and standard entropy change (TΔS°) for the formation of the β-cas/Qct thermodynamically stable complex were obtained (Equations 9 and 10). The standard enthalpy change (ΔH°) was obtained from the van't Hoff approach (Eq. 11 and Fig. S3 of Supplemental Materials).

$$K_b = k_a/k_d \quad (8)$$

$$\Delta G° = -RTlnK_b \quad (9)$$

$$\Delta G° = \Delta H° - T\Delta S° \quad (10)$$

$$ln\frac{Kb_2}{Kb_1} = -\frac{\Delta H°}{R}\left(\frac{1}{T_2} - \frac{1}{T_1}\right) \quad (11)$$

In these equations, R is the universal gas constant (8.3145 J·mol^{-1}·K^{-1}) and T is the temperature (K).

The thermodynamic parameters of β-cas/Qct complex formation are presented in Table 2.

Table 2. Thermodynamic parameters associated with β-casein/Quercetin complex formation at a pH of 7.4 and different temperatures

[a] T	[b] K_b	[c] ΔH°	[c] ΔG°	[c] TΔS°
12	4.35 ± 0.09		-25.32 ± 0.51	51.19 ± 0.91
16	4.89 ± 0.08		-25.97 ± 0.53	51.83 ± 0.90
20	5.55 ± 0.10		-26.62 ± 0.61	52.49 ± 0.93
		25.86 ± 0.52		
24	6.51 ± 0.10		-27.38 ± 0.50	53.25 ± 0.98
25	6.92 ± 0.08		-27.63 ± 0.52	53.49 ± 0.93
28	7.72 ± 0.10		-28.18 ± 0.55	54.04 ± 0.93

The superscripts letters indicate the units: [a] °C, [b] 10^4 L·mol^{-1}, [c] kJ·mol^{-1}.

The K_b values obtained were in the 10^4 L·mol^{-1} region with their temperature dependence indicating that higher temperatures favored β-cas/Qct complex formation. The negative ΔG° values indicated that complex formation was favored in chemical equilibrium.

The thermodynamic process of β-cas/Qct complex formation was entropically driven, as shown by the positive values obtained for both ΔH° and TΔS°, suggesting that hydrophobic interactions are the main driving force for the β-cas/Qct interaction. These hydrophobic interactions potentially arise because when Qct interacts with β-cas, the entropic gain owing to desolvation of both chemical species and consequent release of counterions and water molecules contributes more to these TΔS° positive values than the entropy reduction caused by the decrease in the degree of translational freedom of these molecules as they interact.

Wei et al. (2018) studied the interaction between β-cas and Qct by fluorescence spectroscopy and determined the following thermodynamic parameters for β-cas/Qct complex formation: $\Delta H° = 16.55$ kJ·mol^{-1}, $T\Delta S° = 42.61$ kJ·mol^{-1}, and $\Delta G° = -26.06$ kJ·mol^{-1}, at 25 °C (WEI et al., 2018). Although in the same region, the values of these parameters determined in our study were higher. These differences may arise due to the use of different techniques. In fluorescence spectroscopy, only interactions that occur directly with fluorophore labelled residues are detected (GHOSH; RATHI; ARORA, 2016), while SPR, being a label-free technique, allows all interactions to be detected. Mehranfar et al. (2013) studied the thermodynamics of the interaction between Qct and β-cas in its micellar form (MEHRANFAR; BORDBAR; PARASTAR, 2013b). Absorption spectra of Qct in the presence of different concentrations of β-cas micelles at pH 7.0 were used as experimental data for chemometric analysis, and for determining the thermodynamic parameters. The calculated K_b values were also in the order of 10^4 but in this study complex formation was an enthalpically driven process ($\Delta H° = -28.60$ kJ·mol^{-1}, $T\Delta S° = -3.30$ kJ·mol^{-1}, and $\Delta G° = -25.29$ kJ·mol^{-1}, at 25 °C). As β-cas was used in its micellar form, these results encompass the energy involved in two general processes: Qct transfer to the inner hydrophobic region of the micelles, and the direct interaction of Qct with the β-cas molecule. Therefore, we cannot compare these results with our results.

3.3 Effect of KCl and KSCN on the β-cas/Qct interaction process

It is well known that many processes, including protein folding, protein stability, and protein interactions, are affected by electrolytes, especially those of the Hofmeister series (LO NOSTRO; NINHAM, 2012). In this series, anions generally present more pronounced effects than cations, and are ordered according to their efficiency in precipitating proteins as follows: $SO_4^{2-} > HPO_4^{2-} > F^- > CH_3COO^- > Cl^- > Br^- > NO_3^- > I^- > ClO_4^- > SCN^-$ (SALIS; NINHAM, 2014). The Cl^- is considered a “neutral” ion in terms of specific effects. Ions to its left are known as kosmotropic or “water structure makers”, and tend to precipitate proteins,

while those to its right increase the solubility of proteins and are termed chaotropic ions or "water structure breakers" (BRINI et al., 2017; HIRT et al., 2014). The specific properties of the Hofmeister ions can alter the surface hydration of colloids and their intermolecular interactions (PARSONS et al., 2011). To the best of our knowledge, the effect of Hofmeister ions on the interactions between proteins and bioactive molecules have not yet been systematically studied. Therefore, we evaluate how a neutral (Cl^-) and a chaotropic ion (SCN^-) of the Hofmeister series affects the kinetics and thermodynamics of β-cas/Qct complex formation by studying the formation of these complexes in the presence of KCl and KSCN at five concentrations (25 to 100 mM) using SPR.

The sensorgrams for the β-cas/Qct interaction at 25 °C in the presence of 80 mM KCl and KSCN are shown in Figure 2A and 2B, respectively. The sensorgrams for the β-cas/Qct interaction in the presence of 25, 40, 60, and 100 mM KCl and KSCN at 25 °C are presented in Figures S4 and S5 (Supplemental Materials). The same experiments were performed at 12, 16, 20, 24, and 28 °C, and the sensorgrams are shown in Figures S6 to S15.

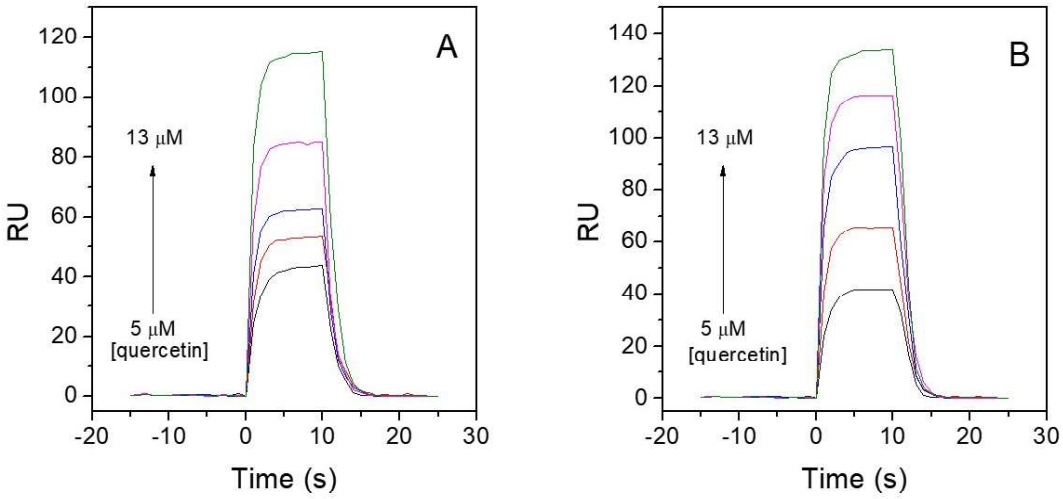

Figure 2. Sensorgrams of immobilized β-casein interacting with different concentrations of quercetin (5, 7, 9, 11 and 13 μM) in the presence of (A) 80 mM KCl and (B) 80 mM KSCN, at 25 °C and at pH 7.4.

The k_a and k_d values, in the presence of KCl and KSCN, were obtained at the six different temperatures. Independent of the concentrations of both salts, the Arrhenius plots were linear (Figure S16). Based on the k_a and k_d values dependence on the temperature, the energetic parameters involved in this process were calculated as described in the section "kinetics of β-cas/Qct complex formation".

Independent of the nature of the ions, the presence of the electrolytes caused a very small decrease in the $\Delta G^{\ddagger}$ values for the association step (from 46.18 to 45.55 $kJ \cdot mol^{-1}$), while in the

dissociation step, these values remained almost constant (from 73.81 to 73.63 kJ·mol^{-1}) (Figure S17). We also determine the effect of the salts from the $\Delta H^{\ddagger}$ and $T\Delta S^{\ddagger}$ values. The $\Delta H^{\ddagger}$ values at different concentrations of KCl and KSCN are shown in Figure 3.

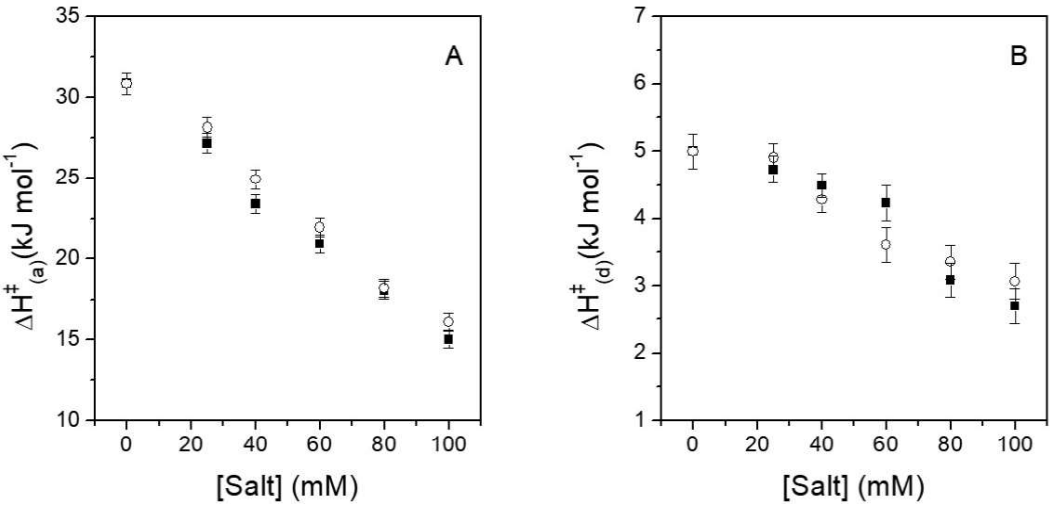

Figure 3. Activated enthalpy changes ($\Delta H^{\ddagger}$) related to activated complex formation between β-casein and quercetin in the (A) association and (B) dissociation steps *versus* [KCl] (■) or [KSCN] (○), at 25 °C.

In the association and dissociation steps, the presence of the salts decreased the $\Delta H^{\ddagger}$ values with a remarkable effect in the association process. Interestingly, the chaotropic (SCN^-) and the neutral (Cl^-) ions showed similar behaviors. The change in the $\Delta H^{\ddagger}$ values could be attributed to two salt effects: i) breakage of the hydrogen-bonded network of water molecules caused by the chaotropic ion SCN^-, which increases the hydrophobic effect favoring the β-cas/Qct interaction (LO NOSTRO; NINHAM, 2012), or ii) by shielding the electrostatic interactions at the electric double layer of the β-cas and Qct molecules, both with net negative charges (HIRT et al., 2014). However, as there was no difference between the two salts, the first effect is unlikely. Therefore, shielding of the electrostatic interactions at the electric double layer of the interacting molecules was the main mechanism which brought about the observed effect. In order to prove this, we determined the dependence of the zeta potential of β-cas and β-cas/Qct complexes on the salt concentration (Figure 4).

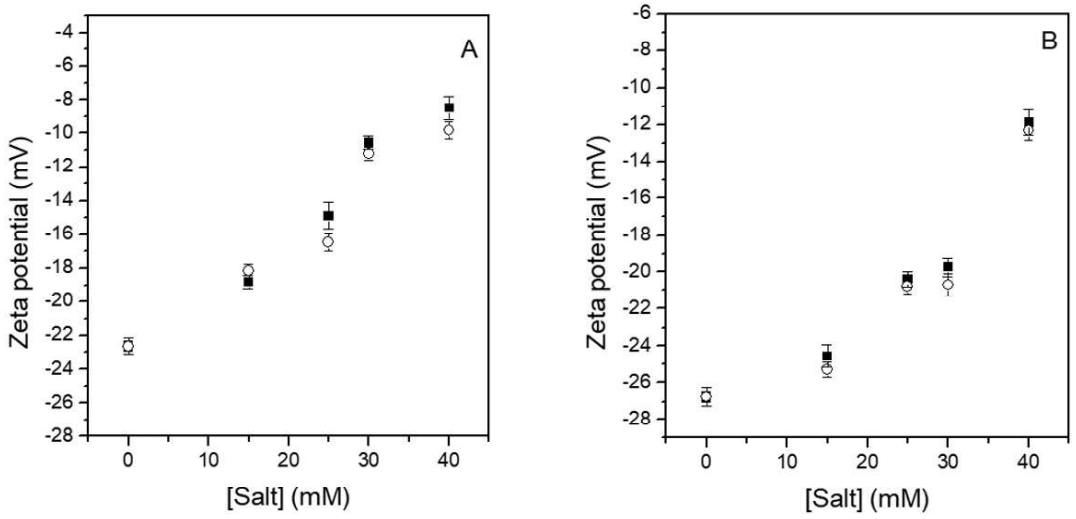

Figure 4. The effect of KCl (■) and KSCN (○) on the zeta potential of β-casein (A) and β-casein/quercetin complexes (B), at pH 7.4 and at 25 °C.

A reduction in the zeta potential was observed as the salt concentration increased with this effect equal for both salts, as expected. Therefore, there was a decrease in the electrostatic repulsion between the negatively charged regions in the interacting molecules, as shown in β-cas (Figure 4A) and β-cas/Qct complexes (Figure 4B). At pH 7.4, both β-cas and Qct carry a net negative charge, since the pKa values of the five OH groups in the Qct molecule (Figure S18) lie between 7.1 and 13.1 (D'ANDREA, 2015), and β-cas has an isoelectric point ranging between 4.8 and 5.1 (ATAMER et al., 2017, MOORE et al., 2015). The decrease in electrostatic repulsion between the interacting molecules caused by both salts favors short-range interactions (hydrophobic, van der Waals, etc.), resulting in decreasing $\Delta H^{\ddagger}$ values. The same behavior was observed for the activation energies, since $E_{act(a)}$ values ranged from 29.63 to 15.01 kJ·mol^{-1} for the system with KCl (25 to 100 mM), and 30.61 to 18.55 kJ·mol^{-1} in the presence of KSCN at the same concentrations, while the $E_{act(d)}$ values ranged from 7.21 to 4.18 kJ·mol^{-1} in the presence of KCl, and 7.39 to 5.55 kJ·mol^{-1} when KSCN was added.

The $T\Delta S^{\ddagger}$ values at different concentrations of KCl and KSCN were also obtained and are shown in Figure S19. Changes in the system entropy during intermolecular interactions depends on three main processes: i) conformational changes at the binding sites, ii) solvation water and counterions release, and iii) decrease of rotational and translational degrees of freedom of the interacting molecules upon complexation (CHANDEL et al., 2018). As the salt concentration increased and shielding of the electrostatic interactions at the electric double layer became more effective, the counterions released, promoted by the β-cas/Qct interaction,

decreases, resulting in lower $T\Delta S^{\ddagger}$ values in both the association (Fig. S19 A) and dissociation (Fig. S19 B) steps.

We evaluated the influence of temperature on the $\Delta H^{\ddagger}$ values related to activated complex formation at different salt concentrations. The $\Delta H^{\ddagger}$ dependence on temperature allowed the heat capacity change ($\Delta C_p^{\ddagger}$) related to activated complex formation to be determined (Eq. 12). The plots of $\Delta H^{\ddagger}$ *versus* temperature in the presence and absence of salt are presented in Figure S20, with the slope representing the $\Delta C_p^{\ddagger}$ value.

$$\Delta C_p^{\ddagger} = d\Delta H^{\ddagger} / \, \mathrm{d}T \qquad (12)$$

The $\Delta C_p^{\ddagger}$ values were negative (Table 3), indicating that new molecular interactions formed in the activated complex were less intense than those disturbed in free β-cas and Qct molecules. In addition, $\Delta C_p^{\ddagger}$ was independent of the presence, concentration, and nature of the ions, suggesting that the molecular processes affecting $\Delta C_p^{\ddagger}$ (such as desolvation of the interacting molecules and conformational changes at the interaction sites) are not influenced by the presence of ions. On the other hand, as $\Delta C_p^{\ddagger}$ was independent of the association and dissociation steps, we can conclude that the main molecular process that affects this parameter is the disruption of amino acid-amino acid interactions and the formation of the amino acid-Qct interactions that occurs at the protein interaction site. We can disconsider the contribution of the desolvation/resolvation processes to the $\Delta C_p^{\ddagger}$ values because water-solute interactions are very different in the association or dissociation steps in activated complex formation.

Table 3. Heat capacity change ($\Delta C_p^{\ddagger}$) associated with activated β-casein/Quercetin complex formation for association (a) and dissociation (d) steps at pH 7.4 and different concentrations of KCl and KSCN

	KCl		KSCN	
[a] Salt concentration	[b] $\Delta C_p^{\ddagger}{}_{(a)}$	[b] $\Delta C_p^{\ddagger}{}_{(d)}$	[b] $\Delta C_p^{\ddagger}{}_{(a)}$	[b] $\Delta C_p^{\ddagger}{}_{(d)}$
0	-8.47 ± 0.17	-8.38 ± 0.16	-8.47 ± 01.5	-8.38 ± 0.13
25	-8.33 ± 0.15	-8.47 ± 0.15	-8.33 ± 0.15	-8.33 ± 0.11
40	-8.33 ± 0.13	-8.47 ± 0.14	-8.07 ± 0.14	-8.07 ± 0.13

60	-8.33 ± 0.15	-8.07 ± 0.13	-8.07 ± 0.13	-8.47 ± 0.15
80	-8.15 ± 0.16	-8.33 ± 0.14	-8.47 ± 0.13	-8.47 ± 0.15
100	-8.47 ± 0.16	-8.33 ± 0.17	-8.47 ± 0.16	-8.38 ± 0.15

The superscripts letters indicate the units: [a] mM, [b] J·mol^{-1}.

3.4. Thermodynamics of β-cas/Qct complex formation in the presence of salts

The van't Hoff plots for the interaction between β-cas and Qct in the presence of KCl and KSCN at different concentrations are presented in Figure S21.

The thermodynamic parameters (K_b, ΔG°, ΔH°, and TΔS°) of β-cas/Qct complex formation in the presence of different concentrations of KCl and KSCN were obtained from equations 8 to 11. As previously discussed, the shielding of electrostatic interactions at the electric double layer of β-cas and Qct molecules in the presence of both salts led to a decrease in the electrostatic repulsion between them. In fact, there was an increase in K_b and a slight decrease in ΔG° values as the salt concentration increased, showing that the amount of β-cas/Qct complex formation increased at higher salt concentrations.

The ΔH° and TΔS° values in the presence of different concentrations of KCl and KSCN, at 25 °C, are shown in Figure 5.

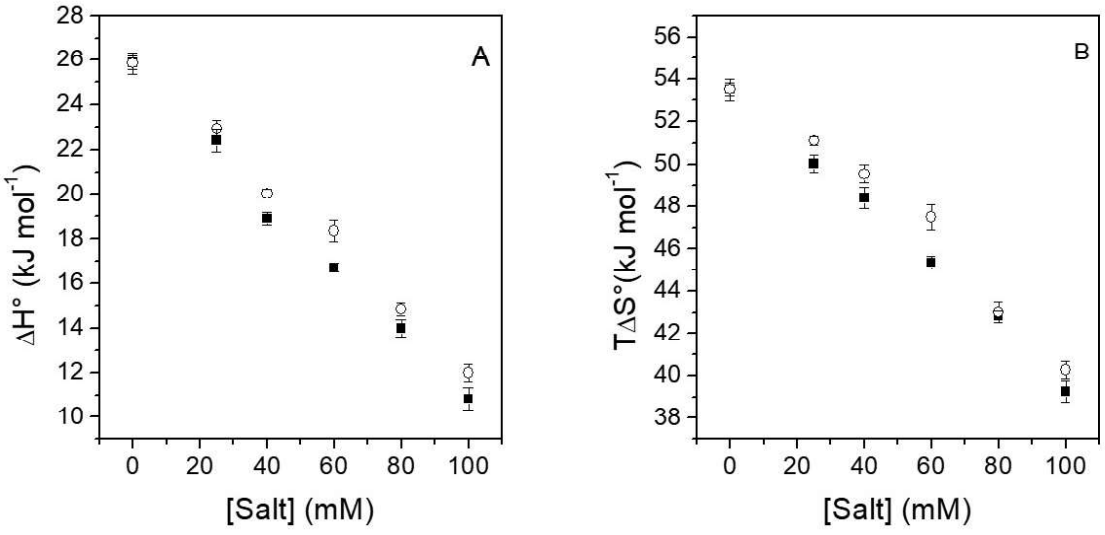

Figure 5. Standard enthalpy (ΔH°) and entropy (TΔS°) changes of β-casein/quercetin complex formation in the presence of different concentrations of KCl (■) and KSCN (○).

As in experiments without the salts, hydrophobic interactions were the main driving forces for thermodynamically stable β-cas/Qct complex formation, since the ΔH° and TΔS° values were positive. However, independent of the electrolyte nature, increasing concentrations

of salt led to a similar decrease in the ΔH° and TΔS° values. The reduction in the electrostatic repulsion between β-cas and Qct favored short-range interactions (hydrophobic, van der Waals, etc.), resulting in decreasing ΔH° values, and reducing the number of counterions released at the electric double layer of the interacting molecules at higher salt concentrations, resulted in a decrease in TΔS° values.

4. Conclusion

In summary, SPR measurements indicated that β-cas and Qct form a thermodynamically stable complex favored at higher temperatures and driven by an increase in entropy. As the association and dissociation rate constants were dependent on temperature, energetic parameters attributed to activated complex formation were calculated, giving insight into the molecular processes driving β-cas/Qct complex formation. The interaction process was equally affected by both of the studied Hofmeister ions (Cl^- and SCN^-), which reduced the enthalpy by shielding electrostatic interactions at the electric double layer of the interacting molecules. The same electrolyte effect was observed during β-cas/Qct activated complex formation. Our results provide insights into the β-cas/Qct interaction process and contribute to the understanding of how Hofmeister ions can modulate intermolecular interactions between proteins and small molecules.

Acknowledgements

This research was supported by the Conselho Nacional de Desenvolvimento Científico e Tecnológico (Brazil), the Coordenação de Aperfeiçoamento de Pessoal de Nível Superior (Brazil), CAPES/Pró-Forenses (Brazil), the Fundação de Apoio à Pesquisa de Minas Gerais (Brazil), the Financiadora de Estudos e Projetos (FINEP) (Brazil), and the Instituto Nacional de Ciências e Tecnologias Analíticas Avançadas (INCTAA) (Brazil).

Conflicts of interest

The authors declare that there is no conflict of interest.

References

ATAMER, Z.; POST, A. E.; SCHUBERT, T.; HOLDER, A.; BOOM, R. M.; HINRICHS, J. Bovine β-casein: Isolation, properties and functionality. A review. **International Dairy Journal**, [s. l.], v. 66, p. 115–125, 2017.

AZZI, J.; JRAIJ, A.; AUEZOVA, L.; FOURMENTIN, S.; GREIGE-GERGES, H. Novel findings for quercetin encapsulation and preservation with cyclodextrins, liposomes, and drug-in-cyclodextrin-in-liposomes. **Food Hydrocolloids**, [s. l.], v. 81, p. 328–340, 2018.

BAHRI, A.; HENRIQUET, C.; PUGNIÈRE, M.; MARCHESSEAU, S.; CHEVALIER-LUCIA, D. Binding analysis between monomeric β-casein and hydrophobic bioactive compounds investigated by surface plasmon resonance and fluorescence spectroscopy. **Food Chemistry**, [s. l.], v. 286, p. 289–296, 2019.

BASU, A.; SURESH KUMAR, G. Thermodynamics of the interaction of the food additive tartrazine with serum albumins: A microcalorimetric investigation. **Food Chemistry**, [s. l.], v. 175, p. 137–142, 2015.

BRINI, E.; FENNELL, C. J.; FERNANDEZ-SERRA, M.; HRIBAR-LEE, B.; LUKŠIČ, M.; DILL, K. A. How Water's Properties Are Encoded in Its Molecular Structure and Energies. **Chemical Reviews**, [s. l.], v. 117, n. 19, p. 12385–12414, 2017.

CAI, X.; FANG, Z.; DOU, J.; YU, A.; ZHAI, G. Bioavailability of Quercetin: Problems and Promises. **Current Medicinal Chemistry**, [s. l.], v. 20, n. 20, p. 2572–2582, 2013.

CHANDEL, T. I.; ZAMAN, M.; KHAN, M. V.; ALI, M.; RABBANI, G.; ISHTIKHAR, M.; KHAN, R. H. A mechanistic insight into protein-ligand interaction, folding, misfolding, aggregation and inhibition of protein aggregates: An overview. **International Journal of Biological Macromolecules**, [s. l.], v. 106, p. 1115–1129, 2018.

CHEN, X.; MCCLEMENTS, D. J.; ZHU, Y.; CHEN, Y.; ZOU, L.; LIU, W.; CHENG, C.; FU, D.; LIU, C. Enhancement of the solubility, stability and bioaccessibility of quercetin using protein-based excipient emulsions. **Food Research International**, [s. l.], v. 114, p. 30–37, 2018.

CHEN, X.; ZOU, L.; LIU, W.; MCCLEMENTS, D. J. Potential of Excipient Emulsions for Improving Quercetin Bioaccessibility and Antioxidant Activity: An in Vitro Study. **Journal of Agricultural and Food Chemistry**, [s. l.], v. 64, n. 18, p. 3653–3660, 2016.

D'ANDREA, G. Quercetin: A flavonol with multifaceted therapeutic applications? **Fitoterapia**, [s. l.], v. 106, p. 256–271, 2015.

DE PAULA, H. M. C.; COELHO, Y. L.; AGUDELO, A. J. P.; REZENDE, J. de P.; FERREIRA, G. M. D.; FERREIRA, G. M. D.; PIRES, A. C. dos S.; DA SILVA, L. H. M. Kinetics and thermodynamics of bovine serum albumin interactions with Congo red dye. **Colloids and Surfaces B: Biointerfaces**, [s. l.], v. 159, p. 737–742, 2017

DEZHAMPANAH, H.; ESMAILI, M.; KHORSHIDI, A. Milk β-casein as a vehicle for delivery of bis(indolyl)methane: Spectroscopy and molecular docking studies. **Journal of Molecular Structure**, [s. l.], v. 1136, p. 50–58, 2017.

FATHI, F.; EZZATI NAZHAD DOLATANBADI, J.; RASHIDI, M.-R.; OMIDI, Y. Kinetic studies of bovine serum albumin interaction with PG and TBHQ using surface plasmon

resonance. **International Journal of Biological Macromolecules**, [s. l.], v. 91, p. 1045–1050, 2016.

FATHI, F.; MOHAMMADZADEH-AGHDASH, H.; SOHRABI, Y.; DEHGHAN, P.; EZZATI NAZHAD DOLATABADI, J. Kinetic and thermodynamic studies of bovine serum albumin interaction with ascorbyl palmitate and ascorbyl stearate food additives using surface plasmon resonance. **Food Chemistry**, [s. l.], v. 246, p. 228–232, 2018.

FERNÁNDEZ-RAMOS, A.; MILLER, J. A.; KLIPPENSTEIN, S. J.; TRUHLAR, D. G. Modeling the Kinetics of Bimolecular Reactions. **Chemical Reviews**, [s. l.], v. 106, n. 11, p. 4518–4584, 2006.

GANG, W.; JIE, W. J.; PING, Z. L.; MING, D. S.; YING, L. J.; LEI, W.; FANG, Y. Liposomal quercetin: evaluating drug delivery in vitro and biodistribution in vivo. **Expert Opinion on Drug Delivery**, [s. l.], v. 9, n. 6, p. 599–613, 2012.

GAO, Y.; WANG, Y.; MA, Y.; YU, A.; CAI, F.; SHAO, W.; ZHAI, G. Formulation optimization and in situ absorption in rat intestinal tract of quercetin-loaded microemulsion. **Colloids and Surfaces B: Biointerfaces**, [s. l.], v. 71, n. 2, p. 306–314, 2009.

GHAYOUR, N.; HOSSEINI, S. M. H.; ESKANDARI, M. H.; ESTEGHLAL, S.; NEKOEI, A.-R.; HASHEMI GAHRUIE, H.; TATAR, M.; NAGHIBALHOSSAINI, F. Nanoencapsulation of quercetin and curcumin in casein-based delivery systems. **Food Hydrocolloids**, [s. l.], v. 87, p. 394–403, 2019.

GHOSH, K.; RATHI, S.; ARORA, D. Fluorescence spectral studies on interaction of fluorescent probes with Bovine Serum Albumin (BSA). **Journal of Luminescence**, v. 175, p. 135-140, 2016.

HIRT, S.; JONES, O. G.; ADIJANTO, M.; GILBERT, J. Influence of sulphate, chloride, and thiocyanate salts on formation of β-lactoglobulin–pectin microgels. **Food Chemistry**, [s. l.], v. 164, p. 63–69, 2014.

HOFMEISTER, F. Zur Lehre von der Wirkung der Salze. **Archiv für Experimentelle Pathologie und Pharmakologie**, [s. l.], v. 24, n. 4–5, p. 247–260, 1888.

HORNE, D. S. Casein structure, self-assembly and gelation. **Current Opinion in Colloid & Interface Science**, [s. l.], v. 7, n. 5–6, p. 456–461, 2002.

HUANG, J.; LIU, Z.; MA, Q.; HE, Z.; NIU, Z.; ZHANG, M.; PAN, L.; QU, X.; YU, J.; NIU, B. Studies on the Interaction between Three Small Flavonoid Molecules and Bovine Lactoferrin. **BioMed Research International**, [s. l.], v. 2018, p. 1–10, 2018.

HUDSON, E. A.; DE PAULA, H. M. C.; FERREIRA, G. M. D.; FERREIRA, G. M. D.; HESPANHOL, M. do C.; DA SILVA, L. H. M.; PIRES, A. C. dos S. Thermodynamic and kinetic analyses of curcumin and bovine serum albumin binding. **Food Chemistry**, [s. l.], v. 242, n. August 2017, p. 505–512, 2018.

KIMPEL, F.; SCHMITT, J. J. Review: Milk Proteins as Nanocarrier Systems for Hydrophobic Nutraceuticals. **Journal of Food Science**, [s. l.], v. 80, n. 11, p. R2361–R2366, 2015.

KLEEMANN, R.; VERSCHUREN, L.; MORRISON, M.; ZADELAAR, S.; VAN ERK, M. J.; WIELINGA, P. Y.; KOOISTRA, T. Anti-inflammatory, anti-proliferative and anti-atherosclerotic effects of quercetin in human in vitro and in vivo models. **Atherosclerosis**, [s. l.], v. 218, n. 1, p. 44–52, 2011.

KUNZ, W.; HENLE, J.; NINHAM, B. W. 'Zur Lehre von der Wirkung der Salze' (about the science of the effect of salts): Franz Hofmeister's historical papers. **Current Opinion in Colloid & Interface Science**, [s. l.], v. 9, n. 1–2, p. 19–37, 2004.

LEE, T.-H.; HIRST, D. J.; KULKARNI, K.; DEL BORGO, M. P.; AGUILAR, M.-I. Exploring Molecular-Biomembrane Interactions with Surface Plasmon Resonance and Dual Polarization Interferometry Technology: Expanding the Spotlight onto Biomembrane Structure. **Chemical Reviews**, [s. l.], v. 118, n. 11, p. 5392–5487, 2018.

LEONTIDIS, E. Investigations of the Hofmeister series and other specific ion effects using lipid model systems. **Advances in Colloid and Interface Science**, [s. l.], v. 243, p. 8–22, 2017.

LI, H.; ZHAO, X.; MA, Y.; ZHAI, G.; LI, L.; LOU, H. Enhancement of gastrointestinal absorption of quercetin by solid lipid nanoparticles. **Journal of Controlled Release**, [s. l.], v. 133, n. 3, p. 238–244, 2009.

LO NOSTRO, P.; NINHAM, B. W. Hofmeister Phenomena: An Update on Ion Specificity in Biology. **Chemical Reviews**, [s. l.], v. 112, n. 4, p. 2286–2322, 2012.

LU, N. T.; CRESPI, C. M.; LIU, N. M.; VU, J. Q.; AHMADIEH, Y.; WU, S.; LIN, S.; MCCLUNE, A.; DURAZO, F.; SAAB, S.; HAN, S.; NEIMAN, D. C.; BEAVEN, S.; FRENCH, S. W. A Phase I Dose Escalation Study Demonstrates Quercetin Safety and Explores Potential for Bioflavonoid Antivirals in Patients with Chronic Hepatitis C. **Phytotherapy Research**, [s. l.], v. 30, n. 1, p. 160–168, 2016.

MEHRANFAR, F.; BORDBAR, A.-K.; PARASTAR, H. A combined spectroscopic, molecular docking and molecular dynamic simulation study on the interaction of quercetin with β-casein nanoparticles. **Journal of Photochemistry and Photobiology B: Biology**, [s. l.], v. 127, p. 100–107, 2013.

METRICK, M. A.; MACDONALD, G. Hofmeister ion effects on the solvation and thermal stability of model proteins lysozyme and myoglobin. **Colloids and Surfaces A: Physicochemical and Engineering Aspects**, [s. l.], v. 469, p. 242–251, 2015.

MIRPOOR, S. F.; HOSSEINI, S. M. H.; NEKOEI, A.-R. Efficient delivery of quercetin after binding to beta-lactoglobulin followed by formation soft-condensed core-shell nanostructures. **Food Chemistry**, [s. l.], v. 233, p. 282–289, 2017.

MOITZI, C.; PORTNAYA, I.; GLATTER, O.; RAMON, O.; DANINO, D. Effect of Temperature on Self-Assembly of Bovine B-Casein above and below Isoelectric pH. Structural Analysis by Cryogenic-Transmission Electron Microscopy and Small-Angle X-ray Scattering. **Langmiur**, [s. l.], v. 24, p. 3020–3029, 2008.

MOORE, T. L.; RODRIGUEZ-LORENZO, L.; HIRSCH, V.; BALOG, S.; URBAN, D.; JUD, C.; ROTHEN-RUTISHAUSER, B.; LATTUADA, M.; PETRI-FINK, A. Nanoparticle colloidal stability in cell culture media and impact on cellular interactions. **Chemical Society Reviews**, [s. l.], v. 44, n. 17, p. 6287–6305, 2015.

PANDEY, S. K.; PATEL, D. K.; THAKUR, R.; MISHRA, D. P.; MAITI, P.; HALDAR, C. Anti-cancer evaluation of quercetin embedded PLA nanoparticles synthesized by emulsified nanoprecipitation. **International Journal of Biological Macromolecules**, [s. l.], v. 75, p. 521–529, 2015.

PARSONS, D. F.; BOSTRÖM, M.; NOSTRO, P. Lo; NINHAM, B. W. Hofmeister effects: interplay of hydration, nonelectrostatic potentials, and ion size. **Physical Chemistry Chemical Physics**, [s. l.], v. 13, n. 27, p. 12352, 2011.

PATEL, R. V.; MISTRY, B. M.; SHINDE, S. K.; SYED, R.; SINGH, V.; SHIN, H.-S. Therapeutic potential of quercetin as a cardiovascular agent. **European Journal of Medicinal Chemistry**, [s. l.], v. 155, p. 889–904, 2018.

PHILLIPS, A. B.; HEBEN, M. J. Activated complex model and surfactant reorganization during SWCNT separations on hydrogels. **Carbon**, [s. l.], v. 95, p. 330–337, 2015.

POÓR, M.; BODA, G.; KUNSÁGI-MÁTÉ, S.; NEEDS, P. W.; KROON, P. A.; LEMLI, B. Fluorescence spectroscopic evaluation of the interactions of quercetin, isorhamnetin, and quercetin-3′-sulfate with different albumins. **Journal of Luminescence**, [s. l.], v. 194, p. 156–163, 2018.

PORTNAYA, I.; BEN-SHOSHAN, E.; COGAN, U.; KHALFIN, R.; FASS, D.; RAMON, O.; DANINO, D. Self-Assembly of Bovine B-Casein below the Isoelectric pH. **Journal of Agricultural and Food Chemistry**, [s. l.], v. 56, p. 2192–2198, 2008.

REZENDE, J. de P.; HUDSON, E. A.; DE PAULA, H. M. C.; COELHO, Y. L.; DA SILVA, L. H. M.; PIRES, A. C. dos S. Thermodynamic and kinetic study of epigallocatechin-3-gallate-bovine lactoferrin complex formation determined by surface plasmon resonance (SPR): A comparative study with fl uorescence spectroscopy. **Food Hydrocolloids**, [s. l.], v. 95, p. 526–532, 2019.

SALIS, A.; NINHAM, B. W. Models and mechanisms of Hofmeister effects in electrolyte solutions, and colloid and protein systems revisited. **Chem. Soc. Rev**., [s. l.], v. 43, n. 21, p. 7358–7377, 2014.

TERAN, M.; NUGENT, M. A. Characterization of receptor binding kinetics for vascular endothelial growth factor-A using SPR. **Analytical Biochemistry**, [s. l.], v. 564–565, p. 21–31, 2019.

VAQUERO, M. J. R.; ALBERTO, M. R.; DE NADRA, M. C. M. Antibacterial effect of phenolic compounds from different wines. **Food Control**, [s. l.], v. 18, n. 2, p. 93–101, 2007.

WANG, H.; YANG, Z.; HE, Z.; ZHOU, C.; WANG, C.; CHEN, Y.; LIU, X.; LI, S.; LI, P. Self-assembled amphiphilic chitosan nanomicelles to enhance the solubility of quercetin for efficient delivery. **Colloids and Surfaces B: Biointerfaces**, [s. l.], v. 179, p. 519–526, 2019.

WANG, W.; SUN, C.; MAO, L.; MA, P.; LIU, F.; YANG, J.; GAO, Y. The biological activities, chemical stability, metabolism and delivery systems of quercetin: A review. **Trends in Food Science & Technology**, [s. l.], v. 56, p. 21–38, 2016.

WEI, J.; XU, D.; YANG, J.; ZHANG, X.; MU, T.; WANG, Q. Analysis of the interaction mechanism of Anthocyanins (Aronia melanocarpa Elliot) with β-casein. **Food Hydrocolloid**s, [s. l.], v. 84, p. 276–281, 2018.

WU, Q.; KROON, P. A.; SHAO, H.; NEEDS, P. W.; YANG, X. Differential Effects of Quercetin and Two of Its Derivatives, Isorhamnetin and Isorhamnetin-3-glucuronide, in Inhibiting the Proliferation of Human Breast-Cancer MCF-7 Cells. **Journal of Agricultural and Food Chemistr**y, [s. l.], v. 66, n. 27, p. 7181–7189, 2018.

Supplementary Materials

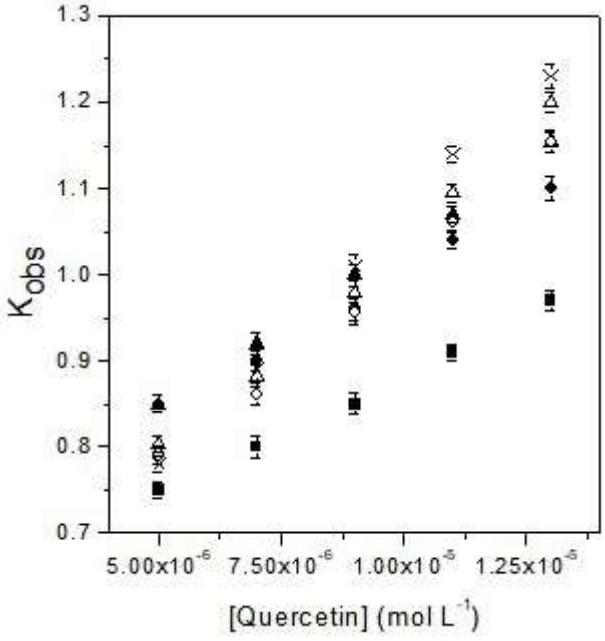

Figure S1. The plot of k_{obs} versus concentration of quercetin for interaction between β-casein and quercetin at pH 7.4 and different temperatures: (■) 12, (●)16, (▲) 20, (○) 24, (Δ) 25 and (x) 28 °C.

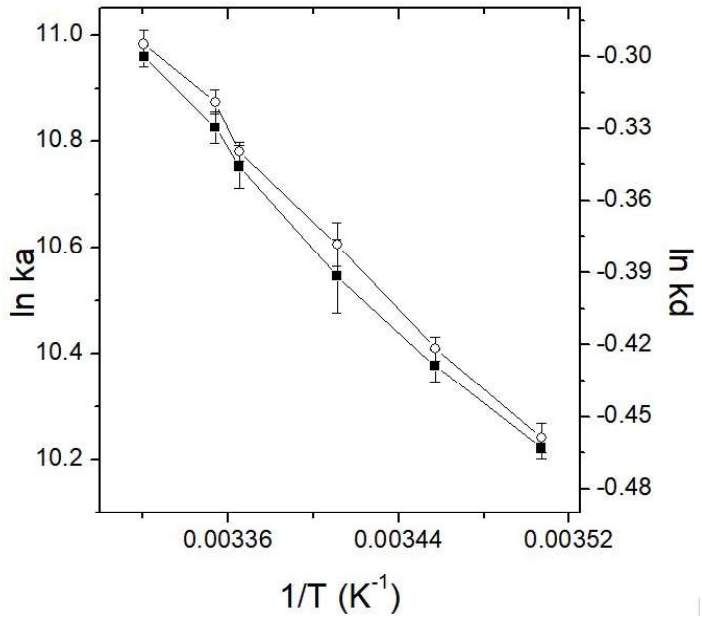

Figure S2. Natural log of the kinetic constants of association (■) and dissociation (○) for activated complex formation between β-casein and quercetin *versus* inverse temperature.

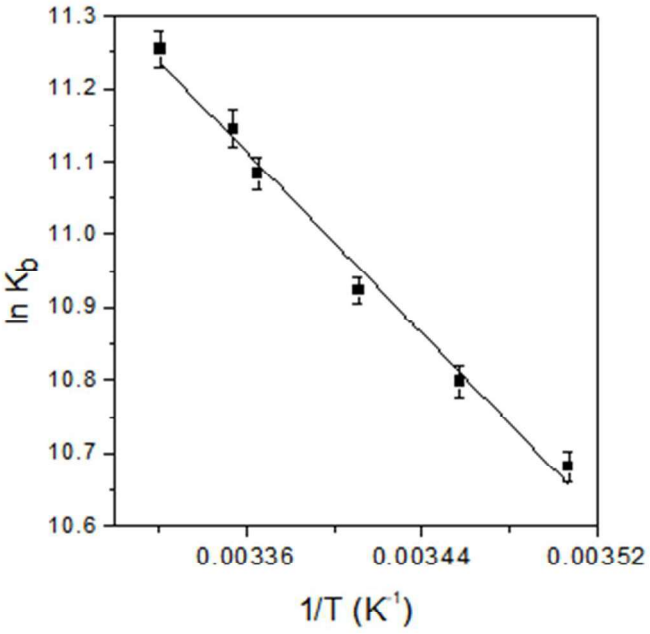

Figure S3. The van't Hoff plot for interaction between β-casein and quercetin at pH 7.4.

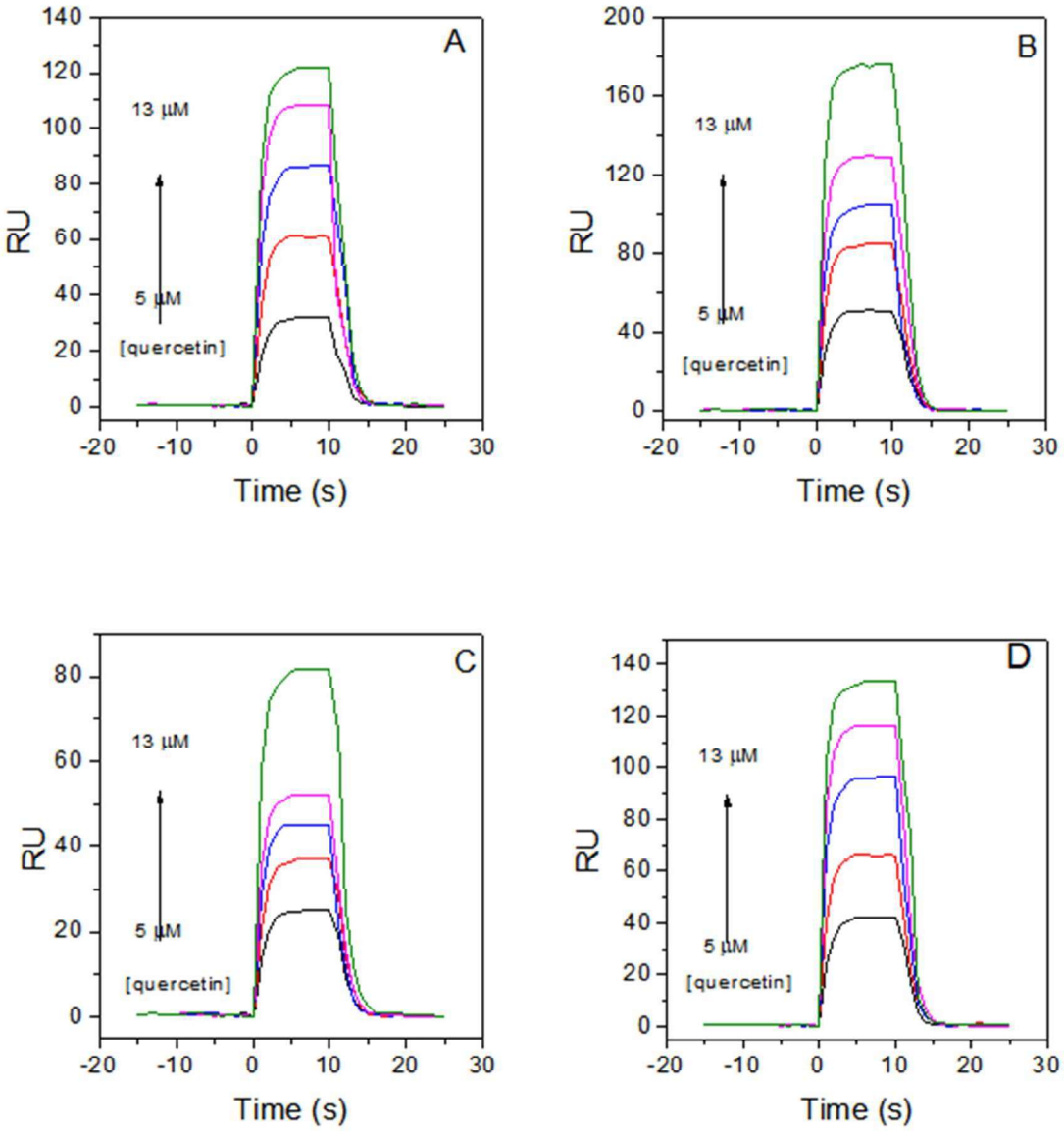

Figure S4. Sensorgrams of immobilized β-casein when it interacts with different concentrations of quercetin (5-13 µM) in the presence of (A) 25 mM, (B) 40 mM, (C) 60 mM and (D) 100 mM of KCl, at 25 °C and a pH of 7.4.

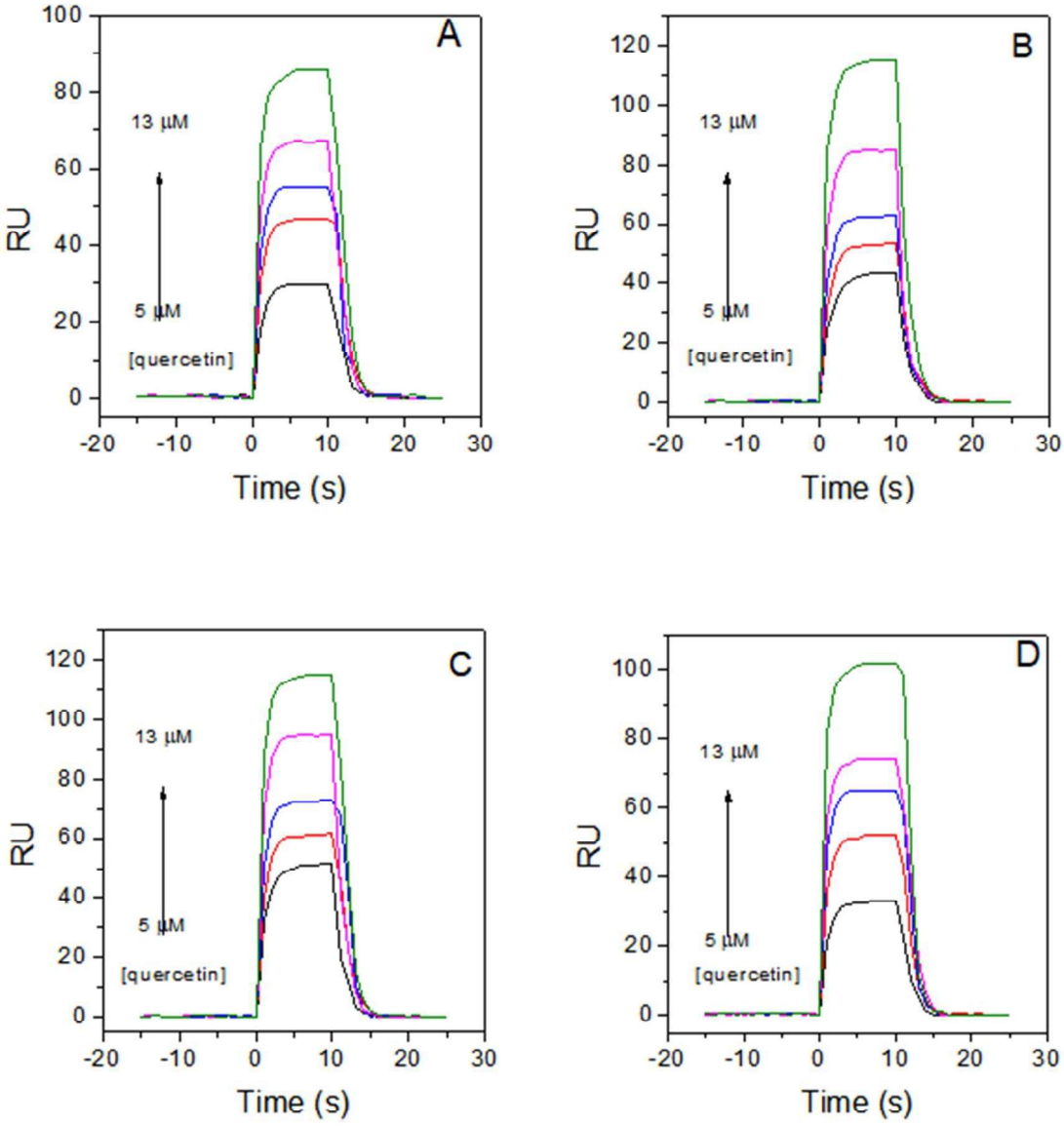

Figure S5. Sensorgrams of immobilized β-casein when it interacts with different concentrations of quercetin (5-13 µM) in presence of (A) 25 mM, (B) 40 mM, (C) 60 mM and (D) 100 mM of KSCN, at 25 °C and a pH of 7.4.

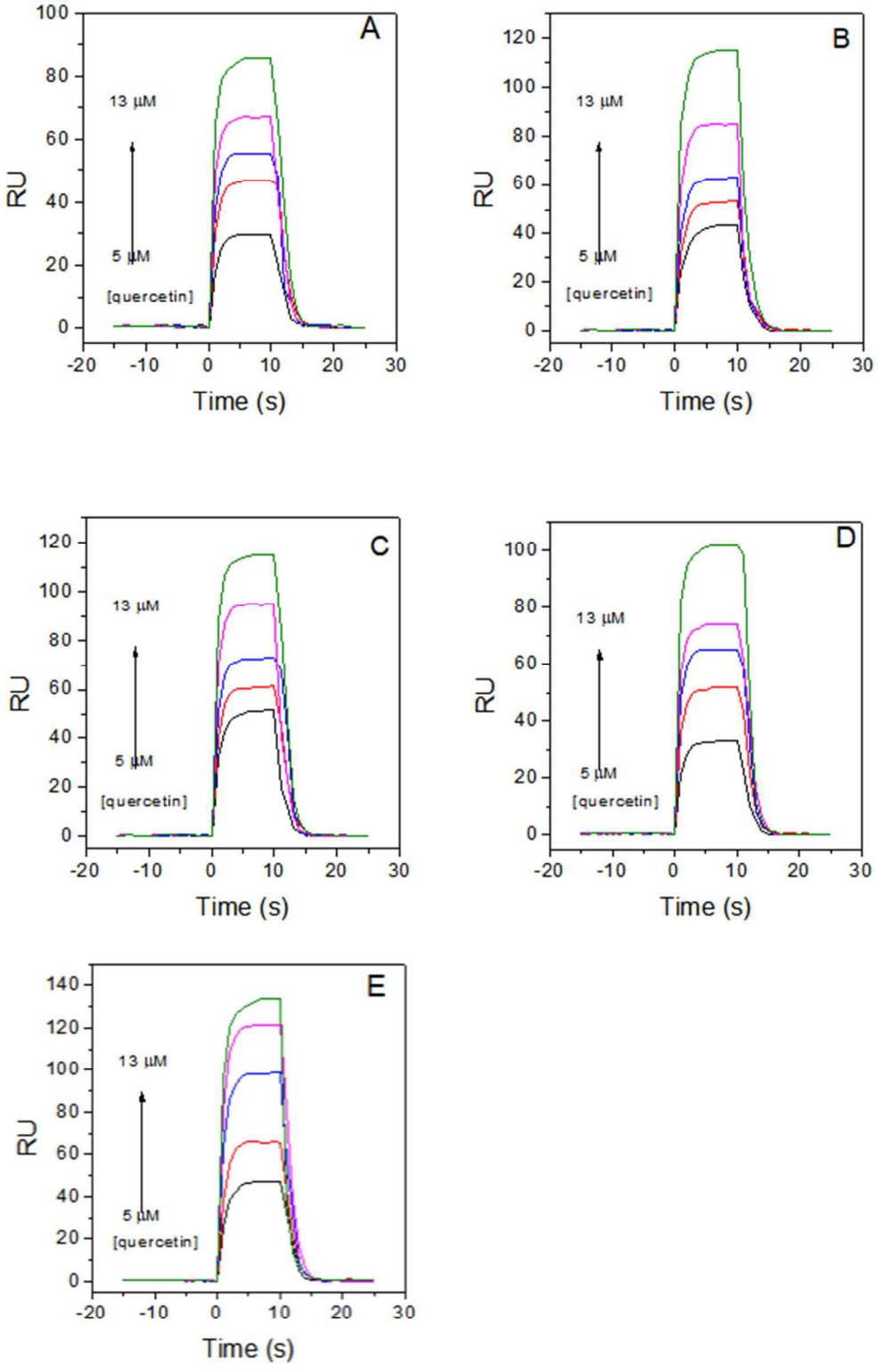

Figure S6. Sensorgrams of immobilized β-casein when it interacts with different concentrations of quercetin (5-13 µM) in the presence of (A) 25 mM, (B) 40 mM, (C) 60 mM, (D) 80 mM and (E) 100 mM of KCl, at 12 °C and a pH of 7.4.

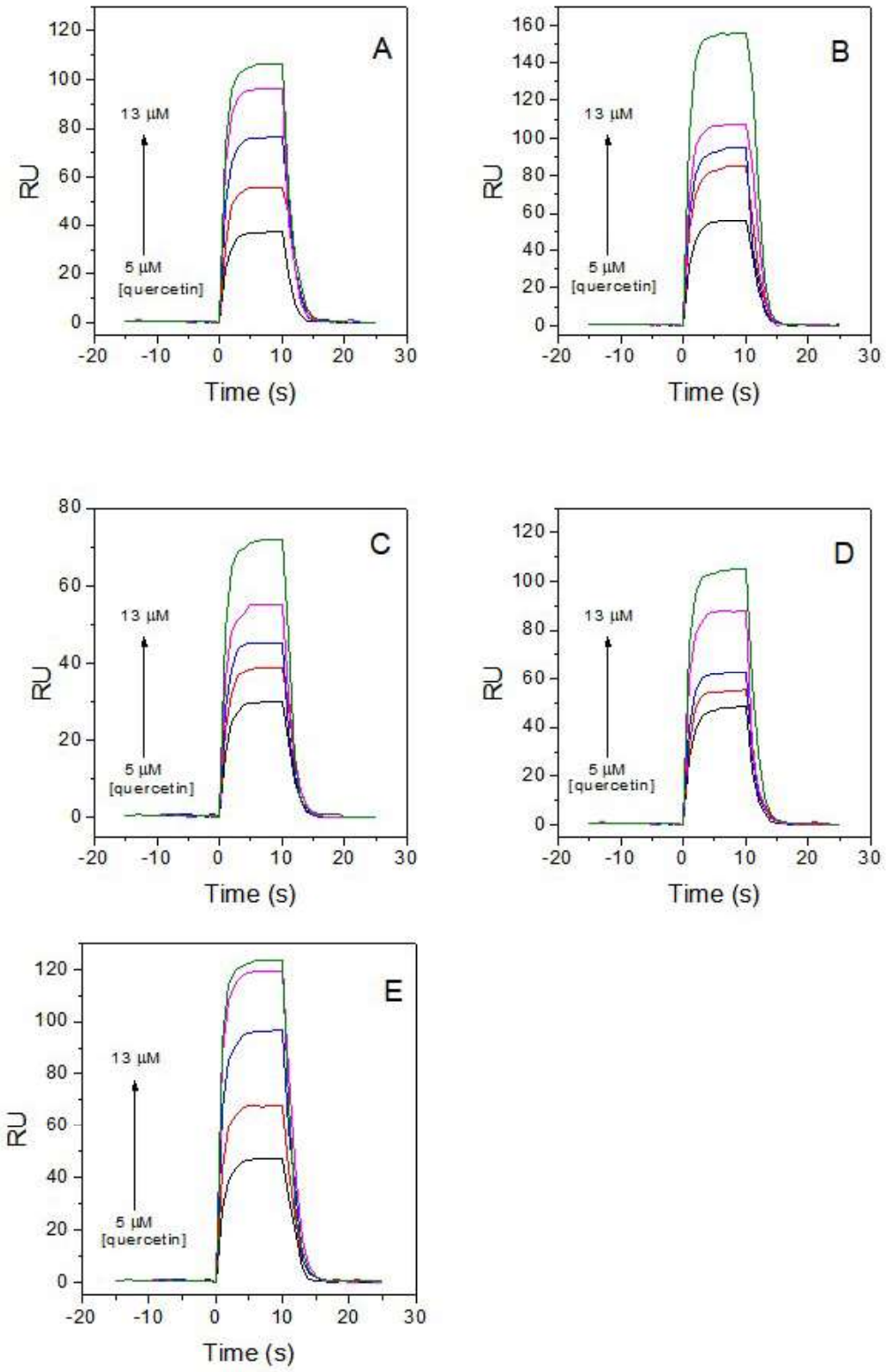

Figure S7. Sensorgrams of immobilized β-casein when it interacts with different concentrations of quercetin (5-13 µM) in the presence of (A) 25 mM, (B) 40 mM, (C) 60 mM, (D) 80 mM and (E) 100 mM of KCl, at 16 °C and a pH of 7.4.

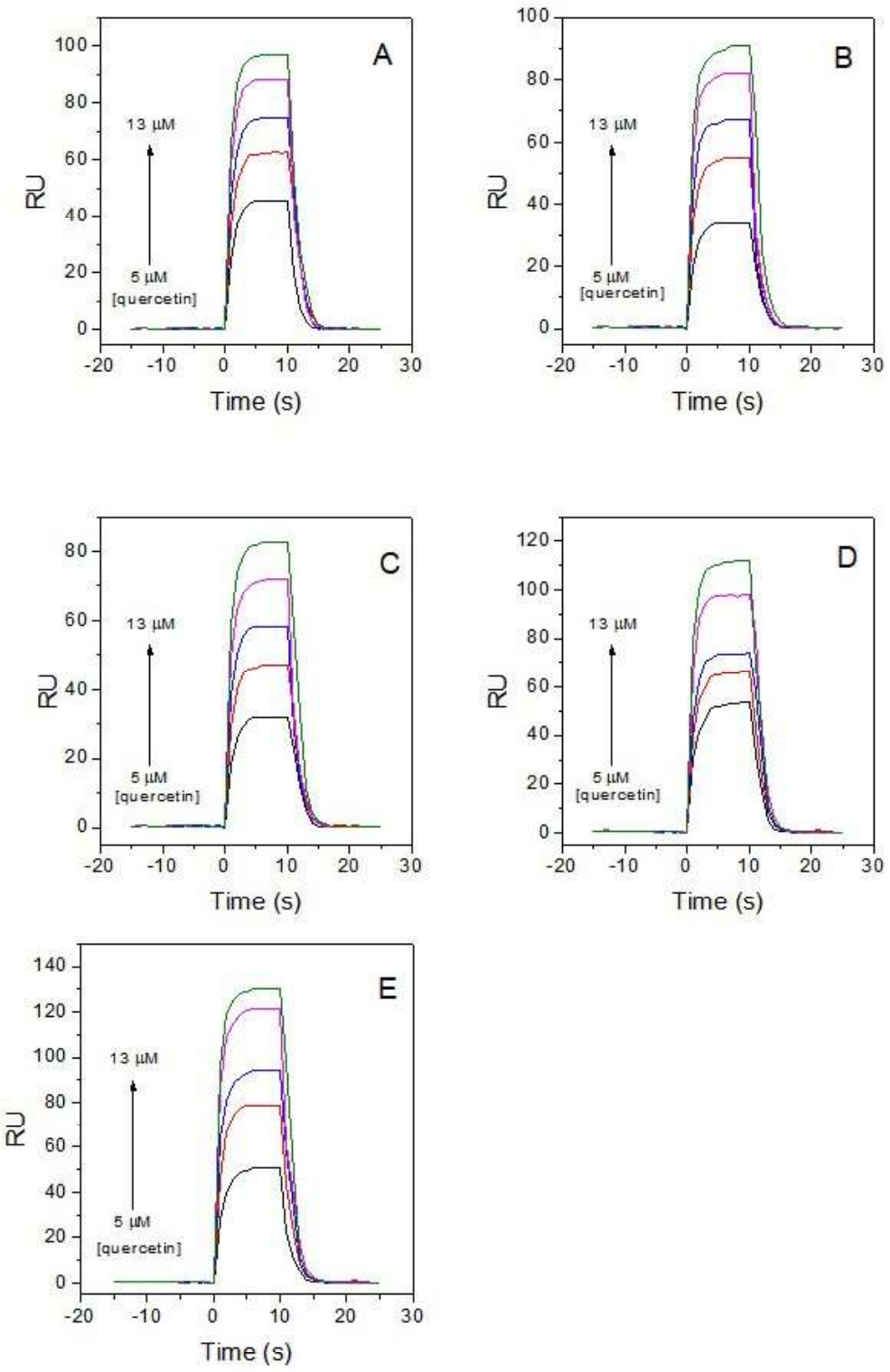

Figure S8. Sensorgrams of immobilized β-casein when it interacts with different concentrations of quercetin (5-13 µM) in the presence of (A) 25 mM, (B) 40 mM, (C) 60 mM, (D) 80 mM and (E) 100 mM of KCl, at 20 °C and a pH of 7.4.

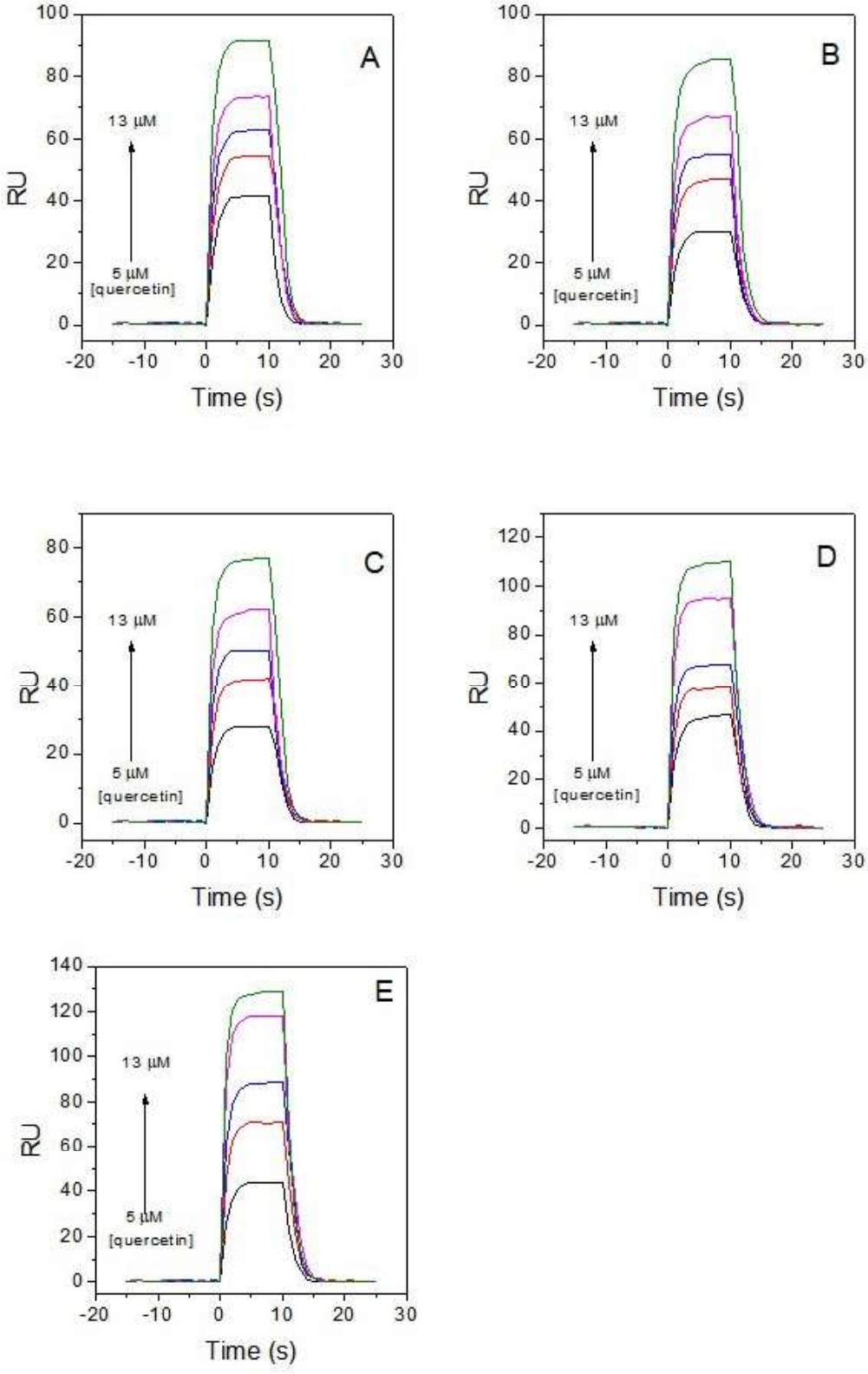

Figure S9. Sensorgrams of immobilized β-casein when it interacts with different concentrations of quercetin (5-13 µM) in the presence of (A) 25 mM, (B) 40 mM, (C) 60 mM, (D) 80 mM and (E) 100 mM of KCl, at 24 °C and a pH of 7.4.

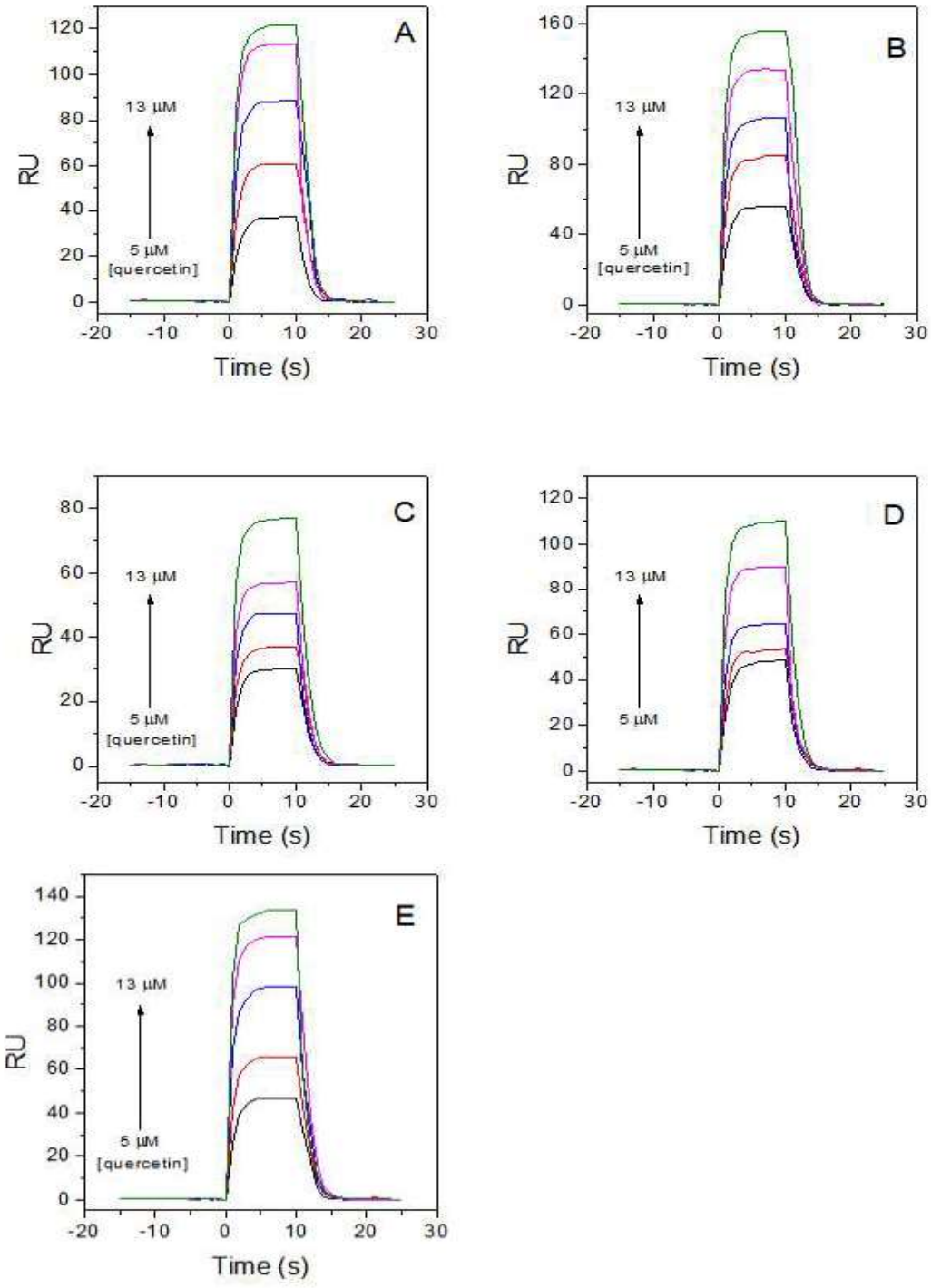

Figure S10. Sensorgrams of immobilized β-casein when it interacts with different concentrations of quercetin (5-13 µM) in the presence of (A) 25 mM, (B) 40 mM, (C) 60 mM, (D) 80 mM and (E) 100 mM of KCl, at 28 °C and a pH of 7.4.

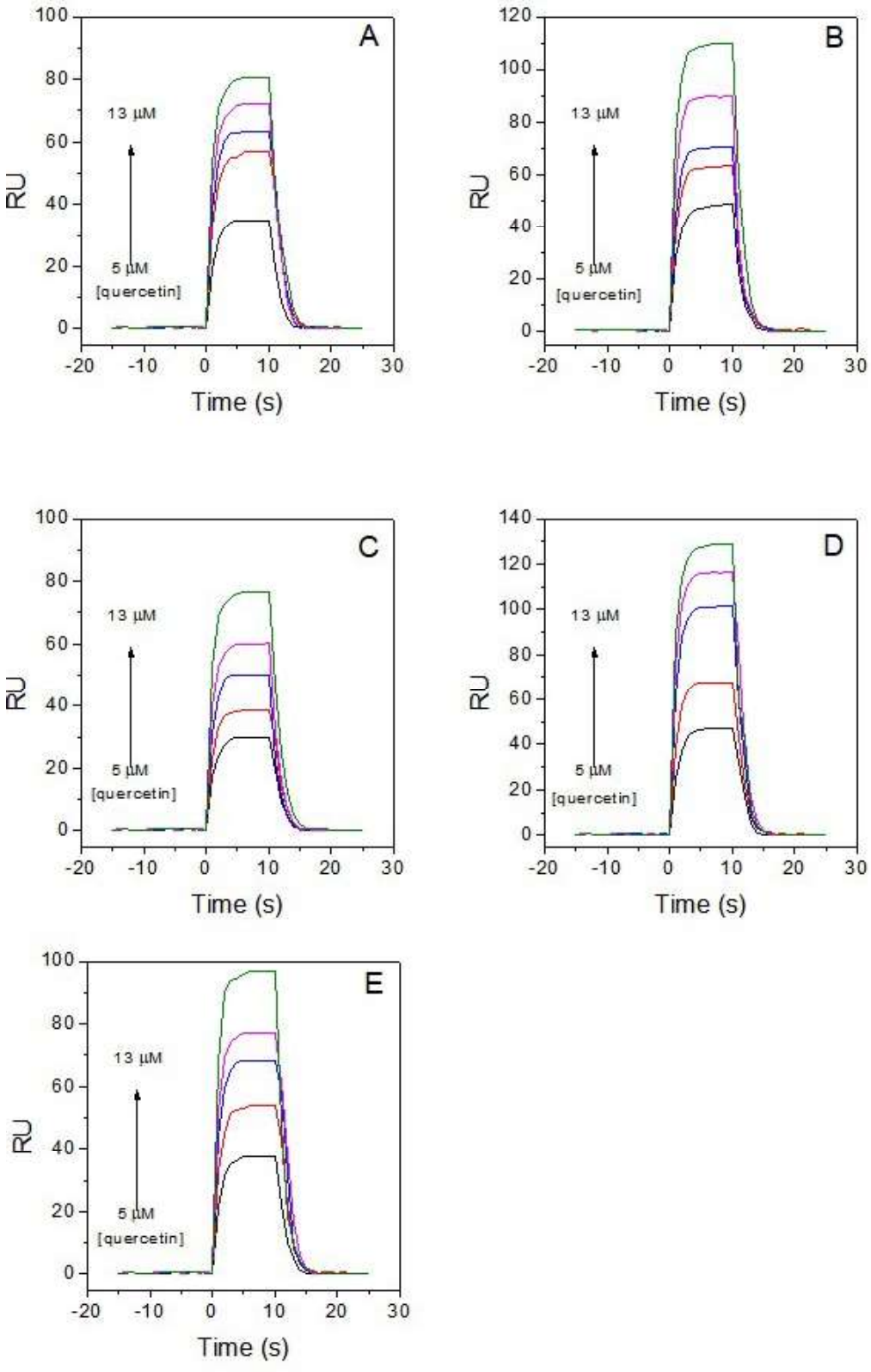

Figure S11. Sensorgrams of immobilized β-casein when it interacts with different concentrations of quercetin (5-13 µM) in the presence of (A) 25 mM, (B) 40 mM, (C) 60 mM, (D) 80 mM and (E) 100 mM of KSCN, at 12 °C and a pH of 7.4.

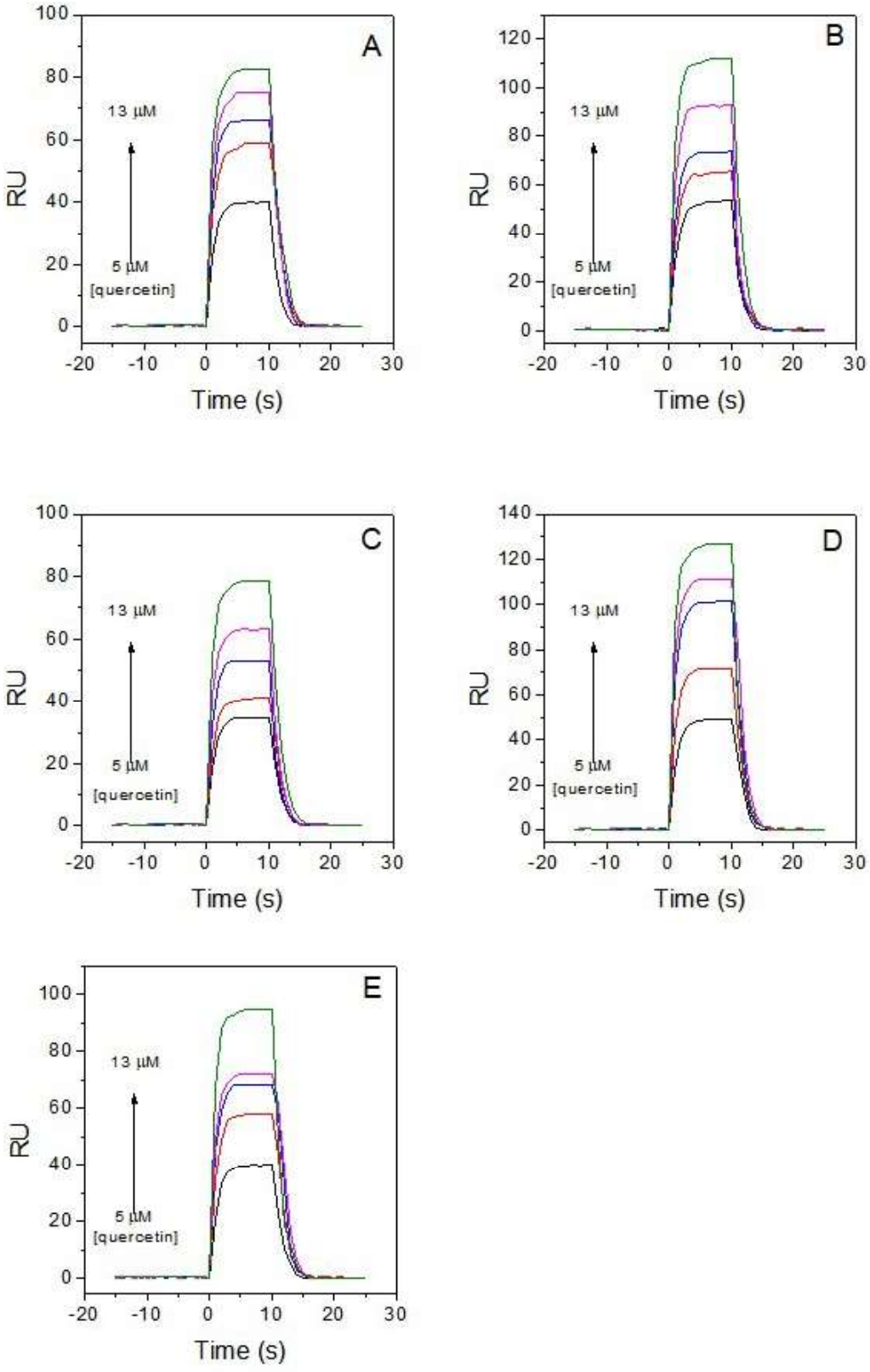

Figure S12. Sensorgrams of immobilized β-casein when it interacts with different concentrations of quercetin (5-13 µM) in the presence of (A) 25 mM, (B) 40 mM, (C) 60 mM, (D) 80 mM and (E) 100 mM of KSCN, at 16 °C and a pH of 7.4.

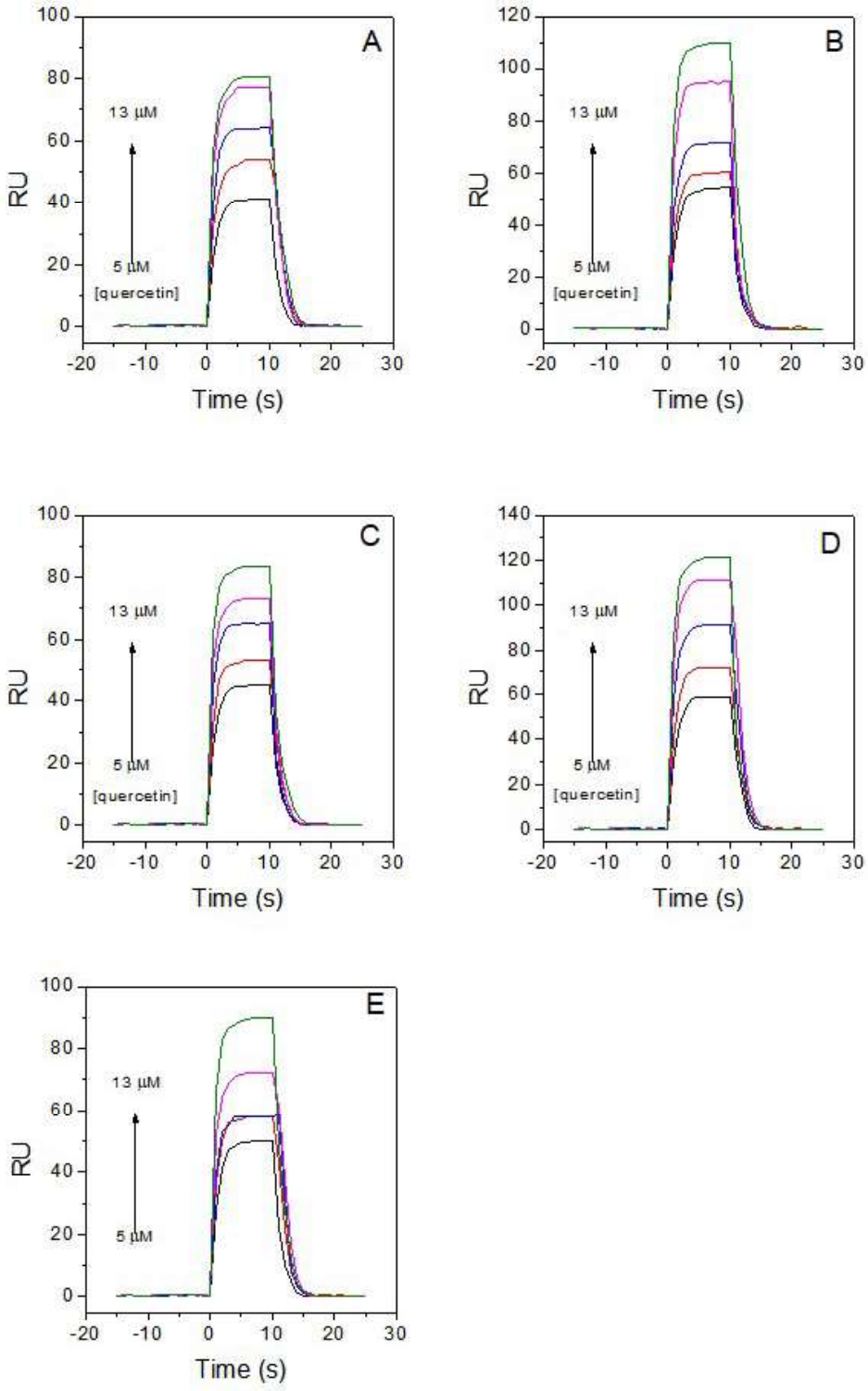

Figure S13. Sensorgrams of immobilized β-casein when it interacts with different concentrations of quercetin (5-13 µM) in the presence of (A) 25 mM, (B) 40 mM, (C) 60 mM, (D) 80 mM and (E) 100 mM of KSCN, at 20 °C and a pH of 7.4.

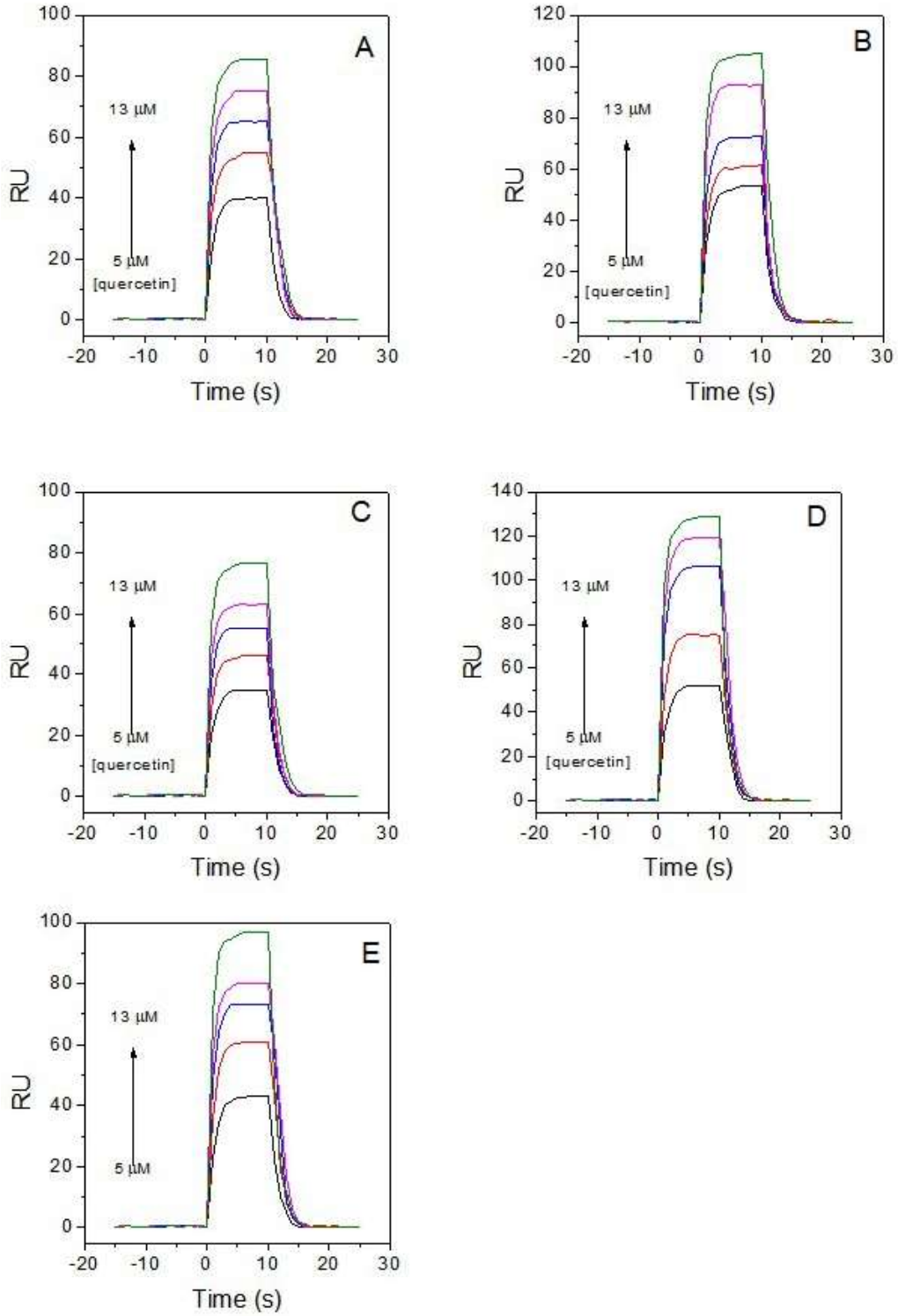

Figure S14. Sensorgrams of immobilized β-casein when it interacts with different concentrations of quercetin (5-13 µM) in the presence of (A) 25 mM, (B) 40 mM, (C) 60 mM, (D) 80 mM and (E) 100 mM of KSCN, at 24 °C and a pH of 7.4.

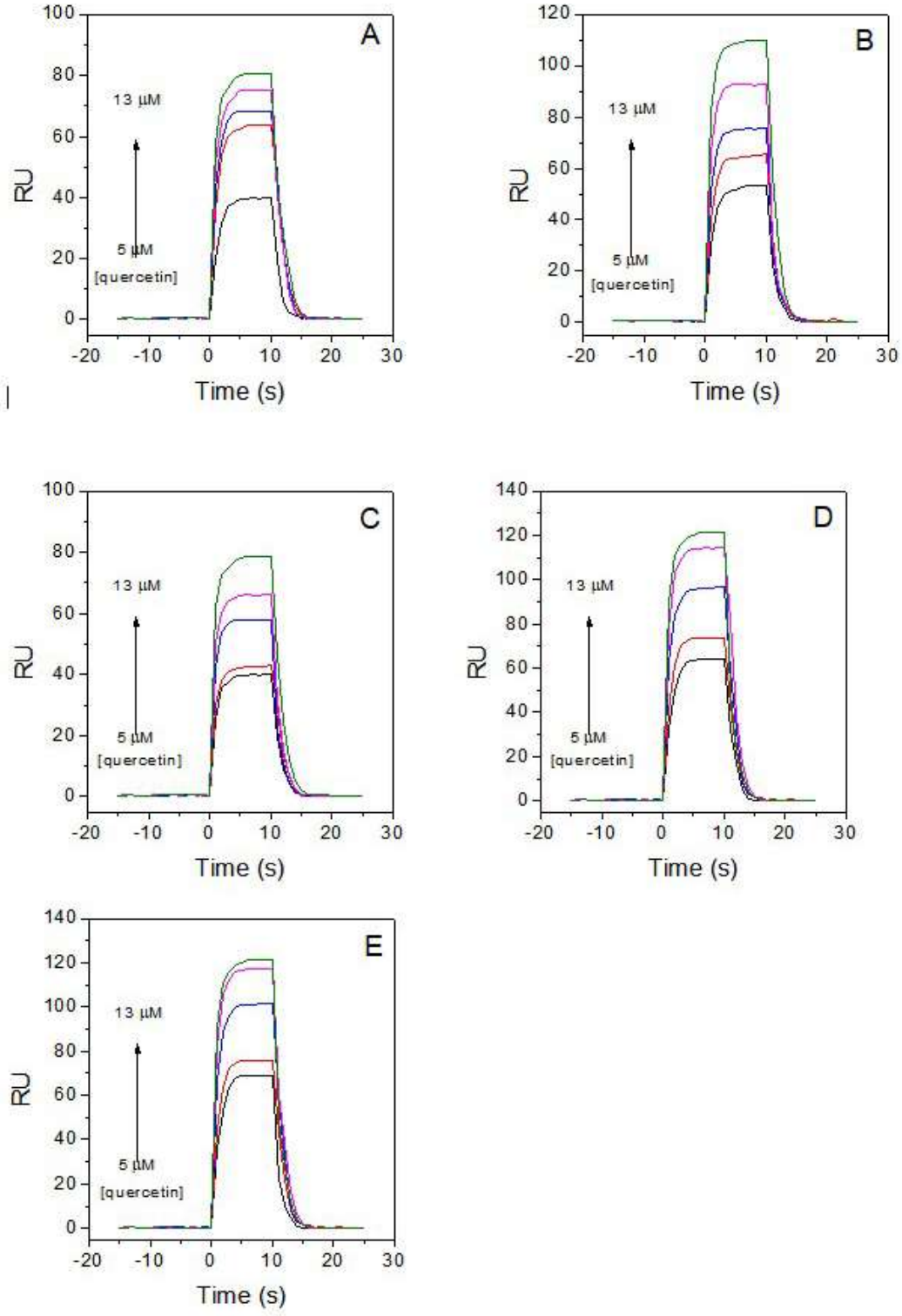

Figure S15. Sensorgrams of immobilized β-casein when it interacts with different concentrations of quercetin (5-13 µM) in the presence of (A) 25 mM, (B) 40 mM, (C) 60 mM, (D) 80 mM and (E) 100 mM of KSCN, at 28 °C and a pH of 7.4.

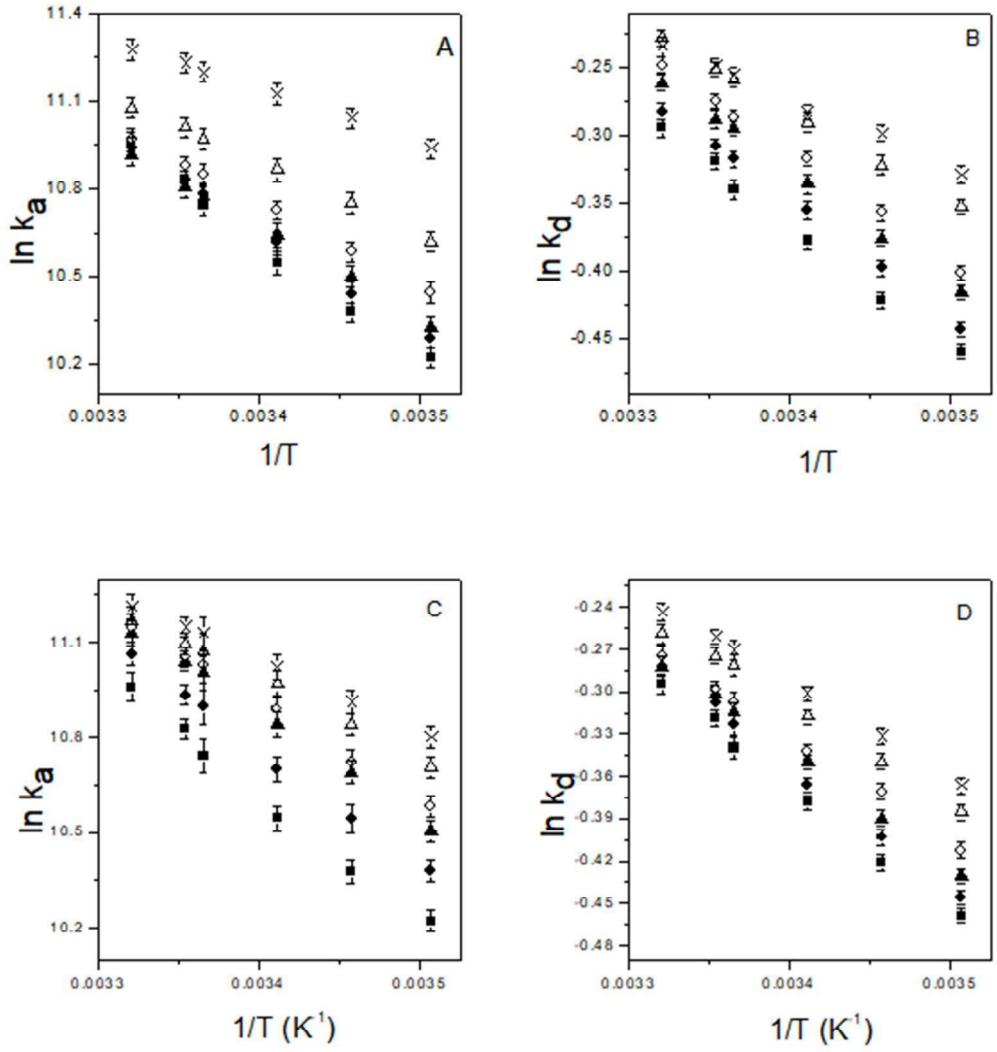

Figure S16. Arrhenius plot for β-casein/quercetin interaction. (A) ln k_a and (B) ln k_d in the presence of KCl, (C) ln k_a and (D) ln k_d in the presence of KSCN, both at the following concentrations: (■) 0 mM, (●) 25 mM, (▲) 40 mM, (○) 60 mM, (Δ) 80 mM, (x) 100 mM.

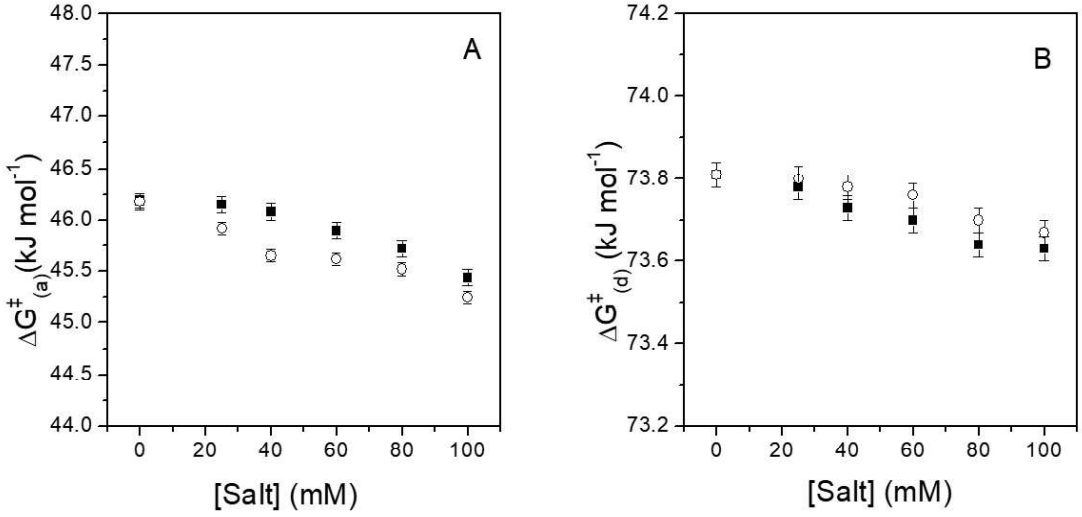

Figure S17. Activated Gibbs free energy change ($\Delta G^{\ddagger}$) related to activated complex formation for (A) association and (B) dissociation steps *versus* [KCl] (■) or [KSCN] (○).

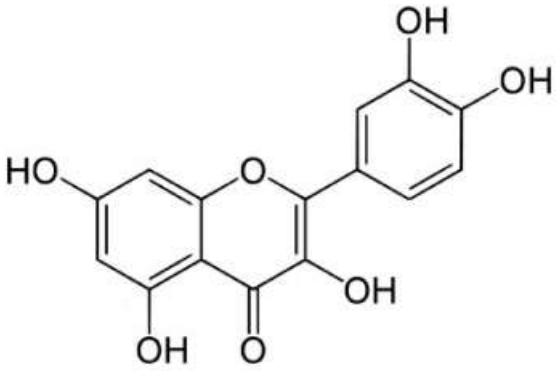

Figure S18. Chemical structure of quercetin.

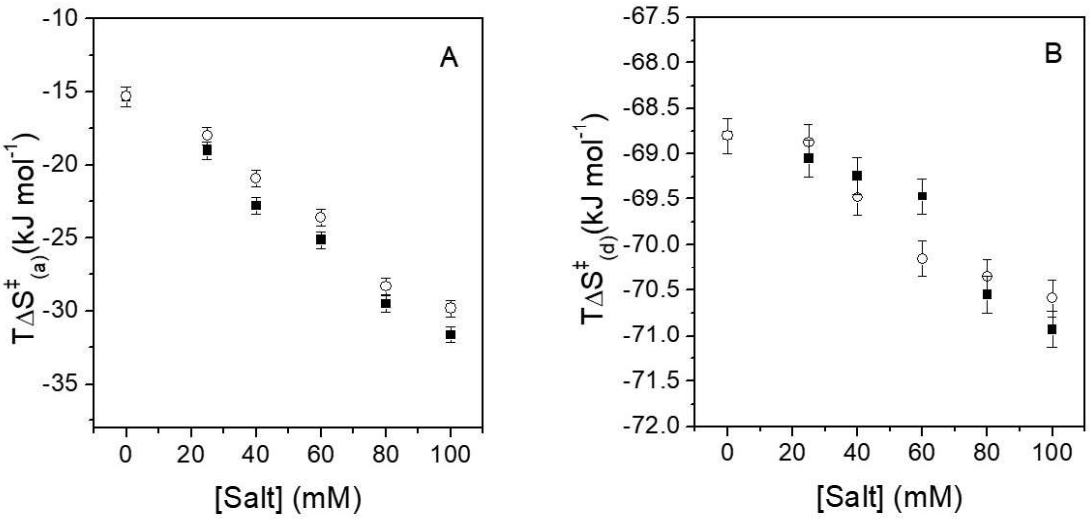

Figure S19. Activated entropy changes ($T\Delta S^{\ddagger}$) related to active complex formation between β-casein and quercetin in the (A) association and (B) dissociation steps *versus* KCl (■) or KSCN (○), at 25 °C.

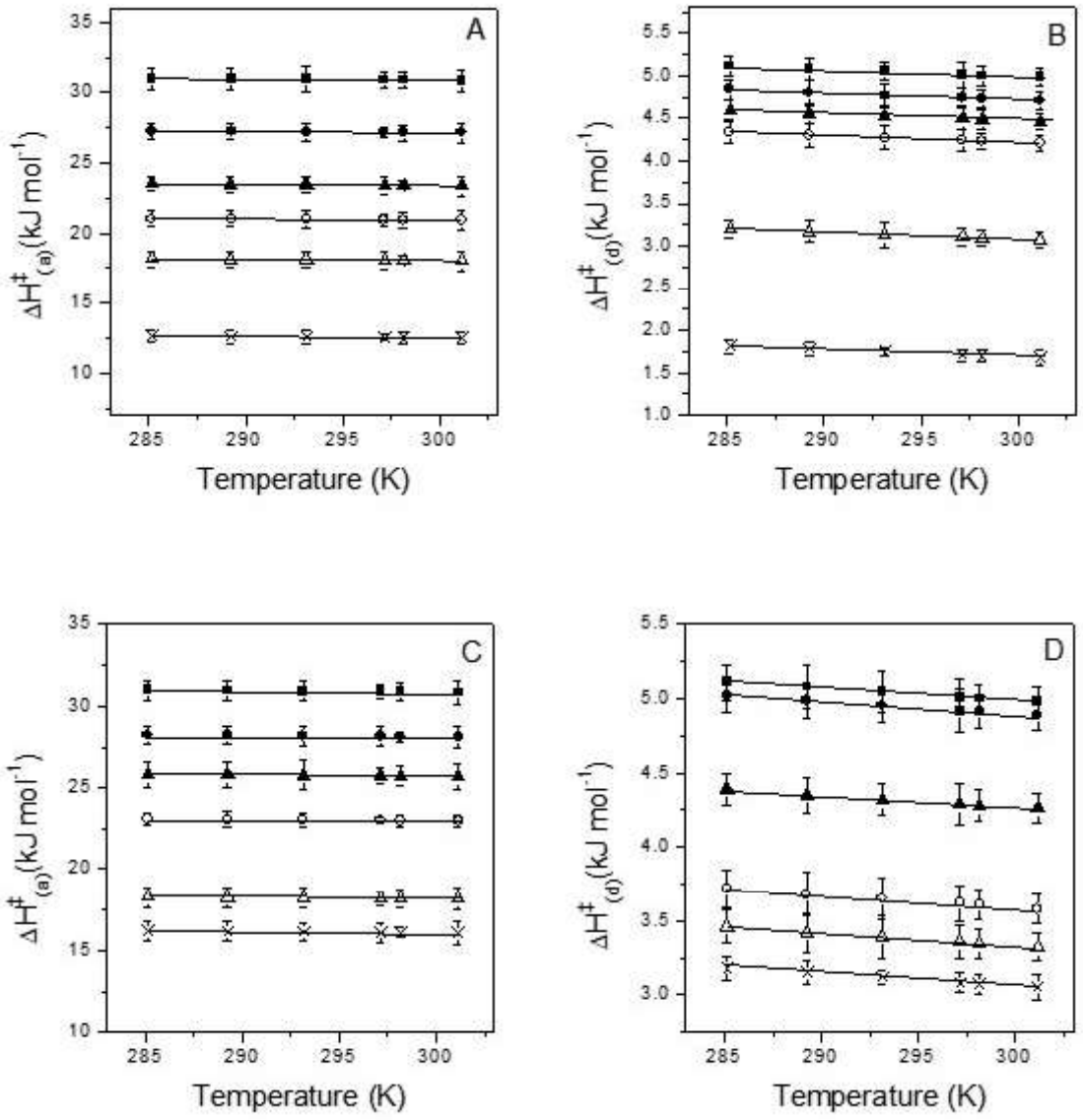

Figure S20. Effect of salt on the dependence of activation enthalpy change ($\Delta H^{\ddagger}$) on temperature. Effect of KCl on the association (A) and dissociation (B) steps of β-casein and quercetin activated complex formation. Effect of KSCN on the association (C) and dissociation (D) steps of of β-casein and quercetin activated complex formation. Salts concentrations were (■) 0 mM, (●) 25 mM, (▲) 40 mM, (○) 60 mM, (Δ) 80 mM, (x) 100 mM.

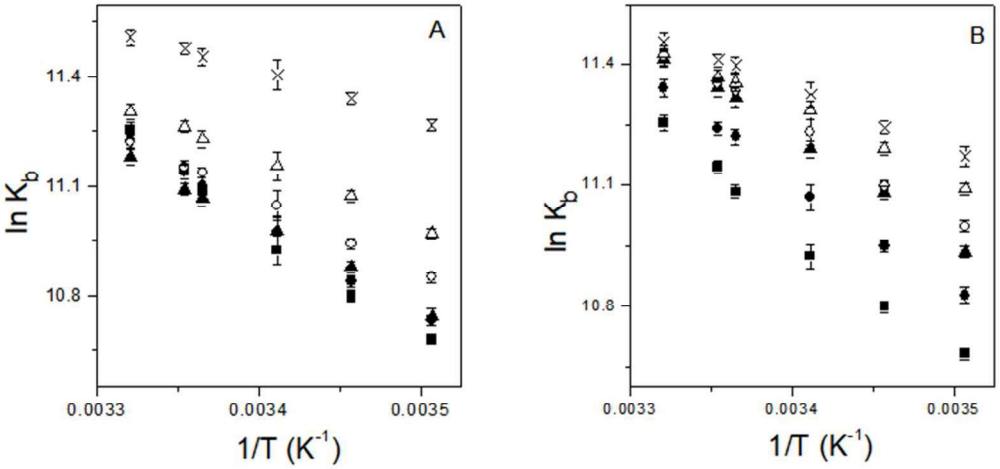

Figure S21. The van't Hoff plots for interaction between β-casein and quercetin at pH 7.4 and different temperatures in the presence of KCl (A) and KSCN (B) at the following concentrations: (■) 0 mM, (●) 25 mM, (▲) 40 mM, (○) 60 mM, (Δ) 80 mM, (x) 100 mM.

ARTICLE 3

The effect of resveratrol chemical structure on the polyphenol-β-cyclodextrin-NH_2 supramolecular complex formation kinetics

Article submitted to the journal *Food Chemistry*

Abstract

The determination of the molecular mechanism of β-cyclodextrin-polyphenol supramolecular complex formation is of great significance, thus, kinetic studies are required. The kinetics of interaction between modified β-cyclodextrin (β-CD-NH_2) and resveratrol (RES), as well as its structural analog (RESAn1), were determined by surface plasmon resonance. RESAn1 inclusion, as well as the β-CD-NH_2 complex dissociation, was found to be faster than a similar process for RES ($k_a^{\beta-CD-\ {}_2/RESAn}$ = 3.10x10^4 M^{-1}s^{-1}, $k_a^{\beta-CD-\ {}_2/RES}$= 1.87 x10^3 M^{-1}s^{-1}; $k_d^{\beta-CD-NH_2/RE}$ = 0.39 s^{-1}, $k_d^{\beta-CD-\ {}_2/RES}$= 0.30 s^{-1}, at 25 °C). The polyphenol structural differences affected the activated complex formation (ACF) energetic parameters of association more than those of dissociation ($E_{act,a}^{\beta-CD-\ {}_2/RES}$ =14.81 kJ·mol^{-1}, $E_{act,a}^{\beta-CD-\ {}_2/RESAn1}$ = -15.01 to 82.35 kJ·mol^{-1}), ($E_{act,d}^{\beta-CD-\ {}_2/RES}$ = 5.19 kJ·mol^{-1} and $E_{act,d}^{\beta-CD-NH_2/RESAn1}$ = 6.29 kJ·mol^{-1}). These parameters differences are mainly due to the desolvation process of interacting molecules, verified by the isokinetic behavior observed in the association step. These results contribute to the elucidation of the dynamics of the molecular inclusion of β-CD with small molecules.

Keywords: activated complex; inclusion complex; β-cyclodextrin; resveratrol; structural analog.

Chemical compounds studied in this article:

β-cyclodextrin (PubChem CID: 444041); Resveratrol (PubChem CID: 445154)

1. Introduction

The formation of complexes between two or more molecules with unique structural characteristics *via* non-covalent interactions is described by supramolecular chemistry. Host-guest chemistry is popular in the biochemical, biomedical, and chemistry fields (TEYSSANDIER; FEYTER; MALI, 2016). In host-guest chemistry, the macrocyclic organic class of cyclodextrins (CDs) is of particular interest because of its availability, safety, and specific structural characteristics, which confer to them the ability to form unique molecular and supramolecular structures (PROCHOWICZ; KORNOWICZ; LEWIŃSKI, 2017).

CDs are cyclic oligosaccharides formed by D-(+)-glucopyranosyl units linked by *α*-1,4-glycosidic bonds. Natural CDs comprise α-, β-, and γ-CDs, which are composed of six, seven, or eight glucose residues, respectively (LIMA et al., 2016). The chair conformation of the glucopyranosyl residues gives CDs the shape of truncated cones, where the primary hydroxyl groups of the glucose residues are at the narrow edges, while the secondary hydroxyl groups are at the wider edges. In addition, the ethereal oxygen and skeletal carbons of the sugar residues are directed towards the central cavity of the natural CDs, giving this region a partial hydrophobic character (JAMBHEKAR; BREEN, 2016). This property gives CDs the ability to form inclusion complexes (ICs) with molecules of low water solubility, such as polyphenolic compounds. The ICs improve the physicochemical and pharmacodynamic properties of these compounds, including water solubility (ROY et al., 2018), antioxidant activity (HO et al., 2017), photostability (KFOURY et al., 2016), and bioavailability (PURPURA et al., 2018).

Resveratrol *trans*-3,4,5′-trihydroxystilbene (RES, Figure 1a) is a polyphenolic exemplar from the oligomeric stilbenoids found in wines and some foods that have numerous biological activities (KEYLOR; MATSUURA; STEPHENSON, 2015). However, the food and nutraceutical use of RES is limited by disadvantageous properties, including low water solubility, chemical instability, and low bioavailability (GUO; YIN; CHEN, 2018). In order to alleviate these disadvantages, IC between RES and β-CD have been extensively studied (BERTACCHE et al., 2006; LU et al., 2009b; LUCAS-ABELLÁN et al., 2007; TROCHE-PESQUEIRA et al., 2013). Among the native CDs, β-CD is commonly used as a carrier because of its suitable cavity size, better IC formation ability, greater availability, and lower cost (DAS; SUBUDDHI, 2015).

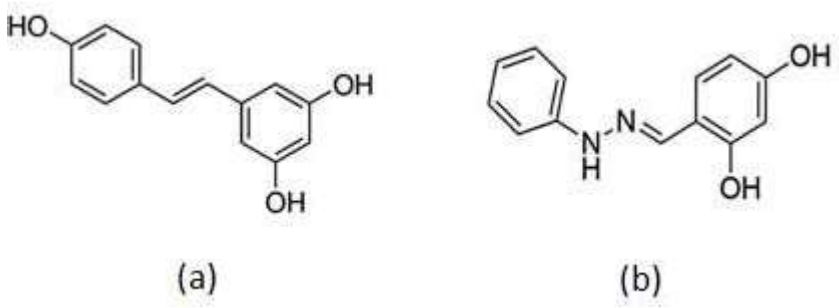

Figure 1. Chemical structures of resveratrol (a) and its analog 2,4-dihydroxybenzaldehyde phenylhydrazone (RESAn1) (b).

IC formation between RES and β-CD improved the solubility, chemical stability, photostability, and antioxidant activity of polyphenols (BERTACCHE et al., 2006; LU et al., 2009b; LUCAS-ABELLÁN et al., 2007). The thermodynamics of the formation of β-CD/RES IC have also been studied. López-Nicolás & García-Carmona (2008) found an enthalpically driven β-CD/RES IC formation process at pH 7.0 ($\Delta H°$ = -22.56 kJ·mol^{-1} − and $T\Delta S°$ = -12.30 kJ·mol^{-1}) using HPLC. Similar results were obtained by Li et al. (2010), who studied IC formation in water using isothermal titration calorimetry ($\Delta H°$ = -26.16 kJ·mol^{-1} and $T\Delta S°$ = -9.16 kJ·mol^{-1}). Fluorescence spectroscopy determined the β-CD/RES IC formation process in water, which proved to be enthalpic and entropically driven ($\Delta H°$ = -4.0 kJ·mol^{-1} and $T\Delta S°$ = 48.25 kJ·mol^{-1}) (LU et al., 2009a). However, despite these advances, there are no reports concerning the kinetics of IC formation between β-CD and RES in the literature. The association and dissociation rate constants obtained by kinetic analysis are significant for the application of ICs as carriers of bioactive molecules to physiological targets (SINGH et al., 2017), as the most stable complex may not always be formed quickly. Moreover, the combination of thermodynamic and kinetic parameters provide more detailed information on IC formation, including data regarding both the thermodynamically stable IC as well as its intermediate states.

In addition, because the structure of guest molecules have a significant impact on IC formation (AL OMARI et al., 2010), we believe that evaluating the IC formation between β-CD and an analog of RES is a strategic approach to determine the structural effects of guest molecules. The 2,4-dihydroxybenzaldehyde phenylhydrazone (RESAn1, Figure 1b) is a structural analog of RES in which the central C=C stilbenoid linkage in RES is substituted by a hydrazone. This analog polyphenol displays the biological activities of RES (antioxidant, anticarcinogenic, anti-inflammatory, etc.) and additional antileishmanial activity. In addition, it has greater bioavailability than RES (DA SILVA et al., 2019). Rezende et al. (2020) studied

the interaction between the human serum albumin (HSA) and RES with RESAn1 and found that this small change in the polyphenolic structure resulted in changes in the HSA-poyphenol complex formation kinetics ($\Delta H_a^{\ddagger\,HSA/RES}$ = 9.0 kJ·mol^{-1}, $\Delta H_a^{\ddagger\,HSA/RESAn1}$ = 28.0 kJ·mol^{-1}) and thermodynamics ($\Delta H_a^{\circ\,HSA/RES}$ = 14.4 kJ·mol^{-1}, $\Delta H_a^{\circ\,HSA/RESAn}$ = 36.0 kJ·mol^{-1}).

Therefore, our main objective was to examine the kinetics of the β-CD/RES IC formation and the effect of the guest structure on the interaction between β-CD and an RES analog (RESAn1), using real-time analysis provided by surface plasmon resonance (SPR). To enable the immobilization of β-CD on the SPR chip surface, the cyclic oligosaccharide structure was functionalized via addition of an amine group (β-CD-NH_2) (da Silva et al., 2019). β-CD-NH_2 was used for all experiments of interaction with RES and RESAn1 in this work.

2. Material and methods

2.1. Material

β-Cyclodextrin (≥ 97 %wt.), resveratrol (≥ 99 %wt.), analytical grade sodium acetate, dimethyl sulfoxide (DMSO), iodine, triphenylphosphine, imidazole, and ethylenediamine were purchased from Sigma-Aldrich (USA). The analog of resveratrol RESAn1 (2,4-dihydroxybenzaldehyde phenylhydrazone) was synthesized following the protocol described by da Silva et al. (2019). Specific products of the Biacore® system (CM5 sensor chips, N-hydroxysuccinimide (NHS), ethanolamine hydrochloride, N-ethyl-N´-(dimethylaminopropyl) carbodiimide (EDC), and HBS-P buffer (pH 7.4)) were purchased from GE Healthcare (USA).

2.2. Obtaining the functionalized β-CD

The synthesis of β-CD functionalized with an amine group (β-CD-NH_2) for polysaccharide immobilization on the SPR sensor chip surface was performed according to the procedures described below. NMR spectra were acquired using a Bruker AVANCE III 500 MHz spectrometer. Chemical shifts (δ) were expressed as ppm relative to tetramethylsilane.

2.2.1. Synthesis of β-CD-6-I

β-CD-6-I was synthesized according to the procedure for iodation of carbohydrates described by Garegg et al. (GAREGG et al., 1982; GAREGG; SAMUELSSON, 1979, 1980), with some modifications. In a round-bottom flask, 300 mg β-CD (0.26 mmol), 74 mg iodine (0.29 mmol), 76 mg triphenylphosphine (0.29 mmol) and 20 mg imidazole (0.29 mmol) were dispersed in 15 mL toluene. The mixture was vigorously stirred at 110 °C for 18 h. The mixture

was the allowed to cool at 298.15K, after which distilled water was added. The two-phase system was stirred for 15 min. The organic phase was then extracted with distilled water in triplicate and the combined aqueous phases were reduced using a rotary evaporator. The solid residue was washed with acetone and then filtered. The remaining solids (insoluble in acetone) were solubilized in a water/methanol mixture (1:3). Acetone was then added dropwise to the solution to precipitate the residual β-CD, which was removed by filtration. The solution was evaporated to yield a brown solid, which was dried in a desiccator; 116 mg (yield = 36 %) of this brown solid was obtained. Applying thin layer chromatography using ethyl acetate/isopropanol/water/ammonium hydroxide (7:7:5:5) as the eluent and a 20 % sulfuric acid solution in ethanol, as visualizing agent, the product was revealed with a retention factor of 0.5. ^{1}H NMR (500 MHz, D_2O) δ 5.08 (d, 7 H, *J* = 3.8 Hz), 3.98 (t, 7 H, *J* = 9.5 Hz), 3.93-3.86 (m, 18 H), 3.78 (t, 1 H, *J* = 4.9 Hz), 3.66 (dt, 7 H, *J* = 9.7, 2.9 Hz), 3.60 (t, 7 H, 9.2 Hz), 3.55 (d, 1 H, *J* = 6.5 Hz), 3.49 (t, 1 H, *J* = 5.3 Hz).

2.2.2. Synthesis of β-CD-6-en

β-CD-6-en (or β-CD-NH_2) was synthesized based on previously described methods (SHENG et al., 2017; SU et al., 2020), where mono-6-deoxy-6-tosyl-β-cyclodextrin was substituted with β-CD-6-I. In a round-bottom flask, 50 mg of β-CD-6-I was dissolved in 10 µL of ethylenediamine (80 % in toluene). The mixture was stirred at 75 °C for 18 h. The resulting oil was washed several times with acetone to remove excess ethylenediamine and acetone-soluble impurities. The remaining solid was dried in a desiccator, and 41 mg of the product was obtained as a brown solid (yield = 85 %). Thin layer chromatography, with ethyl acetate/isopropanol/water/ammonium hydroxide (7:7:5:5) as the eluent and a 20 % sulfuric acid solution in ethanol as the visualizing agent revealed the product with a retention factor of 0.3. ^{1}H NMR (500 MHz, D_2O) δ 5.07 (d, 7 H, *J* = 3.6 Hz), 3.95 (dt, 7 H, *J* = 9.2, 4.8 Hz), 3.88 (d, 7 H, *J* = 3.4 Hz), 3.86-3.83 (m, 12 H), 3.66 (dd, 7 H, *J* = 10.0, 3.4 Hz), 3.29 (t, 7 H, 9.4 Hz), 3.36 (t, 1 H, *J* = 2.6 Hz), 3.29 (t, 2 H, *J* = 5.7 Hz), 3.07 (t, 1 H, *J* = 2.4 Hz), 3.04 (t, 2 H, *J* = 5.7 Hz). A schematic illustration of the synthesis of the functionalized β-CD is shown in Figure S1.

2.3. Immobilization of the β-CD-NH_2 on the sensor chip surface

SPR analyses were conducted in triplicate in a two-channel Biacore® X100 device (GE Healthcare, USA). A standard covalent amine coupling method was followed for the immobilization of functionalized β-CD (β-CD-NH_2) on the dextran surface of the CM5 sensor

chip. Following the insertion of the sensor chip into the SPR machine, its carboxylic groups were activated *via* the injection of an EDC/NHS (0.4 M/0.1 M) mixture for 7 min. A solution of β-CD-NH_2 (2.6 x 10^{-5} M prepared in 10 mM sodium acetate, pH 4.0) was then injected into the sample channel at a flow rate of 10 μL·min^{-1} for 7 min, resulting in a low-density immobilization of approximately 1200 RU, which contributed to the reduced mass transport and crowding phenomena (TERAN; NUGENT, 2019). The carboxylic groups that did not interact with the amine group of β-CD-NH_2 were inactivated by the injection of 1 M ethanolamine for 7 min. In one of the two channels of the SPR device no β-CD-NH_2 was immobilized, thus becoming the reference channel. The carboxylic groups of the reference channel were activated and deactivated, as was done in the sample channel.

2.4. Monitoring the IC formation

IC formation between β-CD-NH_2 and RES or RESAn1 was monitored at six temperatures (12, 16, 20, 24, 25, and 28 °C). HBS-P buffer (0.01 M HEPES pH 7.4, 0.15 M NaCl, and 0.005 %v/v surfactant P20) and DMSO (4 %v/v) were used to prepare the RES and RESAn1 solutions, which were injected into the sample and reference chip channels at a flow rate of 10 μL·min^{-1} for 30 s. Each analysis cycle for all RES or RESAn1 concentrations consisted of injection of the buffer (to obtain the baseline), an injection of RES or RESAn1 solution, and buffer flow over both sample and reference channels. A subtraction of the reference and sample channel signals was performed and the net SPR signals (resonance units, RU) were traced over time. A pseudo-first order kinetic model were fitted to the generated curves for a kinetic analysis of the inclusion processes (REZENDE et al., 2019).

3. Results and discussion

3.1. Data output of the SPR measurements for β-CD-NH_2 and RES or RESAn1 inclusion

The molecular process of IC formation is determined by the contributions of energetic (thermodynamic) and kinetic aspects. The determination of equilibrium parameters as well as the measurement of kinetic properties are essential for elucidating the mechanism of molecular inclusion (BOHNE, 2014). The elucidation of the molecular dynamics that occur during the association and dissociation processes is the basis for supramolecular system formation and in vivo functions of drug-CD complexes (SINGH et al., 2017). Herein, a real-time analysis of the inclusion complex formation between β-CD-NH_2 (ligand or “host” molecule) and RES or RESAn1 (analytes or “guest” molecules) was performed using SPR experiments. This

technique is based on the variation in the mass on the sensor chip surface as the analyte molecules interact with the immobilized ligand and induce a change in the refractive index (RI) of the solution in close vicinity (100 nm) to the chip surface. This change in the refractivity significantly alters the initial incident angle (θ_i) at which resonant surface plasmons occur at the chip gold film, to a new specific angle (θ_f), at which the plasmonic resonance re-occurs. The change in the angle, that is, ($\theta_f - \theta_i$), between the sample flow cell (with immobilized β-CD-NH2) and the reference flow cell (without immobilized β-CD-NH_2), was used to calculate the "resonance units", RU ($RU = (\theta_f - \theta_i)_{sample} - (\theta_f - \theta_i)_{reference}$) (SCHNEIDER et al., 2015). The monitoring of RU over time allows the characterization of intermolecular interactions (NIEGELHELL et al., 2018). In our SPR experiments, the analyte solutions (RES or RESAn1) were injected at variable concentrations over the sensor chip surfaces with and without immobilized β-CD-NH_2, at temperatures ranging between 12 to 28 °C and at a pH 7.4. The resultant sensorgrams (RU versus time) at 25 °C are shown in Figure 2, while the sensorgrams at other temperatures are presented in Figures S2 and S3 (Supplementary Material).

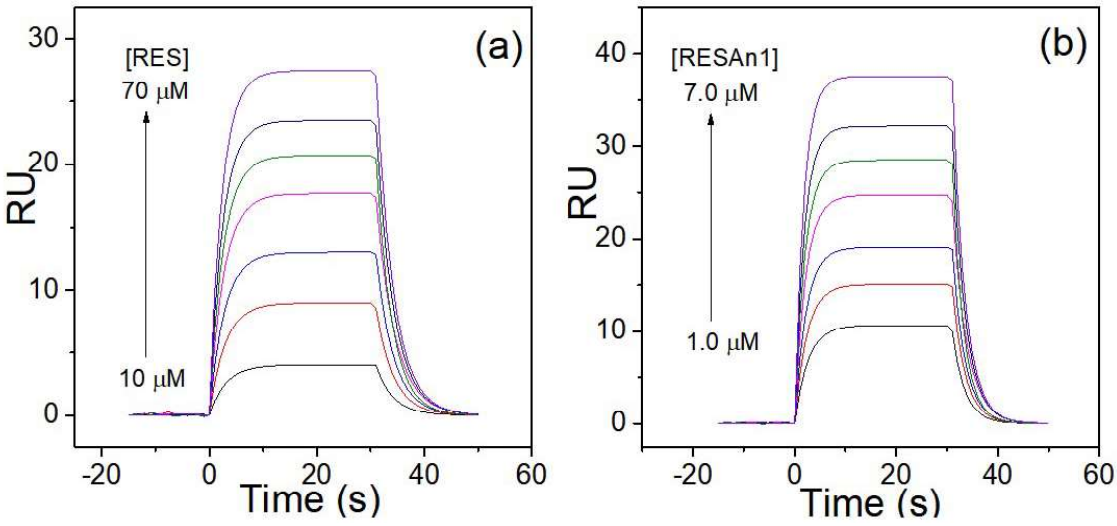

Figure 2. Sensorgrams of immobilized β-CD-NH_2 interacting with (a) resveratrol (RES) ranging from 10 to 70 µM and (b) its analog 2,4-dihydroxybenzaldehyde phenylhydrazone (RESAn1) ranging from 1 to 7 µM, at pH 7.4 and 25 ºC.

The real-time association between free interacting molecules or the break of thermodynamically stable complexes induced a temporal change in the RU values. Thus, while

only the buffer flowed over the chip surfaces (with and without immobilized β-CD-NH_2), the RU values obtained from the difference between both signals remained equal to zero, increasing exponentially as the chip surface was exposed to the analyte (RES or RESAn1). This exponential increase results from the simultaneous processes of association between free β-CD-NH_2 and the analytes and dissociation of the thermodynamically stable [β-CD-NH_2 /RES]° or [β-CD-NH_2 /RESAn1]° complexes. The flow of the analyte solution over the chip surface was maintained until a state of metastable equilibrium was reached, in which the association rate is ≅ the dissociation rate; this was followed by the cessation of the flow of the analyte solution. The buffer flow was then restarted, resulting in the dissociation of the thermodynamically stable complexes formed on the chip surface, promoting an exponential reduction in the RU values over time. The sensorgram profile discussed above confirms the occurrence of the β-CD-NH_2/RES and β-CD-NH_2/RESAn1 complex formation. The global sensorgram data for all analyte concentrations were used to calculate the kinetics of association and dissociation of the ligand-analyte systems, as follows.

3.2. Determination of kinetic association and dissociation rate constants of β-CD-NH_2 /RES or RESAn1 IC formation

It has been established that RES binds to β-CD with a 1:1 stoichiometric ratio (LÓPEZ-NICOLÁS; GARCÍA-CARMONA, 2008; TROCHE-PESQUEIRA et al., 2013). Consequently, for the calculation of the association (k_a) and dissociation (k_d) rate constants, we assumed the bimolecular interaction model "$L + A \leftrightarrows LA$", in which "$L$" represents the immobilized ligand β-CD-NH_2, "A" represents the unbound analyte molecule (RES or RESAn1), and "LA" is the ligand-analyte complex formed. Assuming a pseudo-first-order model for the association process and a first-order model for the dissociation processes, we can apply the overall rate law described in Eq. 1 for the exponential ascendant section of the sensorgrams (REZENDE et al., 2019).

$$\partial[LA]/\partial t = k_a[L][A] - k_d[LA] \quad (1)$$

Assuming that the RU value is proportional to the number of complexes formed ($[LA]$), and that the flow of the analyte solution results in the saturation of the β-CD-NH2 binding sites (RU_{max}) given an infinite amount of time, Eq. 1 can be rewritten as follows (Eq. 2):

$$\partial RU(t)/\partial t = k_a\, RU_{max}(t_\infty) - RU(t) \cdot [A] - k_d\, RU(t) \quad (2)$$

In this equation, "$RU(t)$" is the resonant signal at a time "t" and the term "$RU_{max}(t_\infty)$" is the resonant signal obtained when the ligand is saturated by the analyte.

An observed rate constant (k_{obs}) can further simplify the rate law ($k_{obs} = k_a \cdot [A] + k_d$), and after solving the differential Eq. 2, Eq. 3 can be obtained.

$$RU(t) = RU_{max}(t_\infty)[1 - e^{-k_{obs}(t)}], \quad (3)$$

The integration of first-order exponential decay (Eq. 4) of the complexes in the dissociation phase (decreasing exponential RU signal) results in Eq. 5.

$$\partial RU(t)/\partial t = -k_d\, RU(t) \quad (4)$$

$$RU(t) = RU(t_m)\, e^{-k_d(t-t_m)} \quad (5)$$

Here, "t_m" is the time at the start of the dissociation phase (from 30 s on the sensorgrams in Figures 1a and b).

A global fit for the sensorgram data was performed to determine the k_{obs} and k_d values (Eq. 3 and 5). Consequently, plotting the k_{obs} values as a function of analyte (RES or RESAn1) concentrations (Figure S4), the k_a values were obtained from the slope of the curves. The k_a and k_d values, related to the β-CD-NH_2 /RES or RESAn1 interactions, are presented in Table S1 (Supplementary Material).

The obtained k_a values for the [β-CD-NH_2/RES]° and [β-CD-NH_2/RESAn1]° formation processes were in the order of 10^3 and 10^4, respectively, while the k_d values were in the order of 10^{-1} for both systems. Both k_a and k_d values increased as the temperature increased, indicating that molecular collision optimization favored both the number of β-CD-NH_2/RES or RESAn1 IC formed per second and the fraction of these complexes that decayed per second. It can be seen that the k_a values were influenced by the chemical structure of the analytes. The association between β-CD-NH_2 and RESAn1 was approximately 15- to 21-fold faster than that of the β-CD-NH_2/RES association. However, the k_d values of β-CD-NH_2/RES]° and [β-CD-NH_2/RESAn1]° complexes were less dependent on the analyte structure, which is reflected by a smaller difference. The dissociation of [β-CD-NH_2/RESAn1]° complexes was approximately

1.2-fold faster than that of [β-CD-NH_2/RES]°. A viable hypothesis to explain the effects of different guest molecules on the k_a and k_d values is based on the structural differences between RES and RESAn1 (Figure 1). One of the aromatic ring in RESAn1 lacks a hydroxyl group; this reduces the probability of occurrence of hydrogen bonding between the hydroxyl groups on the outer surface of β-CD-NH_2 with those of RESAn1. These bonds would need to be broken before inclusion of the analyte in the β-CD-NH_2 cavity, which would reduce the association rate, as found in β-CD-NH_2/RES. Consequently, to confirm this hypothesis regarding the role of structure and to better understand the β-CD-NH_2/guest molecule IC formation process, we investigated the energetics involved in the inclusion complex formation via an activated complex formation step (HUDSON et al., 2019b). The rate constants (k_a and k_d) are dependent on temperature, which allows the determination of the activation energy (E_{act}) associated with the activated complex formation ($[\beta-\mathrm{CD}-\mathrm{NH_2}/\mathrm{RES}]^{\ddagger}$ or $[\beta-\mathrm{CD}-\mathrm{NH_2}/\mathrm{RESAn1}]^{\ddagger}$). This is based on the approximation between the RES or RESAn1 free molecules and immobilized β-CD-NH_2 molecules and the dissociation of [β-CD-NH_2/RES]° or [β-CD-NH_2/RESAn1]° complexes (COELHO et al., 2019). The activated complex formation is based on transition state theory, which describes the formation of an intermediate, unstable, and short-lived complex between the reactants species (FERNÁNDEZ-RAMOS et al., 2006b). Characterization of the energetics involved in the formation of activated complexes is useful for understanding the molecular dynamics of IC formation between β-CD-NH_2 and small molecules, such as RES or RESAn1.

3.2. Energetics involved in the formation of $[\beta-\mathrm{CD}-\mathrm{NH_2}/\mathrm{RES}]^{\ddagger}$ or $[\beta-\mathrm{CD}-\mathrm{NH_2}/\mathrm{RESAn1}]^{\ddagger}$due to the association of the interactant molecules

The potential energy barrier needs to be overcome ($E_{act,a}$) for the activated complex formation between RES or RESAn1 and β-CD-NH_2 molecules was calculated by applying the Arrhenius equation (Eq. 6) to the data obtained from the plot of $\ln k_a$ versus $1/T$ (Figure 3).

$$E_{act,a}(T) = -R\left(\frac{\partial \ln k_a}{\partial\, {}^{1}/_{T}}\right), \qquad (6)$$

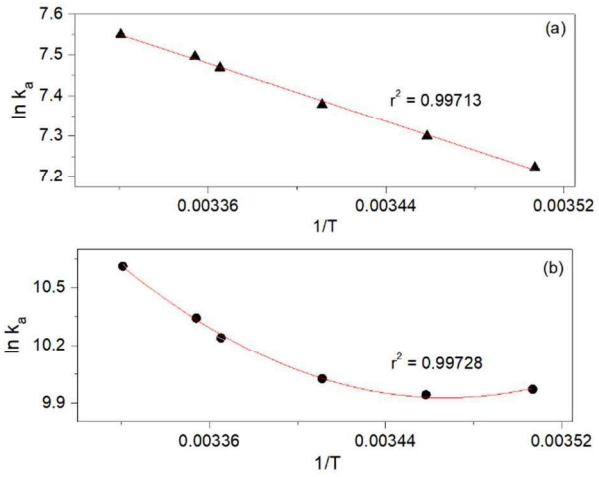

Figure 3. Arrhenius plots for the association between β-CD-NH_2 and (a) resveratrol (RES) or (b) its analog 2,4-dihydroxybenzaldehyde phenylhydrazone (RESAn1).

The $E_{act,a}^{\beta-CD-\ \ _2/RES}$ was determined from the slope of the $\ln k_a$ versus $1/T$ curve for the $[\beta-\mathrm{CD}-\mathrm{NH_2}/\mathrm{RES}]^{\ddagger}$ formation and indicated that an energy barrier of (14.81 ± 0.64) kJ·mol^{-1} needed to be overcome for the association between the interactant molecules and formation of the activated complex.

As the Arrhenius curve for the $[\beta-\mathrm{CD}-\mathrm{NH_2}/\mathrm{RESAn1}]^{\ddagger}$ formation presented a second-order polynomial profile, these data were fitted to a polynomial equation (Eq. 7). After determining the constants (a, b, c, d, $\ln\varphi$), the temperature-dependent $E_{act,a}^{\beta-CD-\mathrm{N}\ _2/RESA}$ values were obtained by applying Eq. 8.

$$ln\ k_a = a + b\left(\frac{1}{T}\right) + c\left(\frac{1}{T}\right)^2 + d\left(\frac{1}{T}\right)^3 + \cdots \ln\varphi \qquad (7)$$

$$E_{act,a} = -R\left[b + 2c\left(\frac{1}{T}\right) + 3d\left(\frac{1}{T}\right)^2 + \cdots\right] \qquad (8)$$

The $E_{act,a}^{\beta-CD-\mathrm{NH_2}/RESAn1}$ ranged from (-15.01 ± 0.75) kJ·mol^{-1} to (82.35 ±4.47) kJ·mol-1 (from 12 to 28 ºC). Consequently, due to high energetic variation in temperature, we should consider the main components of $E_{act,a}^{\beta-CD-\mathrm{NH_2}/RESAn1}$: i) the release of energy by the direct desolvated β-CD-NH_2/RESAn1 interaction ($E_{act,a,int}$< 0), ii) negative energy caused by water molecules released from the cavity of β-CD-NH_2 to the bulk ($E_{act,a,des\ \beta-CD-\ \ _2}$< 0), iii) the energy costs for desolvation of RESAn1 molecules ($E_{act,a,des\ RESAn}$ > 0), and iv) the energy costs for possible conformational fits between β-CD-NH_2 and the guest molecule ($E_{act,a,fit}$>

0). In the lower temperature range (12 ºC≤ T ≤15 ºC, by interpolation), the absorbed energy ("iii" and "iv") required to form the $[\beta-\mathrm{CD}-\mathrm{NH_2}/\mathrm{RESAn1}]^{\ddagger}$ from the association of the free β-CD-$\mathrm{NH_2}$ and RESAn1 molecules was compensated by the energy released when the processes "i" and "ii" occur. At low temperatures, the 3D water structure and hydrogen bonds formed between the water molecules in the bulk are stronger than those at higher temperatures; therefore, more energy is released when these molecules leave the β-CD-$\mathrm{NH_2}$ cavity and interact with each other in the bulk. However, less energy is absorbed by the RESAn1 desolvation effect. Therefore, at low temperatures, $|E_{act,a,des\ RESA}| < |E_{act,a,des\ \beta-\mathrm{CD}-\mathrm{NH_2}}|$. As the temperature increases (T > 15 ºC), the 3D structure of the water molecules breaks in the bulk, weakening $\mathrm{H_2O}-\mathrm{H_2O}$ hydrogen bonding, resulting in less energy released by the liberation of water molecules from the cavity of the β-CD-$\mathrm{NH_2}$ to the bulk and more energy is absorbed via the desolvation of RESAn1, with $|E_{act,a,des\ RESAn}| > |E_{act,a,des\ \beta-\mathrm{CD}-\mathrm{NH_2}}|$.

The temperature-dependence of $E_{act,a}$was not observed in RES as RESAn1 is more hydrophobic than RES due to the lack of a hydroxyl group in the aromatic ring of the RESAn1 molecule. There is no literature kinetic data on the β-CD-$\mathrm{NH_2}$/RES or RESAn1 interaction for a direct comparison of our results, to the best of our knowledge. Recently, our group studied the thermodynamics and kinetics of interactions between RES/RESAn1 and human serum albumin (HSA). Both $E_{act,a}^{HSA/RES}$ and $E_{act,a}^{HSA/RESAn}$ were found to be independent of temperature, while the first (11.37 kJ·mol^{-1}) was lower than the second (30.76 kJ·mol^{-1}). This difference was attributed to a higher conformational change in HSA caused by RESAn1 due to the interaction between its $\mathrm{NNH_2}$ group and amino acid residues of the protein (REZENDE et al., 2020).

To determine the changes in enthalpy ($\Delta H_a^{\ddagger}$), Gibbs free energy ($\Delta G_a^{\ddagger}$), and entropy ($T\Delta S_a^{\ddagger}$) of activation associated with formation of $[\beta-\mathrm{CD}-\mathrm{NH_2}/\mathrm{RES}]^{\ddagger}$ or $[\beta-\mathrm{CD}-\mathrm{NH_2}/\mathrm{RESAn1}]^{\ddagger}$ through the association pathway, we used Eq. 9, 10, and 11, respectively. These values are shown in Table 1.

$$\Delta H_a^{\ddagger}(T) = E_{act,a}(T) - RT, \tag{9}$$

$$\Delta G_a^{\ddagger}(T) = -RTln(k_a h/k_B(T)), \tag{10}$$

$$T\Delta S_a^{\ddagger}(T) = \Delta H_a^{\ddagger}(T) - \Delta G_a^{\ddagger}(T) \tag{11}$$

In these equations, h is Planck's constant (6.62×10^{-34} J·s), k_B is the Boltzmann constant (1.38×10^{-23} J·K^{-1}), and R is the universal gas constant (8.3145 J·mol^{-1}·K^{-1}).

Table 1. The enthalpy ($\Delta H_a^{\ddagger}$), Gibbs free energy ($\Delta G_a^{\ddagger}$) and entropy ($\Delta S_a^{\ddagger}$) changes associated with the $[\beta-\mathrm{CD}-\mathrm{NH_2/RES}]^{\ddagger}$ or $[\beta-\mathrm{CD}-\mathrm{NH_2/RESAn1}]^{\ddagger}$ activated complex formation from the association pathway.

T	$[\beta-\mathrm{CD}-\mathrm{NH_2/RES}]^{\ddagger}$			$[\beta-\mathrm{CD}-\mathrm{NH_2/RESAn1}]^{\ddagger}$		
	$\Delta H_a^{\ddagger}$	$\Delta G_a^{\ddagger}$	$T\Delta S_a^{\ddagger}$	$\Delta H_a^{\ddagger}$	$\Delta G_a^{\ddagger}$	$T\Delta S_a^{\ddagger}$
(°C)		(kJ·mol^{-1})			(kJ·mol^{-1})	
12	12.44 ±0.62a	52.61 ±3.58a	-40.17 ±2.20a	-17.38 ±0.82e	46.09 ±2.38a	-63.47 ±3.17e
16	12.40 ±0.39a	53.19 ±2.59a	-40.79 ±3.22a	2.11 ±0.14d	46.84 ±2.40a	-44.72 ±2.34d
20	12.37 ±0.55a	53.77 ±4.61a	-41.40 ±2.24a	25.01 ±1.50c	47.32 ±2.62a	-22.31 ±1.67c
24	12.34 ±0.42a	54.32 ±2.63a	-41.98 ±2.26a	51.01 ±3.54b	47.47 ±2.35a	3.54 ±0.16b
25	12.33 ±0.37a	54.44 ±3.63a	-42.11 ±3.26a	57.96 ±3.74b	47.38 ±3.01a	10.58 ±0.42b
28	12.30 ±0.46a	54.87 ±2.64a	-42.57 ±2.57a	79.85 ±3.19a	47.21 ±2.68a	32.64 ±1.97a

$\Delta H_a^{\ddagger}$ values are the result of subtracting "R" (universal gas constant) and "T" (temperature) from the $E_{act,a}$ values, therefore, the same explanation is applicable to both activation and enthalpic energy terms.

The net free energy costs expressed by the $\Delta G_a^{\ddagger}$ values indicate that the activated complex formation from the association of β-CD-NH_2 and RESAn1 occurred slightly faster than the same process via the association with β-CD-NH_2/RES. However, the difference in the entropic and enthalpic components of $\Delta G_a^{\ddagger}$ was higher between the two guest molecules. The negative $T\Delta S_a^{\ddagger}$ values for RES associated with β-CD-NH_2 indicate that the $[\beta-\mathrm{CD}-\mathrm{NH_2}/\mathrm{RES}]^{\ddagger}$ formation occurred with a reduction in the entropy of the system over the entire temperature range. As previously discussed, at lower temperatures, the 3D structure of water molecules and H_2O-H_2O hydrogen bonds in the bulk are more structured. Lower temperatures increase 3D water organization and promote two phenomena: i) the system entropy reduction contribution becoming from β-CD-NH_2 cavity desolvation makes higher, and ii) the system entropy increase contribution from the release of water molecules of the solvation layer of RES becoming less, so $|T\Delta S^{\ddagger}_{a,\ des\beta-\mathrm{CD}-\mathrm{N}\ _2}| > |T\Delta S^{\ddagger}_{a,\ des\ RES}|$. The same explanation can be adopted for the negative $T\Delta S_a^{\ddagger\,\beta-\mathrm{CD}-\mathrm{NH_2}\ /RESAn}$ values in the temperature range from 12 to 23.5 °C. However, there was a system entropic gain when the $[\beta-\mathrm{CD}-\mathrm{NH_2}/\mathrm{RESAn1}]^{\ddagger}$ was formed in a certain temperature range (23.5 ºC≤ T ≤28 ºC, by interpolation), resulting in positive $T\Delta S_a^{\ddagger\,\beta-\mathrm{CD}-\mathrm{NH_2}\ /RESAn1}$ values. At higher temperatures (23.5 ºC≤ T ≤28 ºC) occurs a reduction in the 3D water structuring degree and in the strength of the H_2O-H_2O hydrogen bonds in the bulk, making $|T\Delta S^{\ddagger}_{a,\ des\,\beta-\mathrm{CD}-\mathrm{NH_2}}| < |T\Delta S^{\ddagger}_{a,\ des\ RESAn1}|$.

Changes in the interacting molecule structure can affect the kinetics of IC formation, altering the net energetic cost of the process ($\Delta G^{\ddagger}$). The effect of substituent groups on $\Delta G^{\ddagger}$ is generally smaller than on its components ($\Delta H^{\ddagger}$ and $T\Delta S^{\ddagger}$), as an entropic contribution often compensates an enthalpic modification (NUNES et al., 2019). In the association between β-CD-NH_2 and the structurally modified analog RESAn1, the enthalpic increase in the same temperature range mentioned earlier, resulted in an increase in the entropy, indicating the existence of an isokinetic compensation phenomenon, confirmed by the linear relationship between $\Delta H_a^{\ddagger\,\beta-\mathrm{CD}-\mathrm{NH_2}/RESAn1}$ and $T\Delta S_a^{\ddagger\,\beta-\mathrm{CD}-\mathrm{NH_2}\ /RESA}$ (slope = 0.988, R^2 = 0.999, Figure 4) (LIU; GUO, 2001).

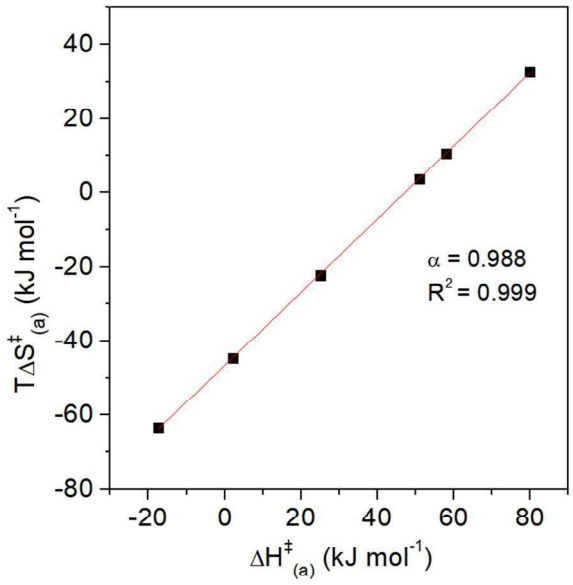

Figure 4. The plot of enthalpic ($\Delta H_a^{\ddagger}$) and entropic ($T\Delta S_a^{\ddagger}$) values of association between β-CD-NH_2 and RESAn1 of the activated complex formation.

This phenomenon reflects the hydrophobic contribution to the formation of the activated complex and the modification of the solvation structures of the molecules involved in the interaction process (PAUL; GHOSH; MUKHERJEE, 2016). The role of the desolvation processes of RESAn1 to $[\beta-\mathrm{CD}-\mathrm{NH_2}/\mathrm{RESAn1}]^{\ddagger}$ formation is highlighted. Isokinetic compensation was not observed in the $[\beta-\mathrm{CD}-\mathrm{NH_2}/\mathrm{RES}]^{\ddagger}$ formation due to the lower hydrophobicity of the RES molecule.

$\Delta H_a^{\ddagger\,\beta-\mathrm{CD}-\mathrm{NH_2}/RESAn1}$ showed a significant variation over the studied temperature range (the exothermicity of the association process decreased with increasing temperature), therefore, we investigated the activation molar specific heat change (ΔCp) and compared it to the association between β-CD-NH_2 and RESAn1 ($\Delta Cp_a^{\ddagger\,\beta-\mathrm{CD}-\mathrm{NH_2}/RESA}$) and $[\beta-\mathrm{CD}-\mathrm{NH_2}/\mathrm{RESAn1}]^{\ddagger}$ formation, using Eq. 12. The slope of the $\Delta H_a^{\ddagger\,\beta-\mathrm{CD}-\mathrm{NH_2}/RESAn1}$ vs the temperature curve gives the $\Delta Cp_a^{\ddagger\,\beta-\mathrm{CD}-\mathrm{NH_2}/RESAn}$ value (Figure S5).

$$\Delta Cp_a^{\ddagger} = \partial \Delta H_a^{\ddagger}/\partial T \qquad (12)$$

The determination of ΔCp from the host-guest interactions elucidate the role of hydrophobic interactions involved in the formation of inclusion complexes as a function of the hydrophobicity of the guest molecule (PAUL et al., 2016). $\Delta Cp_a^{\ddagger\,\beta-\mathrm{CD}-\mathrm{NH_2}/RESAn}$ can be described by Eq. 13.

$$\Delta Cp_a^{\ddagger\,\beta-CD-NH_2/RESAn1} = Cp^{\ddagger\,\beta-CD-NH_2/RESAn} - (Cp^{\,\beta-CD-NH2} + Cp^{\,RESAn1}) \quad (13)$$

, where $Cp^{\ddagger\,\beta-CD-\ \ _2/RESAn1}$ is the molar specific heat of the β-CD-NH_2/RESAn1 activated complex, while $Cp^{\,\beta-CD-\ \ _2}$ and $Cp^{\,RESAn1}$ are the specific heat of the free β-CD-NH_2 and RESAn1 molecules, respectively. All Cp values included the contributions of the solvation layers of these molecules.

We found that $\Delta Cp_a^{\ddagger\,\beta-CD-\ \ _2/RESAn}$ = 6.07 kJ·mol^{-1}·K^{-1}. This value is a result of the difference between the intensity of the intermolecular interactions in the free interactant molecules (β-CD-NH_2 and RESAn1) and $[\beta-CD-NH_2/RESAn1]^{\ddagger}$. Consequently, when the activated complex is formed, the intensity of intermolecular interactions was higher than that in the free host and guest molecules, increasing the potential binding energy of the system ($|Cp^{\ddagger\,\beta-CD-NH_2/RESA}| > (|Cp^{\,\beta-CD-NH_2}| + |Cp^{\,RESAn1}|)$. The contributions of the desolvation of the β-CD−NH_2 cavity and the direct interactions between β-CD−NH_2 and RESAn1 to the increase of the potential energy were higher than the contribution of the RESAn1 desolvation to the decrease in the potential energy of the system.

3.3. Energetics involved in the formation of $[\beta-CD-NH_2/RES]^{\ddagger}$ and $[\beta-CD-NH_2/RESAn1]^{\ddagger}$ from the dissociation of the thermodynamically stable complexes

The energetic parameters related to the process of $[\beta-CD-NH_2/RES]^{\ddagger}$ and $[\beta-CD-NH_2/RESAn1]^{\ddagger}$ formation from the dissociation of $[\beta-CD-NH_2/RES]^{\circ}$ or $[\beta-CD-NH_2/RESAn1]^{\circ}$ were obtained by applying the Arrhenius equation (Eq. 6) to the $\ln k_d$ versus 1/T plot data (Figure S6).

Both $[\beta-CD-NH_2/RES]^{\ddagger}$ and $[\beta-CD-NH_2/RESAn1]^{\ddagger}$ have positive activation energies and temperature-independent ($E_{act,d}^{\beta-CD-NH_2/RES}$= 5.19 ± 0.25 kJ·mol^{-1}, $E_{act,d}^{\beta-CD-NH_2/RESAn1}$= 6.29 ± 0.31 kJ·mol^{-1}). Since the dissociation of thermodynamically stable complexes does not require significant conformational changes and desolvation of the β-CD−NH_2 cavity and guest molecule the temperature variation does not interfere with the energy barriers for the formation of the activated complexes from the dissociation of $[\beta-CD-NH_2/RES]^{\circ}$ or $[\beta-CD-NH_2/RESAn1]^{\circ}$. Therefore, the positive $E_{act,d}$ values are primarily a result of conformational/structural differences between the thermodynamically stable complexes and the activated complexes, which arise due to the difference number and

intensity of intermolecular interactions. Additionally, the kinetic parameters related to the $[\beta - \mathrm{CD} - \mathrm{NH_2}\ /\mathrm{RES}]^{\ddagger}$ and $[\beta - \mathrm{CD} - \mathrm{NH_2}\ /\mathrm{RESAn1}]^{\ddagger}$ formation from the dissociation step ($\Delta H_d^{\ddagger}$, $\Delta G_d^{\ddagger}$, and $T\Delta S_d^{\ddagger}$) were calculated through Eqs. 9–11 and presented in Table 2.

Table 2. The enthalpy ($\Delta H_d^{\ddagger}$), Gibbs free energy ($\Delta G_d^{\ddagger}$), and entropy ($T\Delta S_d^{\ddagger}$) changes associated to the β-CD−NH_2/RES or RESAn1 activated complex formation from the dissociation pathway.

T	β-CD−NH_2/RES			β-CD−NH_2/RESAn1		
	$\Delta H_d^{\ddagger}$	$\Delta G_d^{\ddagger}$	$T\Delta S_d^{\ddagger}$	$\Delta H_d^{\ddagger}$	$\Delta G_d^{\ddagger}$	$T\Delta S_d^{\ddagger}$
(°C)		(kJ·mol^{-1})			(kJ·mol^{-1})	
12	2.82 ±0.14a	72.75 ±3.63a	-69.93 ±2.99a	3.91 ±0.23a	72.20 ±3.17a	-68.28 ±3.35a
16	2.78 ±0.11a	73.72 ±3.92a	-70.93 ±3.12a	3.88 ±0.17a	73.15 ±3.99a	-69.27 ±3.18a
20	2.75 ±0.15a	74.70 ±4.48a	-71.95 ±3.16a	3.85 ±0.21a	74.12 ±3.62a	-70.27 ±3.41a
24	2.72 ±0.13a	75.69 ±5.16a	-72.97 ±3.48a	3.81 ±0.30a	75.08 ±4.02a	-71.26 ±3.62a
25	2.71 ±0.14a	75.93 ±4.55a	-73.22 ±4.39a	3.81 ±0.31a	75.31 ±3.78a	-71.50 ±3.34a
28	2.68 ±0.15a	76.67 ±5.36a	-73.99 ±5.16a	3.78 ±0.28a	76.03 ±3.80a	-72.25 ±3.56a

These kinetic parameters ($\Delta H_d^{\ddagger}$, $\Delta G_d^{\ddagger}$, and $T\Delta S_d^{\ddagger}$) related to the formation of the activated complex from the dissociation of $[\beta-\mathrm{CD}-\mathrm{NH_2}/\mathrm{RES}]^{\circ}$ or $[\beta-\mathrm{CD}-\mathrm{NH_2}/\mathrm{RESAn1}]^{\circ}$ were not affected by the structural differences between RES and RESAn1, as observed in the host-guest molecule association process to the activated complex formation. This can be explained by considering the relevance of the desolvation processes and conformational changes in the $[\beta-\mathrm{CD}-\mathrm{NH_2}/\mathrm{RES}]^{\ddagger}$ and $[\beta-\mathrm{CD}-\mathrm{NH_2}/\mathrm{RESAn1}]^{\ddagger}$ formation from the association step, while these phenomena do not interfere in the dissociation step to the formation of the activated complexes. The $\Delta H_d^{\ddagger}$ values were positive and almost constant over the temperature range for both guest molecules interacting with β-CD−$\mathrm{NH_2}$. Despite $\Delta H_a^{\ddagger} > \Delta H_d^{\ddagger}$, the association pathway was the fastest way to activate complex formation, as indicated by the higher $\Delta G_d^{\ddagger}$ values, in comparison with $\Delta G_a^{\ddagger}$. This can be explained by the greater decrease in the entropy of the system when $[\beta-\mathrm{CD}-\mathrm{NH_2}/\mathrm{RES}]^{\ddagger}$ or $[\beta-\mathrm{CD}-\mathrm{NH_2}/\mathrm{RESAn1}]^{\ddagger}$ were formed from the dissociation of $[\beta-\mathrm{CD}-\mathrm{NH_2}/\mathrm{RES}]^{\circ}$ or $[\beta-\mathrm{CD}-\mathrm{NH_2}/\mathrm{RESAn1}]^{\circ}$.

4. Conclusion

The kinetics of the inclusion complex formation process between β-CD−$\mathrm{NH_2}$ and RES or its structural analog RESAn1 was investigated using SPR. The association and dissociation rate constants showed that a temperature increase favored both the number of inclusion complexes ($[\beta-\mathrm{CD}-\mathrm{NH_2}/\mathrm{RES}]^{\circ}$ or $[\beta-\mathrm{CD}-\mathrm{NH_2}/\mathrm{RESAn1}]^{\circ}$) formed per second and the fraction of these complexes that dissociate per second. In addition, the structural differences between RES and RESAn1 had a significant effect on the kinetic constants, resulting in a higher rate of association between β-CD−$\mathrm{NH_2}$ and RESAn1.

The energetic kinetic parameters (E_{act}, $\Delta H^{\ddagger}$, $\Delta G^{\ddagger}$, and $T\Delta S^{\ddagger}$) revealed that the formation of the activated complex from the association between the interacting molecules was affected by the guest molecule structure and occurred in a multi-step process *via* the β-CD−$\mathrm{NH_2}$/RESAn1 association accompanied by isokinetic compensation. However, the activated complex formation from the dissociation of the thermodynamically stable complexes for both guest molecules occurred in a single-step process, reinforcing the significant relevance of the desolvation processes and conformational changes for the activated complex formation from the host-guest association.

These results provide a detailed characterization of the kinetics of inclusion complex formation between β-CD−$\mathrm{NH_2}$ and RES or RESAn1. The results also highlight the role of the

guest molecule structure, which contributes to the elucidation of the dynamics of molecular inclusion between β-CD and small molecules.

Acknowledgements

The authors wish to thank the Conselho Nacional de Desenvolvimento Científico e Tecnológico (CNPq, Brazil); Coordenação de Aperfeiçoamento de Pessoal de Nível Superior (CAPES, Brazil); CAPES/Pró-Forenses (Brazil); Financiadora de Estudos e Projetos (FINEP, Brazil); Instituto Nacional de Ciências e Tecnologias Analíticas Avançadas (INCTAA, Brazil); and Fundação de Apoio à Pesquisa de Minas Gerais (FAPEMIG, Brazil) for the financial support.

References

AL OMARI, M. M.; EL-BARGHOUTHI, M. I.; ZUGHUL, M. B.; DAVIES, J. E. D.; BADWAN, A. A. The role of drug hydrophobicity in β-cyclodextrin complexes. **Journal of Molecular Liquids**, [s. l.], v. 155, n. 2–3, p. 103–108, 2010.

BERTACCHE, V.; LORENZI, N.; NAVA, D.; PINI, E.; SINICO, C. Host-guest interaction study of resveratrol with natural and modified cyclodextrins. **Journal of Inclusion Phenomena and Macrocyclic Chemistry**, [s. l.], v. 55, n. 3–4, p. 279–287, 2006.

BOHNE, C. Supramolecular dynamics, **Royal Society of Chemistry**, 2014. Disponível em: <www.rsc.org/csr>. Acesso em: 30 jan. 2021.

COELHO, Y. L.; PAULA, H. M. C. De; AGUDELO, A. J. P.; DE CASTRO, A. S. B.; HUDSON, E. A.; PIRES, A. C. S.; DA SILVA, L. H. M. Lactoferrin-phenothiazine dye interactions : Thermodynamic and kinetic approach. **International Journal of Biological Macromolecules**, [s. l.], v. 136, p. 559–569, 2019.

DA SILVA, A. D.; DOS SANTOS, J. A.; MACHADO, P. A.; ALVES, L. A.; LAQUE, L. C.; DE SOUZA, V. C.; COIMBRA, E. S.; CAPRILES, P. V. S. Z. Insights about resveratrol analogs against trypanothione reductase of *Leishmania braziliensis* : Molecular modeling, computational docking and *in vitro* antileishmanial studies. **Journal of Biomolecular Structure and Dynamics**, [s. l.], v. 37, n. 11, p. 2960–2969, 2019.

DAS, S.; SUBUDDHI, U. Studies on the complexation of diclofenac sodium with β-cyclodextrin: Influence of method of preparation. **Journal of Molecular Structure**, [s. l.], v. 1099, p. 482–489, 2015.

FERNÁNDEZ-RAMOS, A.; MILLER, J. A.; KLIPPENSTEIN, S. J.; TRUHLAR, D. G. Modeling the Kinetics of Bimolecular Reactions. **Chemical Reviews**, [s. l.], v. 106, n. 11, p. 4518–4584, 2006.

GAREGG, P. J.; JOHANSSON, R.; ORTEGA, C.; SAMUELSSON, B. Novel reagent system for converting a hydroxy-group into an iodo-group in carbohydrates with inversion of configuration. Part 3. **Journal of the Chemical Society, Perkin Transactions 1**, [s. l.], n. 0, p. 681–683, 1982.

GAREGG, P. J.; SAMUELSSON, B. Novel reagent system for converting a hydroxy-group

into an iodo-group in carbohydrates with inversion of configuration. **Journal of the Chemical Society, Chemical Communications**, [s. l.], n. 22, p. 978–980, 1979.

GAREGG, P. J.; SAMUELSSON, B. Novel reagent system for converting a hydroxy-group into an iodo-group in carbohydrates with inversion of configuration. Part 2. **Journal of the Chemical Society, Perkin Transactions 1**, [s. l.], n. 0, p. 2866–2869, 1980.

GUO, C.; YIN, J.; CHEN, D. Co-encapsulation of curcumin and resveratrol into novel nutraceutical hyalurosomes nano-food delivery system based on oligo-hyaluronic acid-curcumin polymer. **Carbohydrate Polymers**, [s. l.], v. 181, p. 1033–1037, 2018.

HO, S.; THOO, Y. Y.; YOUNG, D. J.; SIOW, L. F. Cyclodextrin encapsulated catechin: Effect of pH, relative humidity and various food models on antioxidant stability. **LWT - Food Science and Technology**, [s. l.], v. 85, p. 232–239, 2017.

HUDSON, E. A.; REZENDE, J. de P.; DE PAULA, H. M. C.; COELHO, Y. L.; DA SILVA, L. H. M.; PIRES, A. C. dos S. Energetic parameters of β-casein/quercetin activated and thermodynamically stable complex formation accessed by Surface Plasmon Resonance. **Colloids and Surfaces B: Biointerfaces**, [s. l.], v. 181, p. 798–805, 2019.

JAMBHEKAR, S. S.; BREEN, P. Cyclodextrins in pharmaceutical formulations I: Structure and physicochemical properties, formation of complexes, and types of complex, **Drug Discovery Today**, v. 21, n. 2, p. 356-362, 2016.

KEYLOR, M. H.; MATSUURA, B. S.; STEPHENSON, C. R. J. Chemistry and Biology of Resveratrol-Derived Natural Products, **American Chemical Society**, 2015.

KFOURY, M.; LOUNÈS-HADJ SAHRAOUI, A.; BOURDON, N.; LARUELLE, F.; FONTAINE, J.; AUEZOVA, L.; GREIGE-GERGES, H.; FOURMENTIN, S. Solubility, photostability and antifungal activity of phenylpropanoids encapsulated in cyclodextrins. **Food Chemistry**, [s. l.], v. 196, p. 518–525, 2016.

LI, H.; XU, X.; LIU, M.; SUN, D.; LI, L. Microcalorimetric and spectrographic studies on host-guest interactions of α-, β-, γ- And Mβ-cyclodextrin with resveratrol. **Thermochimica Acta**, [s. l.], v. 510, n. 1–2, p. 168–172, 2010.

LIMA, P. S. S.; LUCCHESE, A. M.; ARAÚJO-FILHO, H. G.; MENEZES, P. P.; ARAÚJO, A. A. S.; QUINTANS-JÚNIOR, L. J.; QUINTANS, J. S. S. Inclusion of terpenes in cyclodextrins: Preparation, characterization and pharmacological approaches, **Carbohydrate Polymers**, v. 151, p. 965-987, 2016.

LIU, L.; GUO, Q. X. Isokinetic relationship, isoequilibrium relationship, and enthalpy-entropy compensation, **Chemical Reviews**, v. 101, n. 3, p. 673-696, 2001.

LÓPEZ-NICOLÁS, J. M.; GARCÍA-CARMONA, F. Rapid, simple and sensitive determination of the apparent formation constants of trans-resveratrol complexes with natural cyclodextrins in aqueous medium using HPLC. **Food Chemistry**, [s. l.], v. 109, n. 4, p. 868–875, 2008.

LU, Z.; CHEN, R.; LIU, H.; HU, Y.; CHENG, B.; ZOU, G. Study of the complexation of resveratrol with cyclodextrins by spectroscopy and molecular modeling. **Journal of Inclusion Phenomena and Macrocyclic Chemistry**, [s. l.], v. 63, n. 3–4, p. 295–300, 2009. a.

LU, Z.; CHENG, B.; HU, Y.; ZHANG, Y.; ZOU, G. Complexation of resveratrol with cyclodextrins: Solubility and antioxidant activity. **Food Chemistry**, [s. l.], v. 113, n. 1, p. 17–

20, 2009. b.

LUCAS-ABELLÁN, C.; FORTEA, I.; LÓPEZ-NICOLÁS, J. M.; NÚÑEZ-DELICADO, E. Cyclodextrins as resveratrol carrier system. **Food Chemistry**, [s. l.], v. 104, n. 1, p. 39–44, 2007.

NIEGELHELL, K.; CHEMELLI, A.; HOBISCH, J.; GRIESSER, T.; REITER, H.; HIRN, U.; SPIRK, S. Interaction of industrially relevant cationic starches with cellulose. **Carbohydrate Polymers**, [s. l.], v. 179, p. 290–296, 2018.

NUNES, N. M.; DE PAULA, H. M. C.; COELHO, Y. L.; DA SILVA, L. H. M.; PIRES, A. C. S. Surface plasmon resonance study of interaction between lactoferrin and naringin. **Food Chemistry**, [s. l.], v. 297, p. 125022, 2019.

PAUL, B. K.; GHOSH, N.; MONDAL, R.; MUKHERJEE, S. Contrasting effects of salt and temperature on niosome-bound norharmane: Direct evidence for positive heat capacity change in the niosome: β-cyclodextrin interaction. **Journal of Physical Chemistry B**, [s. l.], v. 120, n. 17, p. 4091–4101, 2016.

PAUL, B. K.; GHOSH, N.; MUKHERJEE, S. Direct insight into the nonclassical hydrophobic effect in bile salt:β-cyclodextrin interaction: Role of hydrophobicity in governing the prototropism of a biological photosensitizer. **RSC Advances**, [s. l.], v. 6, n. 12, p. 9984–9993, 2016.

PROCHOWICZ, D.; KORNOWICZ, A.; LEWIŃSKI, J. Interactions of Native Cyclodextrins with Metal Ions and Inorganic Nanoparticles: Fertile Landscape for Chemistry and Materials Science. **Chemical Reviews**, [s. l.], v. 117, n. 22, p. 13461–13501, 2017.

PURPURA, M.; LOWERY, R. P.; WILSON, J. M.; MANNAN, H.; MÜNCH, G.; RAZMOVSKI-NAUMOVSKI, V. Analysis of different innovative formulations of curcumin for improved relative oral bioavailability in human subjects. **European Journal of Nutrition**, [s. l.], v. 57, n. 3, p. 929–938, 2018.

REZENDE, J. de P.; HUDSON, E. A.; DE PAULA, H. M. C.; COELHO, Y. L.; DA SILVA, L. H. M.; PIRES, A. C. dos S. Thermodynamic and kinetic study of epigallocatechin-3-gallate-bovine lactoferrin complex formation determined by surface plasmon resonance (SPR): A comparative study with fl uorescence spectroscopy. **Food Hydrocolloids**, [s. l.], v. 95, p. 526–532, 2019.

REZENDE, J. de P.; HUDSON, E. A.; DE PAULA, H. M. C.; MEINEL, R. S.; DA SILVA, A. D.; DA SILVA, L. H. M.; PIRES, A. C. dos S. Human serum albumin-resveratrol complex formation: Effect of the phenolic chemical structure on the kinetic and thermodynamic parameters of the interactions. **Food Chemistry**, [s. l.], v. 307, 2020.

ROY, P.; DINDA, A. K.; CHAUDHURY, S.; DASGUPTA, S. β-cyclodextrin encapsulated polyphenols as effective antioxidants. **Biopolymers**, [s. l.], v. 109, n. 1, 2018.

SCHNEIDER, C. S.; BHARGAV, A. G.; PEREZ, J. G.; WADAJKAR, A. S.; WINKLES, J. A.; WOODWORTH, G. F.; KIM, A. J. Surface plasmon resonance as a high throughput method to evaluate specific and non-specific binding of nanotherapeutics. **Journal of controlled release : official journal of the Controlled Release Society**, [s. l.], v. 219, p. 331–344, 2015

SHENG, J.; WANG, Y.; XIONG, L.; LUO, Q.; LI, X.; SHEN, Z.; ZHU, W. Injectable doxorubicin-loaded hydrogels based on dendron-like β-cyclodextrin-poly(ethylene glycol)

conjugates. **Polymer Chemistry**, [s. l.], v. 8, n. 10, p. 1680–1688, 2017.

SINGH, V.; HE, Y.; WANG, C.; XU, J.; XU, X.; LI, H.; SINGH, P.; YORK, P.; SUN, L.; ZHANG, J. A comparison report of three advanced methods for drug-cyclodextrin interaction measurements. **Journal of Pharmaceutical and Biomedical Analysis**, [s. l.], v. 134, p. 252–258, 2017.

SU, Q.; WANG, Y.; SUN, W.; LIANG, J.; MENG, S.; WANG, Y.; LI, Z. Synthesis and characterization of cyclodextrin-based acrylamide polymer flocculant for adsorbing water-soluble dyes in dye wastewater. **Royal Society Open Science**, [s. l.], v. 7, n. 1, 2020.

TERAN, M.; NUGENT, M. A. Characterization of receptor binding kinetics for vascular endothelial growth factor-A using SPR. **Analytical Biochemistry**, [s. l.], v. 564–565, p. 21–31, 2019.

TEYSSANDIER, J.; FEYTER, S. De; MALI, K. S. Host-guest chemistry in two-dimensional supramolecular networks. **Chemical Communications**, [s. l.], v. 52, n. 77, p. 11465–11487, 2016.

TROCHE-PESQUEIRA, E.; PÉREZ-JUSTE, I.; NAVARRO-VÁZQUEZ, A.; CID, M. M. A β-cyclodextrin-resveratrol inclusion complex and the role of geometrical and electronic effects on its electronic induced circular dichroism. **RSC Advances**, [s. l.], v. 3, n. 26, p. 10242–10250, 2013.

Supplementary Material

Table S1. Association (k_a) and dissociation (k_d) rate constants related to the interaction between β-Cyclodextrin (β-CD) and resveratrol (RES) or its analog (RESAn1) at different temperatures.

Temperature	β-CD/RES		β-CD/RESAn1	
	k_a	k_d	k_a	k_d
(°C)	(10^3 $M^{-1}s^{-1}$)	(s^{-1})	(10^4 $M^{-1}s^{-1}$)	(s^{-1})
12	1.401 ± 0.056	0.280 ± 0.014	2.141 ± 0.121	0.353 ± 0.021
16	1.523 ± 0.062	0.290 ± 0.016	2.085 ± 0.132	0.367 ± 0.019
20	1.608 ± 0.096	0.298 ± 0.014	2.266 ± 0.135	0.379 ± 0.022
24	1.831 ± 0.111	0.306 ± 0.020	2.809 ± 0.142	0.392 ± 0.023
25	1.867 ± 0.116	0.309 ± 0.022	3.102 ± 0.141	0.397 ± 0.023
28	1.902 ± 0.132	0.315 ± 0.019	4.061 ± 0.191	0.407 ± 0.025

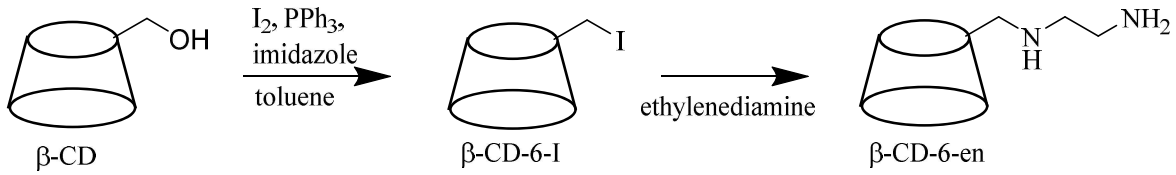

Figure S1. Schematic illustration of the synthesis of the functionalized β-CD.

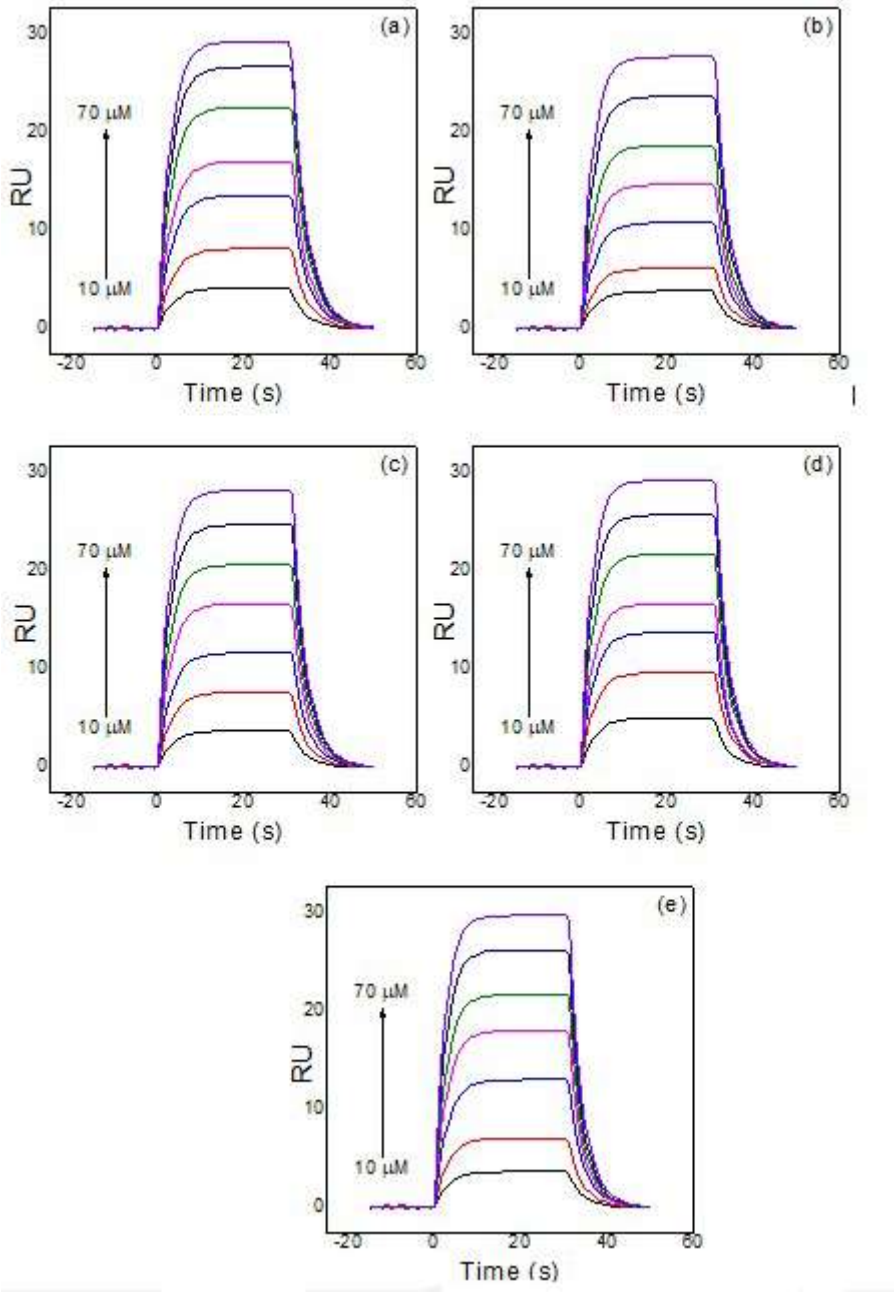

Figure S2. Sensorgrams of immobilized β-cyclodextrin interacting with resveratrol (RES) ranging from 10 to 70 μM at pH 7.4 and (a) 12 °C, (b) 16 °C, (c) 20 °C, (d) 24 °C, (e) 28 ºC.

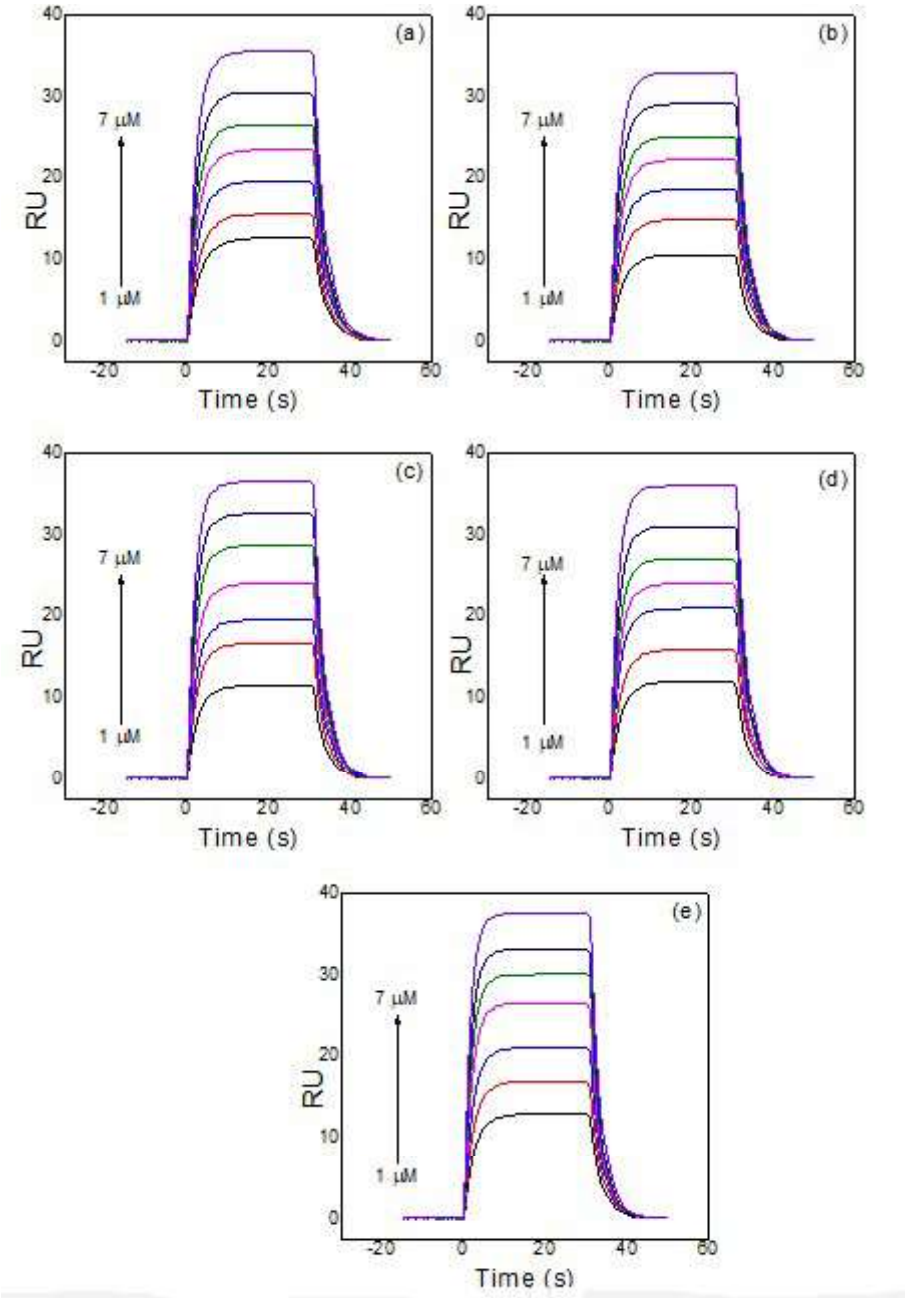

Figure S3. Sensorgrams of immobilized β-cyclodextrin interacting with RESAn1 ranging from 1 to 7 µM at pH 7.4 and (a) 12 °C, (b) 16 °C, (c) 20 °C, (d) 24 °C, (e) 28 ºC.

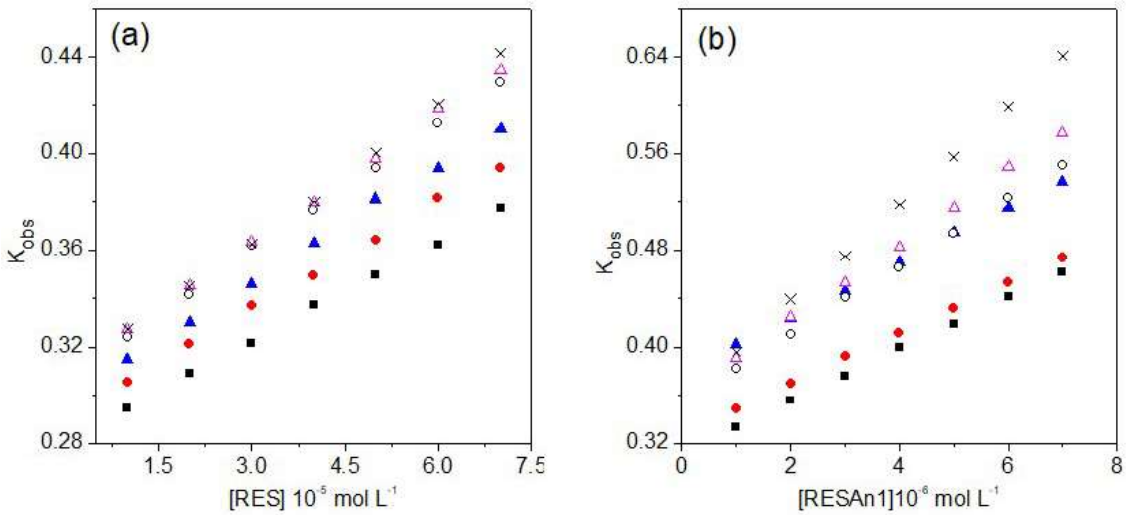

Figure S4. Plot of k_{obs} as a function of (a)RES or (b) RESAn1 concentration, used to determine k_a at temperatures: (■) 12 °C, (●) 16 °C, (▲) 20 °C, (○) 24 °C, (Δ) 25 °C and (X) 28 °C.

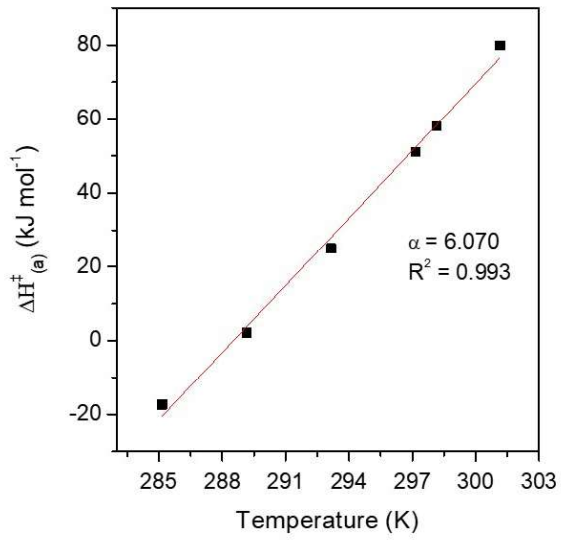

Figure S5. Temperature dependence of activation enthalpy change of association ($\Delta H_a^{\ddagger}$) between β-CD and RESAn1 for the activated complex formation.

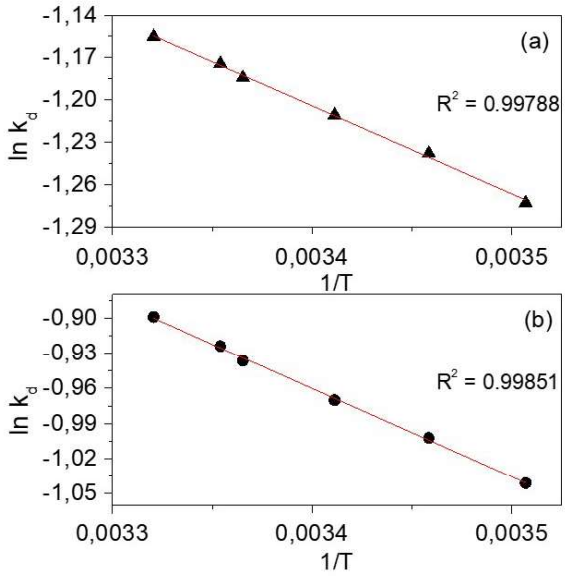

Figure S6. Arrhenius plots for the dissociation of the thermodynamically stable complexes formed by β-cyclodextrin and (a) resveratrol (RES) or (b) resveratrol analog 2,4-dihydroxybenzaldehyde phenylhydrazone (RESAn1).

CONCLUSÕES GERAIS

Neste trabalho foram estudadas as interações intermoleculares de três sistemas: micela de caseína-curcumina, β-caseína-quercetina, β-ciclodextrina-resveratrol e β-ciclodextrina-RESAn1. Para o complexo micela de caseína-curcumina, os experimentos de partição mostraram, que uma micela de caseína pode carrear cerca de 18.000 moléculas de curcumina, destacando o grande potencial carreador dessa estrutura. O processo de formação do complexo micela de caseína-curcumina foi conduzido entalpicamente. A formação desse complexo reduziu em até três vezes a degradação térmica da curcumina. Dessa forma, mostrou-se que a micela de caseína se apresenta como um veículo adequado para curcumina e possivelmente para outros compostos bioativos que podem ser usados como ingredientes funcionais em diferentes sistemas alimentares.

Em relação ao sistema β-caseína-quercetina, os resultados obtidos indicaram que as duas espécies químicas formaram um complexo termodinamicamente estável favorecido em temperaturas mais altas e impulsionado por um aumento na entropia. O processo de interação foi igualmente afetado por ambos os íons de Hofmeister estudados (Cl^- e SCN^-), que reduziram a entalpia blindando as interações eletrostáticas na dupla camada elétrica das moléculas interagentes. O mesmo efeito eletrolítico foi observado durante a formação do complexo ativado por β-caseína-quercetina. Esses resultados forneceram importantes informações sobre

o processo de interação β-caseína-quercetina que contribuem para o entendimento de como os íons de Hofmeister podem modular as interações intermoleculares entre proteínas e pequenas moléculas.

Os dados da cinética de formação de complexo entre β-ciclodextrina e os polifenóis (resveratrol e seu análogo estrutural (RESAn1)) mostraram que a formação dos complexos formados por ambos polifenóis e β-ciclodextrina e a dissociação desses complexos foram favorecidos por um aumento na temperatura do sistema. Além disso, as diferenças estruturais entre o resveratrol e seu análogo mostraram ter um efeito significativo nas constantes cinéticas, resultando em maior taxa de associação entre β-ciclodextrina-RESAn1. Essas diferenças estruturais também afetaram o processo de formação dos complexos ativados e revelaram a importância dos processos de dessolvatação e mudanças conformacionais para a formação do complexo ativado a partir da associação hóspede-hospedeiro, destacando o papel da estrutura da molécula hóspede, o que contribui para a elucidação da dinâmica de inclusão molecular entre β-ciclodextrina e pequenas moléculas.

As estruturas estudadas (micelas de caseína, β-caseína e β-ciclodextrina) apresentam grande potencial carreador para pequenas moléculas, como as moléculas bioativas curcumina, querecetina e resveratrol. Os parâmetros termodinâmicos e cinéticos obtidos nestes estudos, bem como os resultados das análises complementares, são importantes fundamentos para otimização da aplicação desses complexos moleculares bioativos em diferentes sistemas alimentícios ou farmacêuticos.

REFERÊNCIAS

BAHRI, A.; HENRIQUET, C.; PUGNIÈRE, M.; MARCHESSEAU, S.; CHEVALIER-LUCIA, D. Binding analysis between monomeric β-casein and hydrophobic bioactive compounds investigated by surface plasmon resonance and fluorescence spectroscopy. **Food Chemistry**, [s. l.], v. 286, p. 289–296, 2019.

BELLOMARIA, A.; NEPRAVISHTA, R.; MARCHETTI, M.; PACI, M. Profiling proteins in nutraceutical formulations: Characterization of the constituents. **Food Chemistry**, [s. l.], v. 194, p. 733–739, 2016.

CARBONELL-CAPELLA, J. M.; BUNIOWSKA, M.; BARBA, F. J.; ESTEVE, M. J.; FRÍGOLA, A. Analytical methods for determining bioavailability and bioaccessibility of bioactive compounds from fruits and vegetables: A review. **Comprehensive Reviews in Food Science and Food Safety**, [s. l.], v. 13, n. 2, p. 155–171, 2014.

CHENG, H.; DONG, H.; WUSIGALE; LIANG, L. A comparison of β-casein complexes and micelles as vehicles for trans-/cis-resveratrol. **Food Chemistry**, [s. l.], v. 330, p. 127209, 2020.

DAS, S.; SUBUDDHI, U. Studies on the complexation of diclofenac sodium with β-cyclodextrin: Influence of method of preparation. **Journal of Molecular Structure**, [s. l.], v. 1099, p. 482–489, 2015.

DE KRUIF, C. G.; HUPPERTZ, T.; URBAN, V. S.; PETUKHOV, A. V. Casein micelles and their internal structure. **Advances in Colloid and Interface Science**, [s. l.], v. 171–172, p. 36–52, 2012.

FANG, Z.; BHANDARI, B. Encapsulation of polyphenols - A review, **Trends in Food Science & Technology**, v. 21, n. 10, p. 510-523, 2010.

GIACOMELI, R.; IZOTON, J. C.; DOS SANTOS, R. B.; BOEIRA, S. P.; JESSE, C. R.; HAAS, S. E. Neuroprotective effects of curcumin lipid-core nanocapsules in a model Alzheimer's disease induced by β-amyloid 1-42 peptide in aged female mice. **Brain Research**, [s. l.], v. 1721, p. 146325, 2019.

GONZÁLEZ-FERRERO, C.; MORENO-RUIZ, A.; ROMO-HUALDE, A.; GONZÁLEZ-NAVARRO, C. J. Thermal protection of b -carotene in re-assembled casein micelles during different processing technologies applied in food industry. **Food Chemistry**, [s. l.], v. 138, n. 2–3, p. 1581–1587, 2013.

HAHAM, M.; ISH-SHALOM, S.; NODELMAN, M.; DUEK, I.; SEGAL, E.; KUSTANOVICH, M.; LIVNEY, Y. D. Stability and bioavailability of vitamin D nanoencapsulated in casein micelles. **Food & Function**, [s. l.], v. 3, n. 7, p. 737, 2012.

HUDSON, E. A.; DE PAULA, H. M. C.; DA SILVA, R. M.; PIRES, A. C. dos S.; DA SILVA, L. H. M. Curcumin-micellar casein multisite interactions elucidated by surface plasmon resonance. **International Journal of Biological Macromolecules**, [s. l.], v. 133, p. 860–866, 2019.

KEFLIE, T. S.; BIESALSKI, H. K. Micronutrients and bioactive substances: Their potential roles in combating COVID-19, **Nutrition**, p. 111103, 2020.

KHAERUNNISA, S.; KURNIAWAN, H.; AWALUDDIN, R.; SUHARTATI, S.; SOETJIPTO, S. Potential Inhibitor of COVID-19 Main Protease (M pro) from Several Medicinal Plant Compounds by Molecular Docking Study. [s. l.], 2020.

LI, M.; FOKKINK, R.; NI, Y.; KLEIJN, J. M. Bovine beta-casein micelles as delivery systems for hydrophobic flavonoids. **Food Hydrocolloids**, [s. l.], v. 96, p. 653–662, 2019.

MA, G.; TANG, C.; SUN, X.; ZHANG, J. The interaction mechanism of β-casein with oligomeric proanthocyanidins and its effect on proanthocyanidin bioaccessibility. **Food Hydrocolloids**, [s. l.], v. 113, p. 106485, 2021.

O'CONNELL, J. E.; GRINBERG, V. Y.; DE KRUIF, C. G. Association behavior of β-casein. **Journal of Colloid and Interface Science**, [s. l.], v. 258, n. 1, p. 33–39, 2003.

PENG, M.; ZHAO, X.; BISWAS, D. Polyphenols and tri-terpenoids from Olea europaea L. in alleviation of enteric pathogen infections through limiting bacterial virulence and attenuating inflammation. **Journal of Functional Foods**, [s. l.], v. 36, p. 132–143, 2017.

PINHO, E.; GROOTVELD, M.; SOARES, G.; HENRIQUES, M. Cyclodextrins as encapsulation agents for plant bioactive compounds, **Carbohydrate polymers**, v. 101, p. 121-135, 2014.

PORTNAYA, I.; COGAN, U.; LIVNEY, Y. D.; RAMON, O.; SHIMONI, K.; ROSENBERG, M.; DANINO, D. Micellization of Bovine -Casein Studied by Isothermal Titration Microcalorimetry and Cryogenic Transmission Electron Microscopy. **Journal of Agricultural and Food Chemistry**, [s. l.], v. 54, p. 5555–5561, 2006.

RANGSINTH, P.; SILLAPACHAIYAPORN, C.; NILKHET, S.; TENCOMNAO, T.; UNG, A. T.; CHUCHAWANKUL, S. Mushroom-derived bioactive compounds potentially serve as the inhibitors of SARS-CoV-2 main protease: An in silico approach. **Journal of Traditional and Complementary Medicine**, [s. l.], v. 11, n. 2, p. 158–172, 2021.

ROY, P.; DINDA, A. K.; CHAUDHURY, S.; DASGUPTA, S. β-cyclodextrin encapsulated polyphenols as effective antioxidants. **Biopolymers**, [s. l.], v. 109, n. 1, 2018.

SANTOS, D. I.; SARAIVA, J. M. A.; VICENTE, A. A.; MOLDÃO-MARTINS, M. Methods for determining bioavailability and bioaccessibility of bioactive compounds and nutrients. In: Innovative Thermal and Non-Thermal Processing, Bioaccessibility and Bioavailability of Nutrients and Bioactive Compounds. [s.l.] : Elsevier, 2019. p. 23–54.

SCHNEIDER, C. S.; BHARGAV, A. G.; PEREZ, J. G.; WADAJKAR, A. S.; WINKLES, J. A.; WOODWORTH, G. F.; KIM, A. J. Surface plasmon resonance as a high throughput method to evaluate specific and non-specific binding of nanotherapeutics. **Journal of controlled release: official journal of the Controlled Release Society**, [s. l.], v. 219, p. 331–344, 2015.

SHAPIRA, A.; ASSARAF, Y. G.; LIVNEY, Y. D. Beta-casein nanovehicles for oral delivery of chemotherapeutic drugs. **Nanomedicine: Nanotechnology, Biology and Medicine**, [s. l.], v. 6, n. 1, p. 119–126, 2010.

WANG, W.; SUN, C.; MAO, L.; MA, P.; LIU, F.; YANG, J.; GAO, Y. The biological activities, chemical stability, metabolism and delivery systems of quercetin: A review. **Trends in Food Science & Technology**, [s. l.], v. 56, p. 21–38, 2016

WU, Q.; KROON, P. A.; SHAO, H.; NEEDS, P. W.; YANG, X. Differential Effects of Quercetin and Two of Its Derivatives, Isorhamnetin and Isorhamnetin-3-glucuronide, in Inhibiting the Proliferation of Human Breast-Cancer MCF-7 Cells. **Journal of Agricultural and Food Chemistry**, [s. l.], v. 66, n. 27, p. 7181–7189, 2018

ZHANG, J.; LIU, Y.; LIU, X.; LI, Y.; YIN, X.; SUBIRADE, M.; ZHOU, P.; LIANG, L. The folic acid/β-casein complex: Characteristics and physicochemical implications. **Food Research International**, [s. l.], v. 57, p. 162–167, 2014.

ZHENG, Y.; ZHANG, J.; ZHAO, Y.; ZHANG, Y.; ZHANG, X.; GUAN, J.; LIU, Y.; FU, J. Curcumin protects against cognitive impairments in a rat model of chronic cerebral hypoperfusion combined with diabetes mellitus by suppressing neuroinflammation, apoptosis, and pyroptosis. **International Immunopharmacology**, [s. l.], v. 93, p. 107422, 2021.

ZIMET, P.; ROSENBERG, D.; LIVNEY, Y. D. Re-assembled casein micelles and casein nanoparticles as nano-vehicles for ω-3 polyunsaturated fatty acids. **Food Hydrocolloids**, [s. l.], v. 25, n. 5, p. 1270–1276, 2011.